ON THE REGULATION OF EXCITATORY SYNAPSES AND FEEDING BEHAVIOR BY O-GLCNAC TRANSFERASE

By

Karl Olof Lagerlöf

A dissertation submitted to The Johns Hopkins University in conformity with the requirements of the degree of Doctor of Philosophy

Baltimore, MD

February 2016

ABSTRACT

Thought is believed to be created by communication between neurons. Neurons communicate over cell-cell junctions called synapses. The number and function of neuronal synapses are not fixed but can be altered by a number of different mechanisms, so-called synaptic plasticity. For example, experience of the outer world can strengthen or weaken particular sets of synapses, thereby changing how the brain processes information and directs behavior. The work for this dissertation focused on the protein O-GlcNAc transferase (OGT). The activity of OGT is controlled by the metabolic status of the cell and the body. It was known that OGT is expressed in neurons. We hypothesized that if OGT would regulate synaptic plasticity, then investigations into the function of OGT may offer an opportunity to better understand how stimuli from the surrounding environment may influence thinking. Combining biological chemistry and animal behavior, we discovered that OGT maintains normal body weight in αCaMKII neurons of the paraventricular nucleus (PVN) of the hypothalamus. It turns out that these neurons participate in a negative feedback loop that becomes activated upon food intake to turn off further intake. By sensing the caloric content of what is being ingested, OGT sets the threshold of this loop by mediating how many excitatory synapses αCaMKII PVN neurons express. Further studies showed that OGT is enriched in the postsynaptic density of excitatory synapses and regulates their maturity in a range of different types of neurons. The argument of this dissertation holds that nutrient-dependent regulation of synaptic plasticity by OGT is an attractive target for future inquiry of the connection between the outer world and the mind.

DISSERTATION REFEREES

Reader: **Gerald W. Hart, Ph.D.,** Professor, Chair, Department of Biological Chemistry

Faculty sponsor: **Richard L. Huganir, Ph.D.,** Professor, Chair, Department of Neuroscience

ACKNOWLEDGEMENTS

Before entering the Biochemistry, Cellular and Molecular Biology (BCMB) Graduate Program at the Johns Hopkins School of Medicine, Gerald W. Hart, Professor and Chair of the Department of Biological Chemistry, accepted me into his laboratory during two summers as a visiting medical student. It became immediately clear to me that the environment in his laboratory allowed for free pursuit of fundamental questions in biology while upholding high standards for the way in which the problem of your choice should be solved. Dr. Hart is the discoverer of the O-GlcNAc pathway and its chemistry mesmerized me. Thanks to Dr. Hart, research into the mechanism of how O-GlcNAc regulates cellular function has given me a feeling of adventure that must be similar to what the explorers of older times embarking on mapping the world experienced.

Dr. Richard L. Huganir, Professor and Chair of the Department of Neuroscience, is one of the world's leading experts on the molecular basis of learning and memory. The laboratory of Dr. Huganir has had enormous success in reducing mental phenomena to biochemical processes. Dr. Huganir's openness and excitement over testing daring hypotheses are inspiring. He challenged me to question the interpretations of my experiments and I appreciate tremendously his support in becoming a scientist. Dr. Huganir showed me how molecular mechanisms can be harnessed to ask fundamental questions of neuronal information processing. I will be forever grateful for the introduction to Neuroscience given to me by Dr. Huganir.

I have never met so excellent scientists as Dr. Huganir and Dr. Hart. Them allowing me to join both of their laboratories with the aim of elucidating whether, and if so how, the O-GlcNAc pathway regulates synaptic plasticity was a dream come true for me. They opened the world of science to me. On their shoulders, I leave with the hopes of having acquired at least some of their expertise and of being able to apply the same standards to my future work in medicine.

During my two summers before graduate school, in the laboratory of Dr. Hart, Dr. Chad Slawson, now Assistant Professor at the University of Kansas, taught me many of the experimental techniques I would later take advantage of in my dissertation. Similar to Dr. Hart, the mentorship of Dr. Slawson brought great joy and excitement to the day-to-day operations of experimenting and showed the possibility of insight in careful evaluation of often overlooked details of your experiment.

I would also like to thank the rest of my thesis committee for their continuous support; Drs. Alex Kolodkin, Paul Worley and Seth Margolis. I very much appreciate their thoughtful discussion and that they always had time and wanted to help me. I feel honored to have been in their company and experienced their earnest search for how the brain works. I am thankful for the many hours Dr. Margolis has spent helping me with everything from interpreting experiments to writing research grants.

Although not being on my thesis committee, I owe a great deal of credit and appreciation for any progress that we have made to Dr. Seth Blackshaw. Dr. Blackshaw has been instrumental in applying O-GlcNAc and synaptic plasticity onto the biology of metabolic homeostasis. In his laboratory, Dr. Joseph Bedont was very kind in teaching me certain experimental techniques. Similarly, Dr. Yeka Aponte, and her student Julia E.

Slocomb, took time out of their other normal work to share with us experimental expertise as well as giving us intellectual support, of which I am very thankful.

The BCMB program, and its director Dr. Carolyn Machamer in particular, has been very helpful in managing the unusual situtation of writing your thesis in not only two different laboratories but also two different departments.

To my great fortune, coming to Hopkins meant rigorous training in the scientific method and building relationships with people that bring much joy and expertise to my pursuit. I thank all members of the laboratories of Drs. Hart and Huganir for their friendship and support. Dr. Ingie Hong and Richard Johnson, especially, have made substantial contributions to this thesis.

This thesis was supported by NIH R01DK6167, N01-HV-00240, P01HL107153 (G.W.H.); R01NS036715 (R.L.H.).

I have a dream of using medicine to explore questions of philosophy of mind. How is meaning constructed? My journey out into the world and beyond started with reading Ludwig Wittgenstein. On his life, I would like to build my own.

TABLE OF CONTENTS

LIST OF FIGURES

Chapter 2

Chapter 3

Chapter 4

LIST OF ABBREVIATIONS

ACSF	artificial cerebrospinal fluid
AMPA	α-amino-3-hydroxy-5-methyl-4-isoxazolepropionic acid
AN	anorexia nervosa
BED	binge eating disorder
BN	bulimia nervosa
CaMK	calcium/calmodulin-dependent kinase
C-terminus	carboxyl terminus
CNS	central nervous system
DIV	days *in vitro*
FRET	fluorescence resonance energy transfer
HEK 293	human embryonic kidney cell 293
kb	kilobase pair
K_M	the Michaelis constant
KO	knockout
LTP	Long-term potentiation
LTD	Long-term depression
MAPK	mitogen-activated kinase
MeCP2	methyl CpG binding protein 2
NMDA	N-methyl D-aspartate
N-terminus	amino terminus
OGA	O-GlcNAc hydroxylase
O-GlcNAc	O-linked β-N-acetylglucosamine

OGT	O-GlcNAc transferase
PIP3	phosphatylinositol (3,4,5)-triphosphate
PPF	paired-pulse facilitation
PSD	postsynaptic density
SDS-PAGE	sodium dodecyl sulfate polyacrylamide gel electrophoresis
UDP-GlcNAc	uridine diphosphate β-N-acetylglucosamine
Wb	Western blot
Wt	wildtype

CHAPTER 1.

INTRODUCTION

Notes

Most content (e.g. text and experimental results) included here is modified from work published previously or work that will be submitted for publication. These publications include:

1. **Lagerlöf O**, Slocomb JE, Hong I, Aponte Y, Blackshaw S, Hart GW, Huganir RL. The nutrient sensor OGT in PVN neurons regulates feeding. In press (*Science*)

2. **Lagerlöf O**, Hart GW, Huganir RL. OGT is a synaptic protein that regulates excitatory synapse maturity. In preparation.

3. **Lagerlöf O** and Hart GW (2014). O-GlcNAcylation of Neuronal Proteins: Roles in Neuronal Functions and in Neurodegeneration. *Book Chapter in the book 'Glycobiology of the nervous system'*. Springer.

1.1 Abstract

O-GlcNAc is the attachment of β-N-acetylglucosamine to the hydroxyl group of serine and threonine in nuclear and cytoplasmic proteins (1). It is generally not further elongated but exists as a monosaccharide that can be rapidly added or removed (2). Thousands of proteins involved in gene transcription, protein translation and degradation as well as the regulation of signal transduction contain O-GlcNAc (3, 4). Brain is one of the tissues where O-GlcNAc is the most highly expressed and deletion of neuronal O-GlcNAc leads to death early in development (5, 6). O-GlcNAc is also important for normal adult brain function, where dynamic processes like learning and memory at least in part depend on the modification of specific proteins by O-GlcNAc (7, 8). Conversely, too much or too little O-GlcNAc on other proteins participates in neurodegenerative processes underlying

diseases such as Alzheimer's and Parkinson's (9-13). In this chapter, I describe the expression and regulation of O-GlcNAc in the nervous system.

1.2 O-GlcNAc is a ubiquitous monosaccharide that cycles onto and off serine and threonine

1.2.1 O-GlcNAc is not elongated to yield complex oligosaccharides

O-GlcNAc is the covalent modification of nuclear and cytoplasmic proteins by β-N-acetylglucosamine (1). O-GlcNAc is formed as a derivative of glucose through the hexosamine biosynthesis pathway (HBP). In the HBP, the oxygen on the second carbon of fructose-6-phosphate is exchanged for nitrogen forming GlcN-6-P, prior to acetylation of the nitrogen to yield GlcNAc-6-P. This is then coupled to the high-energy molecule uridine diphosphate (UDP), UDP-GlcNAc. Upon modification of proteins by O-GlcNAc, the GlcNAc is cleaved from the UDP and attached in β-position to the hydroxyl group of serine or threonine (O-β-GlcNAc, O-GlcNAc). The reaction is catalyzed by the O-GlcNAc transferase, OGT. The removal of GlcNAc is catalyzed by the O-GlcNAc hydrolase, O-GlcNAcase (OGA).

Unlike 'classical' O- and N-linked protein glycosylation the GlcNAc is generally not elongated but exists as a monosaccharide. In fact, when O-GlcNAc is artificially capped by galactose, its biological function is lost (14). Although O-GlcNAc is smaller than complex oligosaccharides, it is still much larger than many other protein modifications, such as protein methylation or protein phosphorylation (2).

1.2.2 O-GlcNAc is mostly expressed on the inside of cells in multicellular organisms

O-GlcNAc is a highly conserved posttranslational modification. It has been found in evolutionarily distinct clades like plantae, fungi and animalia (5, 15). In multicellular organisms, all types of cells investigated so far contain O-GlcNAc (2). O-GlcNAc has also been identified in some unicellular organisms, e.g. giardia - the oldest eukaryote, and inside several types of virus (16-18). Nonetheless, most studies on unicellular organisms fail to report the presence of β-O-GlcNAc. Protozoans modify proteins by O-linked GlcNAc but primarily on extracellular proteins and in α-linkage rather than in β-linkage. Yeasts appear to lack O-GlcNAc entirely, but recent studies suggest that they use O-mannose cycling for similar functions carried out by O-GlcNAc in higher organisms (19). Bacteria are also largely devoid of cytoplasmic O-GlcNAc even though some bacterial proteins have been shown to carry O-linked GlcNAc (20, 21). Interestingly, the bacterium *Clostridium novyi* exploits O-GlcNAc by encoding an O-GlcNAc transferase that modifies small G-proteins in the infected cell (2, 22, 23).

O-GlcNAc is expressed almost exclusively on the inside of cells (1). Until the discovery of O-GlcNAc protein glycosylation was known to occur only on proteins exposed to the extracellular matrix, or in cellular organelles topographically similar to the outside of the cell such as the endoplasmic reticulum (ER) and the Golgi apparatus. In contrast, nearly all proteins that contain O-GlcNAc are expressed in the cytosolic or nuclear fraction of the cell. Proteins anchored to the cell membrane are modified with O-GlcNAc but usually only on parts stretching into the cytosol. This comes as no surprise as the O-GlcNAc transferase, OGT, is mainly nucleocytoplasmic rather than present in the

Golgi or ER as other glycosyltransferases (there are at least two O-GlcNAc transferases with their active sites in the lumen of the ER, called, eOGTs, but these enzymes are distinct from the enzyme regulating nucleocytoplasmic O-GlcNAc. O-GlcNAc has been detected on extracellular domains of a handfull of proteins, e.g. notch) (see section 2.2; (4). Also the hexosaminidase removing O-GlcNAc, OGA, is cytosolic and active at neutral pH (see section 2.3). By comparison, cellular glycosidases breaking down glycoconjugates retrieved from the cell surface are primarily found in the lysosome and prefer an acidic milieu.

Importantly, the concentration of O-GlcNAc is not uniform across the cell. Some parts, like the nuclear membrane, are heavily modified whereas other parts, like the mitochondria, contain O-GlcNAc but to a lesser degree. All major organelles and other cytosolic substructures, e.g. the proteasome and ribosome, express O-GlcNAc (24-26). The precise level varies over time and is finely tuned to meet the conditions of the cell (see sections 1.3, 3 and 4).

1.2.3 O-GlcNAc can be dynamically attached and removed

Whether or not a protein is modified by O-GlcNAc varies substantially over time. On many proteins, including the heat-shock protein αB-crystallin, the O-GlcNAc half-life is much shorter than the half-life of the peptide backbone (27). In fact, studies using selective inhibitors of the enzyme that removes O-GlcNAc from proteins, OGA, show that cycling rates are often on the order of minutes, making O-GlcNAc more akin to protein phosphorylation than 'classical' protein glycosylation. 'Classical' N- and O-linked glycosylation of proteins, glycosylation of proteins exposed to the extracellular matrix or within the secretory pathway, is, largely, stable once the mature glycan has been attached.

There are examples of proteins, e.g. the nucleoporins that form pores through the nuclear membrane, where the O-GlcNAc does not appear to turnover faster than the protein itself (28, 29).

It has been proposed that O-GlcNAc cycling works like a light switch with only two modes of operation - either 'on' or 'off'. One argument in favor of this idea is the fact that there are only two enzymes that add and remove O-GlcNAc from proteins, OGT and OGA, respectively (see section 2). Indeed, in some situations cells react by either elevating or suppressing global O-GlcNAc levels. For example, abundant nutrient supply leads to a general increase in O-GlcNAc and scant supply to a general decrease (see sections 2.2 and 4.3). Likewise, cellular stress is associated with raised O-GlcNAc throughout the cell (30). All the same, early studies showed that activation of lymphocytes causes O-GlcNAc levels in the cytosol to go up while they go down in the nucleus (31). A recently developed FRET (fluorescence resonance energy transfer) reporter that measures OGT activity in real-time demonstrated further that during serum stimulation of transformed cell lines, OGT was activated many fold in some parts of the cytosol whereas in nearby areas OGT activity remained at baseline (32). Work on the regulation of signal transduction by O-GlcNAc describes the same picture; upon stimulation, in a single pathway there can be proteins that become better substrates for OGT but also proteins that become worse substrates for OGT (33). Thus, despite there being only two enzymes that add and remove O-GlcNAc, changes in O-GlcNAc can occur 'locally' within the cell. For example, by forming dynamic multi-partner complexes OGT and OGA can be directed towards select targets among a broader range of available substrates (see sections 2.2-3; (34-36)).

The spatiotemporal regulation of O-GlcNAc cycling is complex and occurs on many levels. While nutrients and stress can cause global changes in O-GlcNAc, binding partners to OGT and OGA tune O-GlcNAc occupancy locally. Below I will discuss in detail how O-GlcNAc cycling is controlled in the nervous system and how the dynamic modification of proteins by O-GlcNAc helps the brain to develop and respond to challenges in the environment.

1.3 O-GlcNAc is added to proteins by OGT and removed by OGA

1.3.1 Only two enzymes regulate the cycling of O-GlcNAc

O-GlcNAc exists as a monosaccharide on nuclear and cytoplasmic proteins and can cycle rapidly and repeatedly over the lifetime of the polypeptide chain (see section 1). In a single cell, including neurons, thousands of proteins carry O-GlcNAc ((3); see section 3.2). Changes in O-GlcNAc can happen globally throughout the cell but also locally on individual proteins or sites within a protein (see section 1.3). In mammals, there are only two enzymes that add and remove O-GlcNAc. The O-GlcNAc transferase (OGT) adds O-GlcNAc to proteins (5, 37). The O-GlcNAc glycosidase, O-GlcNAcase (OGA), removes O-GlcNAc from proteins (38, 39). As we will see in section 3, loss or deregulation of O-GlcNAc cycling leads to severe developmental brain defects, impaired brain function in the adult and risk for many neurodegenerative disorders, e.g. Alzheimer's disease. In this section we will discuss how OGT and OGA are both promiscuous in order to accept a broad range of targets while at the same time specific to ensure that O-GlcNAc cycles on the correct site at the correct time and place.

1.3.2 O-GlcNAc transferase; a highly conserved glycosyltransferase present in the nucleus & cytosol

In mammals, O-GlcNAc transferase (OGT) is encoded by a single gene. The gene is highly conserved and lies close to the centromeric region of the X chromosome (Xq13) (5, 40, 41). It spans about 45 kilobase pairs (kb) and its locus is linked to Parkinsonian dystonia, a neurodegenerative movement disorder (41, 42). In most organs there are five major OGT transcripts ranging from 4.2kb to 9.5kb. The transcripts undergo alternative splicing. In brain the larger 9.5kb and 6.4kb transcripts, which include exons located 5' of the internal promoter, dominate (41, 43). Most studies so far argue that the total expression of *OGT* is stable during most conditions. However, little is known about the regulation of the OGT gene and at least in neuroblastoma cells OGT mRNA increases after depriving the cells of glucose (35).

The protein encoded by *OGT* contains two major domains. The N-terminal half is comprised of several tetratricopeptide (TPR) repeats and the C-terminal half binds UDP-GlcNAc and harbors the glycosyltransferase activity. The TPR repeats form a flexible superhelix that can accommodate many protein-protein interactions (5, 44-46). The C-terminus exhibits a more compact structure and resembles members of the GT-B superfamily of glycosyltransferases (Gtfs) but adopts some unique folds as well (47). While most OGT-interacting proteins are believed to bind the TPR repeats the C-terminus includes regions that are necessary and sufficient for some interactions, e.g. to the mitogen-activated kinase (MAPK) p38 in neurons (35). The C-terminus also mediates translocation to the cell membrane upon insulin stimulation, probably via a cluster of

lysines that pairs electrostatically with negatively charged phosphatylinositol (3,4,5)-triphosphate (PIP3) (48).

Catalysis occurs by an ordered sequential mechanism where OGT binds first UDP-GlcNAc and then the substrate. A hydroxyl group on the incoming substrate performs a direct nucleophilic attack on the anomeric carbon on GlcNAc, thereby inverting the glycosidic bond from UDP-α-GlcNAc to (serine/threonine-) O-β-GlcNAc. There is a general base and a general acid that catalyze the nucleophilic attack by activating the hydroxyl group (47, 49). *In vitro* experiments have shown that if the TPR domain is removed from OGT, the C-terminus alone can modify peptides with O-GlcNAc. In contrast, for protein substrates to be modified, the TPR domain is required (44, 45). It has been hypothesized based on computer simulations that the TPRs induce a conformational change in the substrate that enables the O-GlcNAc site to dock at the catalytic groove. Most likely, OGT goes through a conformational change as well; the TPR helix pivots around the intervening region between the TPRs and the C-terminus exposing the entrance to the groove (3, 47).

Three major isoforms of OGT have been described (43). All share the same catalytic domain but differ in their N-terminus. Nucleocytoplasmic OGT (ncOGT) is the full-length variant and includes 11-12 TPRs, depending on the species. Mitochondrial OGT (mOGT) starts with a mitochondrial targeting sequence, followed by a membrane-spanning region and continues with the last 9 TPRs found in ncOGT. The third, and shortest, isoform is soluble OGT (sOGT). It contains only 3 TPRs. According to most studies, only ncOGT is present in total brain lysate (5, 50). However, sOGT may become upregulated in older animals and little is known about whether mOGT or sOGT is present

in specific regions of the brain or in specific subcellular compartments (51). Apart from mOGT, which is anchored to the inner membrane of the mitochondria, almost all OGT activity is found in the nucleocytoplasm or as a non-integral membrane protein associated with the cytosolic face of cell membranes (37, 43).

In vivo, OGT oligomerizes into a dimer or trimer (5, 50). OGT was first purified from rat liver and described as a heterotrimer consisting of two ncOGT and one 78kDa unit. The 78kDa unit is enriched in certain tissues and may correspond to sOGT, but may also be a proteolytic fragment of ncOGT (5, 52). The major form of OGT expressed in brain is more likely a homodimer of ncOGT (50). Dimerization occurs over an evolutionary conserved hydrophobic region in the TPR domain (TPR 6). Dimerization is stable even in very high salt concentrations and probably not subject to posttranslational regulation (45, 46).

OGT is exquisitely regulated adding O-GlcNAc only to particular sites at any given time and place. *In vitro*, OGT exhibits sequence specificity. If purified OGT is mixed with UDP-GlcNAc and a peptide that contains several possible O-GlcNAc sites, often only one or a few sites become significantly modified. Likewise, substrate peptides derived from different proteins are often modified with different efficiency (45). Also UDP-GlcNAc levels influence peptide substrate specificity (45, 53). Nevertheless, there is no absolute substrate consensus sequence for OGT. Indeed, the catalytic site of OGT interacts primarily with the peptide backbone of the substrate and not particular side chains (47). *In vivo*, O-GlcNAc sites concentrate on disordered regions of proteins and close to proline and valine, so called PVS motifs (2-4). Presumably, the reason is that such regions can be made to fit OGT's catalytic groove more easily.

Primary sequence plays a role in determining the major O-GlcNAc sites on a given protein. However, in cells, whether a particular protein will be modified depends also on OGT-binding proteins. OGT operates as a holoenzyme, where its interacting proteins direct OGT to its substrates (34-36, 50, 54, 55). For example, in neurons, neurofilaments become O-GlcNAcylated only after activated p38 binds OGT (54). OGT-interacting proteins can enhance OGT activity towards peptide substrates as well (50). Moreover, OGT is multiply phosphorylated and it modifies itself with O-GlcNAc (5, 34, 56). Phosphorylation of OGT can both activate OGT, e.g. via calcium/calmodulin-dependent kinase IV (CaMKIV) during neuronal depolarization, and alter OGT's substrate specificity (34, 56, 57). OGT is strongly inhibited by free UDP but, unlike most other glycosyltransferases that utilize a UDP-bound sugar as donor, OGT does not require divalent cations (37).

OGT has emerged as a key cellular nutrient sensor. The donor for O-GlcNAc, UDP-GlcNAc, is produced by the hexosamine biosynthesis pathway, the HBP (see section 1.1). UDP-GlcNAc is an abundant high-energy small molecule and ranges in concentrations within cells from 0.1 to 1mM. Almost all metabolic pathways feed into the HBP and contribute to the production of UDP-GlcNAc, including fatty acids, nitrogen and 2-5% of all cellular glucose. A rich energy supply elevates UDP-GlcNAc, and, subsequently, protein O-GlcNAcylation whereas a scarce supply is associated with reduced levels of both UDP-GlcNAc and O-GlcNAc (2, 23). Also in the brain fasting has been shown to decrease O-GlcNAc generally, a change reversed upon re-feeding (10, 58). Interestingly, depending on the substrate, the K_m for UDP-GlcNAc can vary more than 20-fold but most become better substrates in the presence of higher concentrations

of UDP-GlcNAc (45, 53). Therefore, although metabolic flux is associated with global changes in O-GlcNAc, some proteins are more sensitive to nutrient supply than others. In section 4.3 we will discuss how OGT as a nutrient sensor is involved in the pathology behind neurodegenerative disease.

1.3.3 O-GlcNAcase; a cytosolic O-β-GlcNAc hydrolase with neutral pH optima

In accord with the O-GlcNAc transferase, the enzyme that removes O-GlcNAc from proteins, O-GlcNAcase (OGA), is expressed from a single gene. The gene was first cloned as an antigen associated with meningioma and it is localized to the long arm of chromosome 10 (10q24), a locus tightly linked to late-onset Alzheimer's disease (59, 60)). In addition, alternatively spliced OGA transcripts have been associated with sporadic cases of Alzheimer's disease (61).

OGA hydrolyses GlcNAc from proteins using substrate-assisted catalysis. Two aspartates activate the acetamido group on GlcNAc's second carbon to perform a nucleophilic attach on its anomeric carbon. This results in the displacement of GlcNAc from the protein (62). Contrary to most hexosaminidases, OGA has neutral pH optima and is not inhibited by GalNAc. Nor does it remove GalNAc from proteins but is specific for β-linked O-GlcNAc (38). OGA is also genetically and immunogenically distinct from other glycosidases (39).

OGA has been identified in all tissues so far investigated. It is expressed in the nucleus and cytoplasm of cells and the highest expression is found in brain (39). OGA is highly conserved but contains a middle, intrinsically unfolded region that exhibits more variability (39, 59, 63). Like OGT, OGA consists of two major domains. The glycosidase domain is C-terminal. The N-terminus contains a histone acetyl transferase (HAT)

domain. While the HAT domain was reported to be functionally active (64, 65), other groups have not been able to repeat this finding (63). Caspase 3 cleaves OGA between the glycosidase domain and the HAT domain during apoptosis without any loss of O-GlcNAcase activity (63).

Very little is known about the regulation of OGA. It is believed that OGA forms multi-partner complexes that direct OGA to its substrates, much like how OGT is regulated ((2); see above). Recently, highly specific pharmacological inhibitors of OGA have been developed (11, 66). In section 4 we will learn more about the way in which OGA is important for the brain's ability to learn and form memories and serves as a drug target for neurodegenerative disorders.

1.4 O-GlcNAc is highly expressed in the nervous system

1.4.1 O-GlcNAc is found throughout the brain

Brain is one of the organs where O-GlcNAc is the most abundant. OGT and OGA are expressed in comparatively high levels in the brain (5, 39, 67). Both enzymes are present across brain regions, including cortex, the cerebellum and subcortical nuclei such as the amygdala (8, 51). Within neurons, O-GlcNAc has been identified in all subcellular structures investigated, albeit to differing degrees. Biochemical fractionation was used to show that O-GlcNAc transferase activity was present in synapses (68). Immunoelectron microscopy indicated that OGT and O-GlcNAc were present in both the post- and pre-synapse. In the presynapse, OGT is concentrated on synaptic vesicles storing neurotransmitter (69). Most research on O-GlcNAc in the brain has focused on O-GlcNAc's role in neurons of the central nervous system. Less is known about its expression in neurons of the peripheral nervous system or in glia.

1.4.2 Thousands of neuronal proteins are modified by O-GlcNAc

One difficulty in studying the role of O-GlcNAc for brain function is its vast abundance. Technical breakthroughs have allowed identification of O-GlcNAc sites *en masse* by coupling selective enrichment of O-GlcNAc modified proteins with electron capture dissociation (ECD) or electron transfer dissociation (ETD) mass spectrometry (types of mass spectrometry that can fragment peptides without losing the GlcNAc) (3, 70). According to some estimates, about 40% of all neuronal proteins are modified by O-GlcNAc (3). Some proteins, like bassoon, which is important for neurotransmitter release, have more than a dozen O-GlcNAc sites. On other proteins, e.g. CaMKII, only a single site has been detected (3). As discussed in section 2.2 O-GlcNAc sites concentrate on structurally disordered regions of proteins and there is some preference for a sequence context rich in proline and valine. For any particular site, O-GlcNAc is usually present in substochiometric levels (23). The absolute occupancy is dynamic and depends on the activity of the neuron, possibly due to CaMK-dependent stimulation of OGT (56, 71, 72).

Proteins modified by O-GlcNAc belong to all functional classes. Many O-GlcNAc proteins are shared across cell types and underlie constitutive cellular functions such as transcription, translation and protein degradation. Nevertheless, the role played by O-GlcNAc on these factors is often neuron-specific. For example, in neurons, the common transcription factor cyclic AMP-response element binding protein (CREB) is modified by O-GlcNAc on serine 40 upon cell depolarization. Once modified, CREB is prevented from binding to its co-activator CRTC (CREB-regulated transcription coactivator). This inhibits CREB and leads to an inactivation of several transcription pathways involved in synaptic plasticity (see section 4.2; (8)). Other O-GlcNAc proteins

are particular to neurons, including certain scaffolding proteins, signaling proteins and cytoskeletal proteins. Many of these are proteins found in the synapse. One interesting case is αCaMKII. αCaMKIIα is modified by O-GlcNAc in a small region known to contain one phosphorylation site that can activate the enzyme and another phosphorylation site that deactivates it (3). The regulation of αCaMKII activity is crucial for synaptic events that underlie learning and memory (73). Therefore, elucidation of how O-GlcNAc may fine tune αCaMKII activity is important not only to our understanding of synapse biology but also higher-order brain function. Moreover, in the synapse, there is a significant overrepresentation of kinases, the enzymes that add O-phosphate to proteins, among the proteins that are modified by O-GlcNAc (3).

Several proteins that contribute to the development of neurocognitive disease carry O-GlcNAc. The transcription factor methyl CpG binding protein 2 (MeCP2) coordinates activity-dependent gene transcription and is modified by O-GlcNAc. Loss of MeCP2 causes Rett syndrome, a developmental disorder classically associated with repetitive and stereotypical hand movements and mental retardation. It has been shown that only the MeCP2 molecules that do not carry O-GlcNAc were activated in response to neuronal depolarization (8, 70). Seemingly on MeCP2, O-GlcNAc serves as a checkpoint for turning on or off activity-dependent gene transcription. Other O-GlcNAc proteins that are intimately involved in neurocognitive disease include tau (Alzheimer's disease) and α-synuclein (Parkinson's disease) (9, 70).

1.4.3 O-GlcNAc regulates diverse cellular processes

Proteins modified by O-GlcNAc regulate diverse cellular processes such as gene transcription, protein translation and degradation and signal transduction. The function of

the O-GlcNAc modification depends on the specific protein that is modified as well as the site on that protein that is modified (2, 74). Here we will briefly discuss different mechanisms by which O-GlcNAc underlies normal cell function.

Gene transcription

RNA polymerase II. O-GlcNAc may directly affect basal transcription by inactivating RNA polymerase II. RNA polymerase II in the so-called pre-initiation complex is heavily modified by O-GlcNAc in its carboxyl terminal domain (CTD). However, the RNA polymerase II in the so-called elongation complex is devoid of O-GlcNAc. Instead, upon transcription initiation the CTD of RNA polymerase II becomes phosphorylated. It has been suggested that the loss of O-GlcNAc is required before it can be phosphorylated and thereby activated (75-77).

Histones. Histones are modified by multiple posttranslational modifications, including O-GlcNAc (78). The combination of these modifications are hypothesized to form a 'code' that either facilitates or prevents the access of transcription factors to DNA. The O-GlcNAc on serine 112 enhances the (mono-) ubiquitination of histone 2B thereby activating gene transcription (79).

Transcription factors. O-GlcNAc takes advantage of several different mechanisms to regulate the activity of transcription factors toward gene transcription (80). O-GlcNAc activates NeuroD by promoting its shuttling from the cytosol to the nucleus and protects p53 by saving it from ubiquitin-mediated degradation (81). O-GlcNAc on serine 228 on Oct4 does not affect its general activity but influences its promoter specificity (82).

Protein translation

O-GlcNAc plays several distinct roles during the translation of messenger RNA to polypeptide chains. OGT and OGA bind very tightly to the ribosome and overexpression of OGT was shown to facilitate ribosome assembly. Several ribosomal proteins are modified by O-GlcNAc, including the mammalian target of rapamycin (mTOR) pathway protein S6 (26). Also associated translational factors are modified by O-GlcNAc. The eukaryotic initiation factor 2 (eIF2) initiates translation by forming a complex with p67. It has been suggested that the O-GlcNAc on p67 is required for p67's ability to protect eIF2 from phosphorylation and thereby inactivation (83, 84).

Protein and vesicle trafficking

The subcellular distribution of multiple proteins has been shown to depend on O-GlcNAc (85, 86). For instance, E-cadherin is a cell junction protein that, among other things, is important for inhibitory synapse formation (87). If the O-GlcNAc on E-cadherin's cytosolic tail is not removed, E-cadherin becomes trapped in the endoplasmatic reticulum (ER) and cannot be transported further to the Golgi apparatus (86). O-GlcNAc may also play a role in the transport of microvesicles within cells, e.g. vesicles that mediate the release of neurotransmitter. There is no direct evidence showing that O-GlcNAc regulates microvesicle trafficking *per se*. However, proteins such as adaptor protein complex 2 (AP-2) that mediates clathrin-dependent endocytosis and N-ethylmaleimide-sensitive fusion protein (NSF), which is an ATPase involved in vesicle fusion, are modified by O-GlcNAc (88).

Protein degradation

O-GlcNAc is intimately involved in the control of protein degradation. O-GlcNAc sites often fall in regions with high PEST-scores (the Pro-Glu-Ser-Thr sequence is associated

with rapid degradation of proteins) and an increase in global O-GlcNAc leads to an increased ubiquitination of proteins whereas a decrease in global O-GlcNAc decreases protein ubiquitination (23, 89). In addition, O-GlcNAc can directly inhibit the proteasome by modifying the 26S and 19S proteasomes (25).

Signaling and the crosstalk between O-GlcNAc and O-phosphate

An emerging theme in the regulation of signal transduction pathways is the crosstalk between O-GlcNAc and O-phosphate. Many O-phosphorylated proteins are also O-GlcNAc proteins (3). O-GlcNAc and O-phosphate can directly and reciprocally inhibit each other by sharing the same site, as in the case of threonine 58 in the trans-activation domain of the transcription factor c-myc (90, 91). On other proteins the crosstalk is indirect and can be both negative and positive. Removal of O-GlcNAc from threonine 57/serine 58 on CaMKIV, for example, prevents the phosphorylation of threonine 200, the main activation site on CaMKIV. At the same time, loss of O-GlcNAc on serine 189 facilitates threonine 200 phosphorylation (92). In fact, on a global level, the occupancy of most dynamic phosphorylation sites is affected by acute inhibition of O-GlcNAc cycling (93). As a group, kinases, the enzymes that add O-phosphate to proteins, are more often modified by O-GlcNAc than other kinds of proteins (3, 94). Furthermore, as discussed in section 2.2, phosphorylation of OGT can activate OGT and influence its substrate specificity.

1.5 O-GlcNAc is essential for brain function

In sections 1-3 we have learned that O-GlcNAc dynamically modifies a vast array of neuronal proteins involved in many cellular processes, such as gene transcription and signal transduction. In the following section I will discuss how the regulation of neuronal

function by O-GlcNAc underlies normal brain function and contributes to neurocognitive disease.

1.5.1 Early and late brain development depend upon O-GlcNAc cycling

In vertebrates, O-GlcNAc is essential for normal development. In many different cell types, it has been shown that perturbations of O-GlcNAc cycling interrupt the cell cycle by preventing cytokinesis (70, 95, 96). In the embryo, this leads to failure of stem cell proliferation and subsequent death at the single cell stage (40). Studies taking advantage of partial depression of OGT expression, where cell proliferation is preserved, indicated that renewal of stem cell pluripotency and stem cell differentiation depend upon O-GlcNAc. In fact, two members of the core pluripotency network in embryonic stem cells, Oct4 and Sox2, are modified by O-GlcNAc. Loss of O-GlcNAc on threonine 228 of Oct4 alters its promoter specificity disrupting transcription of dozens of genes, including some that are involved in neuronal differentiation (e.g. Nanog) (82, 97).

Later in development, O-GlcNAc plays a role in brain morphogenesis and patterning. Loss of OGT decreases brain size, while overexpression of OGT blurs the organization and distinction of hind-, mid- and forebrain regions in zebra fish (15). Likewise, when OGT was deleted from neurons specifically by crossing floxed OGT mice with mice expressing Cre recombinase under the synapsin I promoter, viability until term was reduced. The pups that survived failed to develop any locomotor activity and died within ten days (6). In postmitotic neurons, the O-GlcNAc glycosylation of CREB underlies both axonal and dendritic growth and may, at least partly, explain the impaired development of brain function (8). O-GlcNAc is also known to affect axonal branching (98).

1.5.2 O-GlcNAc is associated with learning and memory

Learning and memory are fundamental properties of the brain. Over the past decades it has been shown that the brain is a highly malleable organ that dynamically responds to challenges in the environment. It is believed that memories are encoded by neurons through changes in their synaptic communications with other neurons, so-called synaptic plasticity. A prevailing model for how such changes occur is long-term potentiation (LTP) and depression (LTD) (see, e.g., (99, 100). Multiple disorders involving mental retardation such as Fragile X and Rett syndrome have been linked to proteins underlying synaptic plasticity (101, 102). OGT is present in the synapse and many postsynaptic proteins involved in LTP and LTD carry O-GlcNAc (see section 3.1 and 3.2). Using electrophysiology, it was further established that O-GlcNAc cycling is necessary for normal expression of LTP; pharmacological inhibition of OGT diminished LTP whereas OGA inhibition elevated LTP (7). The effect may relate to the synaptic relocation of the α-amino-3-hydroxy-5-methyl-4-isoxazoleproprionic (AMPA) receptor, the glutamate neurotransmitter receptor responsible for most fast synaptic transmission in the central nervous system (CNS). O-GlcNAc modifies CaMKII in close proximity to a phosphorylation site that regulates its activity (see section 3.2). CaMKII, in turn, is one of the major pathways that can induce the synaptic insertion of the AMPA receptor (7, 103). Interestingly, an OGT-dependent increase in AMPA receptor conductivity was absent in AMPA receptors where the main CaMKII phosphorylation site was mutated to alanine (104).

O-GlcNAc cycling is important for dynamic synaptic function at the presynapse. Acute OGA inhibition *in vivo* decreases paired-pulse facilitation (PPF). PPF is a

measurement of vesicle release of neurotransmitter. O-GlcNAc may regulate PPF via synapsin I. The presynaptic protein synapsin I is extensively modified by O-GlcNAc and inhibition of OGA increases the phosphorylation of synapsin I (7).

The studies investigating the effect of O-GlcNAc on learning and memory have so far relied heavily upon pharmacological manipulation of OGT and OGA. Unfortunately, some of the drugs used are known to cause off-target effects in cells. This may explain some apparent contradictions in published results; one report argues that O-GlcNAc does not affect basal synaptic (7) transmission whereas another does see a large effect on basal AMPA receptor function (104). For future research, it will be important to develop mouse models of O-GlcNAc function and focus on mechanisms for the way in which O-GlcNAc may underlie learning and memory. One good example is a recent study that compared wildtype CREB with an O-GlcNAc loss-of-function mutant of CREB. This study overexpressed these proteins *in vivo* and showed that the O-GlcNAc mutant enhanced CREB-dependent transcription of several synaptic plasticity associated genes as well as short-term memory in mice (8).

1.5.3 Impaired O-GlcNAc cycling contributes to neurodegenerative disease

Neurodegenerative disease is a collection of disorders that are characterized by general cognitive decline and loss of neurons and neuronal synapses. They become more common with age but early-onset variants exist (105, 106). Impaired O-GlcNAc cycling is implicated in the development of several types of neurodegenerative disease, including Alzheimer's, Parkinsonism and Huntington's (2, 9, 74, 97). The loci for the genes encoding OGT and OGA are linked to Parkinsonian dystonia and Alzheimer's disease,

respectively. In addition, OGA transcripts are alternatively spliced in the brain in patients with sporadic Alzheimer's (see sections 2.2-3).

Two pathological hallmarks of Alzheimer's disease are neurofibrillary tangles and amyloid plaques (74, 105). The neurofibrillary tangles consist of paired helical filaments of tau, a protein that is important for microtubuli stability. Tau is extensively modified by O-GlcNAc, including in the region that binds to microtubuli (9, 12). Results from both *in vitro* and *in vivo* experiments indicated that increasing O-GlcNAc on tau protected it from filament precipitation (11). O-GlcNAc may save tau from precipitating either directly or indirectly by protecting it from hyperphosphorylation (11, 66). Alzheimer's patients present with hyperphosphorylated and hypo-O-GlcNAc glycosylated tau. No O-GlcNAc can be found on the tau tangles isolated from these patients (10). Importantly, in mouse models of neurodegenerative disease resulting from expressing mutant forms of tau prone to precipitate, elevating global O-GlcNAc, including O-GlcNAc on tau, by selectively inhibiting OGA pharmacologically, slowed symptom progression (11). Interestingly, the main constituent amyloid plaques, amyloid precursor protein (APP), is also modified by O-GlcNAc (107).

Alzheimer's disease is intimately associated with dysregulated glucose metabolism and insulin resistance (108, 109). Due to the regulation of O-GlcNAc by nutrient supply and metabolic hormones, OGT has emerged as a key nutrient sensor in cells (see section 2.2). Much of the toxicity associated with excessive intake of glucose is mediated by the hexosamine biosynthesis pathway, the same pathway that produces the O-GlcNAc donor substrate UDP-GlcNAc. Many forms of insulin resistance are also related to OGT (23). Overexpression of OGT can independently lead to insulin resistance

(48). From this perspective, impaired O-GlcNAc signaling represents a model, and pharmacological target, for how metabolic dysfunction may result in neurodegenerative disease.

O-GlcNAc may also be involved in neurodegenerative diseases other than Alzheimer's. For example, in transgenic models where a polyglutamine expansion of huntingtin (the protein that causes Huntington's disease) was overexpressed, deletion of OGT attenuated neuron loss while deletion of OGA exacerbated neuron loss (97). In addition, α-synuclein, the protein found in lesions overrepresented in Parkinson's disease, carries O-GlcNAc in the region known to induce self-aggregation (12). It should also be noted that O-GlcNAc in other cell types becomes elevated from many different types of stress and that deletion of OGT makes cells more vulnerable to stress (30, 110).

1.6 Synaptic plasticity underlies adaptive behavior

Neuronal synapses, the cell-cell junctions over which neurons communicate, are formed and eliminated throughout life and their turnover has for decades been associated with the way neuronal circuits adapt to environmental challenges to optimize behavior (111, 112). In both humans and animals, early development is characterized by massive generation of new synapses. About half of all synapses are then lost during adolescence (112, 113). Most mature excitatory synapses occur on dendritic protrusions called spines and essentially all spines contain an excitatory synapse (114-116). *In vivo* imaging of individual spines for days to months has shown that adult spines are largely stable but a small subpopulation remains plastic (113, 117) and spine turnover is increased by novel experience (115, 118-120). While most new spines are thin and withdraw rapidly, some enlarge and form stable synaptic contacts (112, 113, 117, 121-124). In fact, the

stabilization of a subset of new spines correlates with behavioral performance in several different tasks in multiple animal species (123, 125-127). Rather than synapse formation or density, the selection of which spines are retained once formed has been suggested to match circuit architecture with behavioral needs (128). Without affecting spine formation, deleting β-adducin, which regulates actin, perturbed the process by which nascent spines establish functional synapses and impaired long-term memory (129). Fragile X Syndrome, a common form of mental retardation, exhibits a higher than normal density of spines but more of them exhibit an immature morphology and their turnover is not affected by sensory experience (119, 130). Conversely, the protein Telencaphalin arrests the maturation of spines and its removal enhances several forms of learning (123, 131).

The association between learning and spine survival suggests that synaptic maturation is regulated by neuronal activity (112). Long-term synaptic potentiation (LTP) caused by repeated stimulation of excitatory synapses, a predominate model for encoding of learning and memory on a cellular level, protects activated spines from removal (132, 133). Likewise, Hill and Zito induced LTP specifically on individual newly formed spines through glutamate uncaging and observed potent stabilization (134). While also causing some spines to be eliminated, LTP does not consistently lead to a lasting increase in overall spine density (114, 132, 135, 136). It is widely believed that LTP is caused by insertion of α-amino-3-hydroxy-5-methyl-4-isoxazolepropionic acid (AMPA) receptors into the synaptic membrane. AMPA receptors are glutamate-gated tetrameric ion channels composed of different combinations of subunits GluA1-4 and conduct the majority of the fast excitatory neurotransmission in the brain (103). AMPA receptors may

not be obligatory for spine formation in early development as knocking out (KO) GluA1-3 shortly after birth did not change spine density (137). However, knocking down GluA1-3 increases the number of inactive presynaptic terminals and overexpression of the GluA2 as well as the GluA4 subunits recruits synapses (138-140). Nascent spines incorporate AMPA receptors within a few tens of minutes of formation and so-called 'silent spines', where AMPA receptors cannot be detected, do not correspond to the age of the spine but only its size (123, 141-144). Live imaging has shown that the frequency of local postsynaptic calcium transients within seconds to minutes upon contact between a dendritic protrusion and an axon correlates with the retention of that contact (122). While blocking glutamate signaling did not affect these early events, it did arrest subsequent molecular organization of the spine, including decreasing its long-term stability (122, 124, 133). AMPA receptor stimulation, rather than overall neuronal activity, can rescue the loss of spines that occurs upon removal of presynaptic inputs (111, 145). Similar to LTP, which occurs mainly at small spines, inhibiting AMPA receptor signaling decreases spine density by reducing the number of small and thin spines (114, 146-148). Long-term depression (LTD) of excitatory synapses involves synaptic removal of AMPA receptors and leads to fewer and smaller spines (114, 149). A downstream target of AMPA receptor-dependent regulation of spine maturation is actin, e.g. via modulation of the RhoA signaling cascade (148, 150).

In addition to their effect on synapse number, the function of the synapse, once it is formed, is heavily modified by the absolute abundance and relative efficacy of the AMPA receptors in the synaptic cleft (103). In fact, recent evidence from *in vivo* imaging of AMPA receptor trafficking argues that in mature circuits, some experience-dependent

synaptic plasticity is based mostly on a relative change in AMPA receptor abundance rather than turnover of synapses (142). AMPA receptors undergo both activity-dependent and constitutive recycling to and from the synaptic plasma membrane. AMPA receptors reach the cell membrane via vesicle-mediated extrasynaptic exocytosis and then by lateral diffusion enter the synapse. It has also been hypothesized that some synaptic translocation occurs by direct insertion into the synapse (103, 151, 152). Upon endocytosis, the receptor can either recycle back to the plasma membrane or undergo lysosmal and proteasomal degradation (103, 153).

The trafficking of AMPA receptors is regulated by AMPA receptor-binding proteins such as protein 4.1N and protein kinase C-alpha-binding protein (PICK1) (153). Many AMPAR interactions occur through its C-terminal PSD95/Dlg1/ZO1 (PDZ) ligand, but also through a membrane-adjacent domain. The AMPAR cytoplasmic tail is modified by several posttranslational modifications, e.g. phosphorylation, ubiqutination and palmitoylation, which can affect both AMPA receptor channel properties and protein-protein interactions (154).

The AMPA receptor functions in a context of its auxiliary subunits called TARPs (transmembrane AMPA receptor regulatory proteins). TARPs regulate AMPAR conductance and trafficking (155, 156). While some evidence shows that AMPA receptor translocation can occur independent of their C-terminal tails, behaviorally relevant trafficking likely depends on the C-terminus. For example, point mutations of specific phosphorylation sites in the C-terminus affect both LTP and memory retention (157-159).

Experience-dependent trafficking of AMPA receptors can occur in a subunit-specific manner (160). It has been suggested that GluA1 homomers move into the synapse first to be replaced later by more stable GluA2/A3 heteromers (159, 161).

Synapse formation and termination and AMPA receptor trafficking are multi-step processes where the stability, or maturity, and function of the spine are continuously surveyed by activity-dependent processes. Though many molecules that affect synapse number and function have been identified over the last decade, it is still unclear how these are regulated to refine information processing to optimize behavior (162).

1.7 Feeding behavior is regulated by diverse neuronal circuits in the brain

Eating disorders, including obesity, bring enormous emotional, physical and economic costs to society (163, 164). Feeding behavior is a consequence of personal habits, social cues and chemical factors associated with ingested food. Although it has been known for decades that particular feeding centers in the brain integrate this information to either promote or inhibit food intake, their function has remained elusive. The main difficulty lies in resolving the many categories of neurons that often have contrasting roles contained in these centers (165).

While disorders like anorexia and bulimia nervosa (AN and BN, respectively) have been correlated with abnormal activity of several neurotransmitters, the heterogeneity of affected brain circuits make a related change hard to interpret as causative or compensatory (166). For example, palatable food increases dopaminergic release in the nuccleus accumbens but so do aversive stimuli like restraint stress. Although dopamine is associated with reward pathways, antagonizing dopamine strongly

inhibits feeding mostly due to motor dysfunction in the neostriatum (167). The problem is magnified by the fact that non-invasive methodology applied in human studies like fMRI cannot distinguish between anorectic and obesogenic neurons as they often lie intermingled and in areas technically challenging to image with high resolution (168). The basic sciences, on the other hand, have described many peripheral hormones, e.g. leptin, that potently regulate food intake depending on the energy need of the body (169). Curiously, these hormones often affect brain regions that have been difficult to link to common eating disorders directly (170).

The current confusion over where in the brain the pathology behind eating disorders lies is reflected by the lack of available long-term treatment for any of the major eating disorders like AN, BN or binge eating disorder (BED). Anti-depressants modulating serotonin and cognitive behavioral therapy decrease the frequency of binge episodes in BN and BED in the first six months, but the patients quickly relapse and there is no change in their body weight. Data from clinics specializing in eating disorders show that available treatment options do not lead to improvement in core symptoms over a five year period (171, 172).

Recently developed methods in rodents to identify and manipulate genetically defined neurons make it possible to disentangle those neuronal circuits that mediate feeding behavior (165) . A case in point is the medial hypothalamus. In the medial hypothalamus, there are several types of neurons that have strong effects on food intake. Obesogenic Agouti-related peptide (AgRP) neurons are mixed with anorectic proopiomelanocortin (POMC) neurons in the arcuate nucleus, adjacent to the third ventricle (173). Cell-specific neuronal tracing and opto- and pharmacogenetic methods

have shown that these neurons respond in opposite directions, where AgRP become activated and POMC neurons become inactivated, upon the antecipation of caloric ingestion and signal through multiple downstream targets. Some targets appear to directly modulate ascending information from the gastrointestinal system while other targets relate to more complex, higher-order processing of food intake (165, 174, 175)).

The need for effective treatment of eating disorders is pressing. Obesity is one of the world's leading causes of morbidity and mortality. 7-10% of the female population suffer from some eating disorder as defined in psychiatry. The prevalence among males is increasing. In addition to being unable to keep a normal weight, a problem which is common also in the general population, diseases like AN and BN are associated with grave psychological despair, for example depression, anxiety and substance abuse. In fact, eating disorders have the highest mortality rate of all psychiatric disorders, many times above the normal, in large part due to suicide (170).

Until now, progress in preventing and treating eating disorders has been stymied by a lack of techniques identifying defined networks of neurons. Without this knowledge, it is not possible to synthesize how the many disparate brain regions associated with food intake together may produce abnormal feeding behavior (165).

CHAPTER 2.

THE NUTRIENT SENSOR OGT IN PVN NEURONS REGULATES FEEDING

Notes

Most content (e.g. text, figures and experimental results) included here is modified from work that has been submitted for publication:

1. **Lagerlöf O**, Slocomb JE, Hong I, Aponte Y, Blackshaw S, Hart GW, Huganir RL. The nutrient sensor OGT in PVN neurons regulates feeding. In press (*Science*)

2.1 Abstract

Maintaining energy homeostasis is crucial for the survival and health of organisms. The brain regulates feeding by responding to dietary factors and metabolic signals from peripheral organs. It is unclear how the brain interprets these signals. O-GlcNAc transferase (OGT) catalyzes the posttranslational modification of proteins by O-GlcNAc and is regulated by nutrient access. Here we show that acute deletion of OGT from αCaMKII-positive neurons in adult mice caused obesity due to overeating. The hyperphagia derived from the paraventricular nucleus (PVN) of the hypothalamus where loss of OGT was associated with impaired satiety. These results identify O-GlcNAcylation in αCaMKII neurons of the PVN as a novel molecular mechanism that regulates feeding behavior.

2.2 Results and Discussion

Obesity is a major contributor to disease throughout the world (163). Currently, there is no successful and available treatment for the majority of obese patients. One of the genes most commonly linked to human obesity, *Gnpda2*, affects flux through the hexosamine biosynthesis pathway (HBP) (176-178). The HBP produces uridine-diphosphate:N-acetylglucosamine (UDP-GlcNAc), which is the donor substrate for the enzyme O-

GlcNAc transferase (OGT). OGT cleaves UDP-GlcNAc and covalently attaches GlcNAc to the hydroxyl group of serine or threonine in nuclear and cytoplasmic proteins in β-linkage (O-GlcNAc). Nutrient access directly via the HBP and metabolic hormones such as insulin regulate the activity of OGT (2, 58). Like many other human obesity genes, *Gnpda2* is believed to act mainly in the brain (176, 177). Although OGT has been shown to be important for neuronal development, the role of OGT for mature brain function is almost completely unknown (6, 8, 179). To study the function of OGT in normal behavior we created conditional OGT knock out (KO) mice by crossing floxed OGT mice (OGT^{Fl}) with mice expressing a tamoxifen-inducible version of Cre recombinase under the αCaMKII promoter (αCaMKII-$CreER^{T2}$). This cross enables acute brain-specific deletion of OGT in αCaMKII-expressing neurons in adult mice, which we confirmed by immunohistochemistry, Western blotting and PCR (Fig. 2.S1). It has been reported previously that KO of OGT leads to lower cell number, probably due to impaired mitosis and in fact constitutive KO of OGT leads to early embryonic lethality (6, 40, 95, 110). In contrast, in postmitotic neurons, deletion of OGT did not affect cell number *in vitro* or *in vivo* (Fig. 2.S2A-B).

Acute and brain-specific loss of OGT in adult mice caused rapid weight gain (Fig. 2.1A-B, 2.S3A-B). Within three weeks the amount of adipose tissue tripled whereas the lean weight had not changed as quantified by whole-body nuclear magnetic resonance (NMR) (fat mass: Wt n=7, 2.5 +/- 0.21 g; KO n=6, 8.3 +/- 0.86 g, Fig. 2.S3C-D). Measuring the increase of adipose tissue intra-abdominally, subcutaneously, and in the liver showed that the incorporation of fat was general and not particular to any specific body region (Fig. 2.S3E-G). Obesity can result from either excessive caloric intake or

insufficient energy expenditure. Daily food intake rapidly increased upon KO of OGT and plateaued at a level more than twice as high (Fig. 2.1C). If access to food was restricted to the same amount consumed by wildtype (Wt) mice (pair-feeding), the KOs retained normal body weight. When free access to food was re-introduced, the KOs quickly approached the weight of KO littermates who had been fed *ad libitum* throughout the experiment (Fig. 2.1D). In order to quantify food intake and energy expenditure simultaneously in real-time, we took advantage of comprehensive laboratory animal monitoring system (CLAMS). CLAMS confirmed that loss of OGT leads to hyperphagia (Fig. 2.S3H). Energy expenditure was actually increased, which is inconsistent with changes in energy expenditure contributing to the weight gain (Fig. 2.S3I). The accelerated energy expenditure resulted from, at least in part, hyperactivity (Fig. 2.S3J). As expected from a combination of hyperphagia and hyperactivity, knocking out OGT caused higher vO_2 and vCO_2 leading to a respiratory exchange ratio (RER) above 1 (Wt n=17, 0.94 +/- 0.004; KO n=20, 1.04 +/- 0.007, Fig. 2.S3K-M).

Daily food intake is a factor of both the size of each meal and meal frequency. A normal diurnal rhythm was preserved in OGT KOs where physical activity and food intake showed clear preference for dark hours in both Wts and KOs (Fig. 2.1E, 2.S4A-B). While there was no difference in meal frequency, loss of OGT increased meal size as well as meal duration (meal size: Wt n=268, 0.25 +/- 0.02 g; KO n=330, 0.42 +/- 0.02 g, Fig. 2.1E, 2.S4C-E). The point at which a meal is terminated depends on the total caloric content of the food but also non-caloric determinants of the food, mainly its volume and composition. When fed either regular carbohydrate-rich pellets or fat-based food paste with higher caloric density, the OGT KOs overate the same amount of calories (Fig.

2.S4F). This indicates that the hyperphagia did not correlate with the composition of the food or its volume but only with its total caloric content. Our observations suggest that OGT-dependent hyperphagia is caused by impaired meal termination due to uncoupling of caloric intake from caloric need.

Immunohistochemistry for OGT showed that within the core feeding circuitry, the major loss of OGT in the KO mice occurred in medial nuclei of the hypothalamus, most notably in the paraventricular nucleus (PVN) (Fig. 2.2A, 2.S5A). There was only minor loss of OGT from nuclei of the midbrain and the brainstem (Fig. 2.2A, 2.S5A). Taking advantage of αCaMKII-CreER^{+} x TdT^{Fl} mice and immunohistochemistry, we noticed that some αCaMKII PVN cells expressed thyroid-releasing hormone (TRH) and some Oxytocin (Fig. 2.S6A). Before any major weight gain, OGT deletion reduced the expression of TRH, as determined by *in situ* hybridization, in a subpopulation of cells in the PVN without affecting their viability, whereas several other known neuropeptides regulating feeding behavior were largely unaltered; proopiomelanocortin (POMC), cocaine and amphetamine regulated transcript (CART), orexin, agouti-related peptide (AgRP), neuropeptide Y (NPY), vasopressin (AVP) and oxytocin (TRH: Wt n=4, 40 +/- 4.1 cells / 150 x 10^3 μm^2; KO n=4, 23 +/- 2.9 cells / 150 x 10^3 μm^2, Fig. 2.2B, 2.S6B-E, 2.S7A) (165, 180). Next, we infected hypothalamic organotypic cultures with a virus that expresses GFP under the αCaMKII promoter and treated the explants with varying concentrations of glucose. The PVN retained its normal morphology and expression of neuropeptide during the extent of the experiment (about 2.5 weeks, Fig. 2.S8A). Immunohistochemistry for O-GlcNAc demonstrated that 1 h treatment with 5 mM glucose, simulating physiological and meal-derived fluctuations in glucose, increased O-

GlcNAc in αCaMKII-positive cells (1 mM n=360, 134 +/- 10 intensity / cell (a.u.); 5 mM n=330, 211 +/- 12 intensity / cell (a.u.), Fig. 2.2C) (181-183). In contrast, there was no change in O-GlcNAc levels in neighboring αCaMKII-negative cells (Fig. 2.S8B). Incubation for 16 hours with 25 mM glucose raised the O-GlcNAc levels in αCaMKII cells to a larger extent (5 mM n=390, 156 +/- 9 intensity / cell (a.u.), 25 mM n=375, 298 +/- 14 intensity / cell (a.u.), Fig. 2.S8C-D). Unlike cortex and the hippocampus where O-GlcNAc levels mirror food intake it has recently been reported that fasting increased O-GlcNAc in AgRP neurons, which has been proposed to be due to stimulation of OGT expression by ghrelin in these cells (58, 179, 182). In the PVN, fasting decreased O-GlcNAc, but only in αCaMKII-positive cells (αCaMKII-positive cells: fed n=455, 158 +/- 5 intensity / cell (a.u.); starved n=259, 81 +/- 6 intensity / cell (a.u.), Fig. 2.S8E). In addition, we compared the expression of the immediate early gene c-Fos in αCaMKII PVN cells *in vivo* in mice fed *ad libitum* or refed upon starvation. This enables us to characterize cellular responses to food intake as mice start eating after a period of starvation. We found that food intake appeared to activate αCaMKII cells in the PVN and that loss of OGT blocked this activation completely (Fig. 2.S8F-G). Thus, within the PVN, OGT activity is directly sensitive to fluctuations in energy availability in αCaMKII neurons and may be crucial for their normal response to food intake.

O-GlcNAc is highly expressed in neuronal synapses in the brain (3). We crossed αCaMKII-CreER^{+} x OGT$^{Fl/Wt}$ x TdT^{Fl} mice to assess whether OGT regulates excitatory synaptic input onto αCaMKII PVN cells using whole-cell patch-clamp techniques. If deleting OGT attenuates excitatory input, it would explain, at least in part, how OGT regulates the activity of these cells. The mean capacitance of labeled cells averaged

around 15pF and did not differ between Wts and KOs (Fig. 2.S9A). The mean miniature EPSC (mEPSC) frequency was more than three-fold lower in OGT KO cells (Wt n=6, 1.7 +/- 0.11 Hz; KO n=6, 0.50 +/- 0.10 Hz, Fig. 2.3A-B). The mean mEPSC amplitude was also decreased but to a much smaller degree (Wt n=6, 19.7 +/- 1.16 pA; KO n=6, 15.6 +/- 0.867 pA, Fig. 2.3A, 2.3C). Waveform analysis showed that neither the rise time nor the decay time of the EPSCs changed upon deleting OGT (Fig. 2.S9B-C). Pharmacological inhibition of glutamatergic signaling in the PVN has been shown previously to elicit intense feeding (*18*). The sharp decrease in mEPSC frequency suggests that OGT is essential for maintaining the number of functional excitatory synapses onto αCaMKII PVN neurons.

Selectively deleting OGT in the αCaMKII cells of the PVN by stereotactic virus injection caused concurrent obesity and hyperphagia (Fig. 2.4A-C, 2.S9D). As deletion of OGT in αCaMKII cells in the PVN prevents their feeding-induced activation and leads to hyperphagia, we predicted that stimulating those cells would decrease food intake. Activating αCaMKII PVN cells optogenetically decreased cumulative food consumption over 24 h (baseline n=11, 3.6 +/- 0.14 g; 50 Hz n=11, 2.6 +/- 0.33 g, Fig. 2.4D-E) (184). Consistent with OGT's regulation of meal size, the main change in food intake came from smaller amounts of food ingested per meal while there was no significant effect on meal frequency (meal size: baseline n=125, 0.25 +/- 0.014 g; 50 Hz n=110, 0.20 +/- 0.014 g, Fig. 2.4F, 2.S9E). In a second experiment, we started the stimulation at the onset of darkness after fasting the mice during the light phase to assay whether activation of these cells is able to override hunger-induced feeding. Fasting increased food intake and 20 Hz optogenetic stimulation for 4 hours produced a significant decrease in food intake, while

50 Hz stimulation for 1 or 4 hours produced large significant drops in feeding (Fig. 2.S9F). The decrease in meal size with 50 Hz stimulation was evident in the first meal without any change in latency to initiation of feeding (Fig. 2.S9G-H).

Together, our data favor a model where the function of OGT is to couple energy intake with energy need, at least in part, by regulating the excitatory synaptic input in αCaMKII PVN cells (Fig. 2.4G). The select effect on meal termination suggests that OGT regulates satiation. αCaMKII neurons are often excitatory. Although vGlut2-positive excitatory neurons in the PVN decrease food intake, there appears to be only partial overlap between αCaMKII and vGlut2 expression in the PVN (185, 186). As glucose remains elevated in the cerebrospinal fluid more than 1 h upon eating, the feeding-related changes in O-GlcNAc integrates nutrient availability on a time scale longer than a single meal (181, 187). The brain promotes satiation by coordinating adipokines reflecting body energy depots and acute food-derived signals into circuits that turn off feeding. Rather than constituting a link in meal-to-meal satiety feedback loops, our observations suggest that OGT controls the threshold of such loops through its regulation of excitatory synaptic transmission onto αCaMKII PVN neurons. The observation that OGT KOs quickly reached a plateau in daily food intake supports this idea. Thresholding satiation between meals confers the behavioral advantage of stabilizing caloric intake over time such that the previous meal informs on the caloric need of the next. These data do not exclude additional, faster regulation of OGT activity and levels via metabolic hormones. In conclusion, the findings of this paper identify the regulation of excitatory synapses onto αCaMKII PVN neurons by OGT as a novel mechanism underlying satiation, representing a new medicinal target for human obesity

Figure 2.1

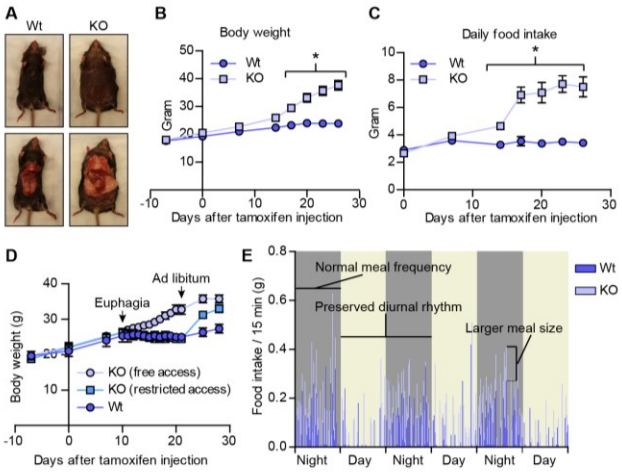

Fig. 2.1. Acute deletion of OGT in αCaMKII-positive neurons causes hyperphagia-dependent obesity. (A) Photo of mice four weeks after OGT deletion. (B) Body weight time course (Wt n=8, KO n=8; repeated-measures two-way ANOVA with *post hoc* Bonferroni test: $P<0.05$). (C) Daily food intake time course (Wt n=6, KO n=6; repeated-measures two-way ANOVA with *post hoc* Bonferroni test: $P<0.05$). (D) Body weight time course upon pair-feeding (free n=4, restricted n=4, Wt n=3). (E) Food intake every 15 minutes from sample mice. Quantifications represent mean +/- s.e.m.

Figure 2.2

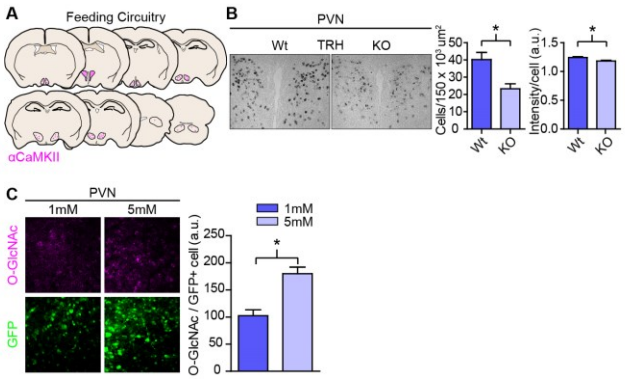

Fig. 2.2. OGT-mediated hyperphagia is associated with feeding circuitry function in the PVN. (A) αCaMKII expression within feeding circuitry (schematized from Fig. S5A). (B) TRH expression. Left; image of probe staining, right; quantification (Wt n=4, KO n=4; two-tailed *t*-test: $P<0.05$). (C) Left; GFP and O-GlcNAc in the PVN. Right; quantification of O-GlcNAc intensity in GFP-positive cells (1 mM n=240, 5 mM n=270; two-tailed *t*-test: $P<0.05$). Quantifications represent mean +/- s.e.m.

Figure 2.3

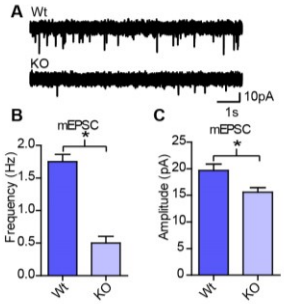

Fig. 2.3. OGT regulates excitatory synaptic function in αCaMKII PVN neurons. (A) Sample traces from Wt and KO cells. (B-C) mEPSC frequency (B) and amplitude (C) in αCaMKII-positive PVN neurons (Wt n=6, KO n=6; two-tailed *t*-test: $P<0.05$). Quantifications represent mean +/- s.e.m.

Figure 2.4

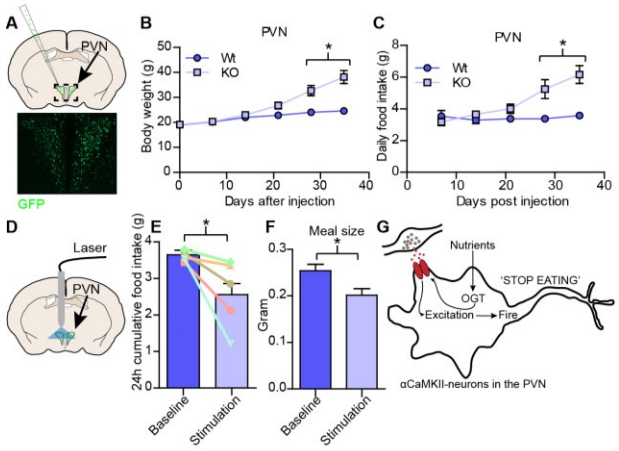

Fig. 2.4. OGT regulates feeding behavior in αCaMKII neurons of the PVN. (A) Top; schematic of stereotactic PVN injection. Bottom; GFP expression in the PVN after stereotactic injection. (B-C) Body weight (B) and daily food intake (C) time course (Wt n=5, KO n=7; repeated-measures two-way ANOVA with *post hoc* Bonferroni test: $P<0.05$). (D) Schematic of optogenetic setup with αCaMKII-driven expression of channelrhodopsin-2 in the PVN with the abutting laser. (**E-F**) Food intake after optogenetic stimulation. (E) 24 h cumulative food intake. Bars represent average intake over all mice and lines represent average intake per individual mouse. (baseline n=11, stimulation n=11; two-tailed *t*-test: $P<0.05$). (F) Average meal size (baseline n=125, stimulation n=110; two-tailed *t*-test: $P<0.05$). (G) Model of OGT-dependent hyperphagia. Quantifications represent mean +/- s.e.m.

Figure 2.S1

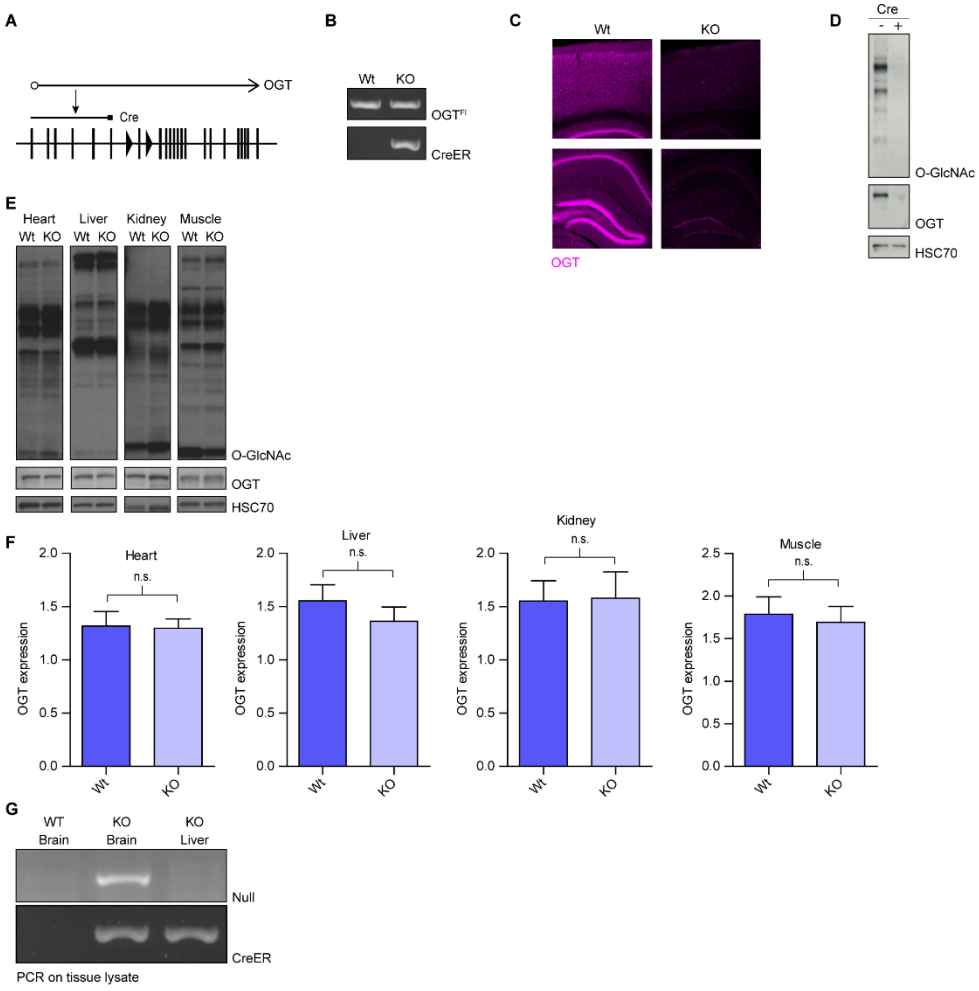

Fig. 2.S1. αCaMKII-CreER x OGT^{Fl} deletes OGT in αCaMKII-positive neurons of adult mice but does not affect OGT expression in peripheral organs. (A) Schematic of the *Ogt* locus, including loxP sites (triangles) in OGT^{Fl} mice and translational start site (empty circle). (B) PCR analysis showing the genotype of Wt (αCaMKII-CreER^{-} x OGT^{Fl}) and KO (αCaMKII-CreER^{+} x OGT^{Fl}) mice. (C) Immunohistochemistry for OGT. Top: neocortex. Bottom: the hippocampus. (D) Primary cultured OGT^{Fl} neurons were infected with either a wildtype (Wt) virus or a virus expressing Cre recombinase (KO).

Western blot characterizing the O-GlcNAc and OGT expression in Wt and KO neurons. (E) Western blot characterizing O-GlcNAc and OGT expression in peripheral tissues. (F) Quantification of OGT expression in peripheral tissues from (E) (Wt n=7, KO n=8; two-tailed *t*-test: $P<0.05$). (G) PCR analysis detecting Cre-dependent *Ogt* recombination in the brain but not in the liver. Quantifications represent mean +/- s.e.m.

Figure 2.S2

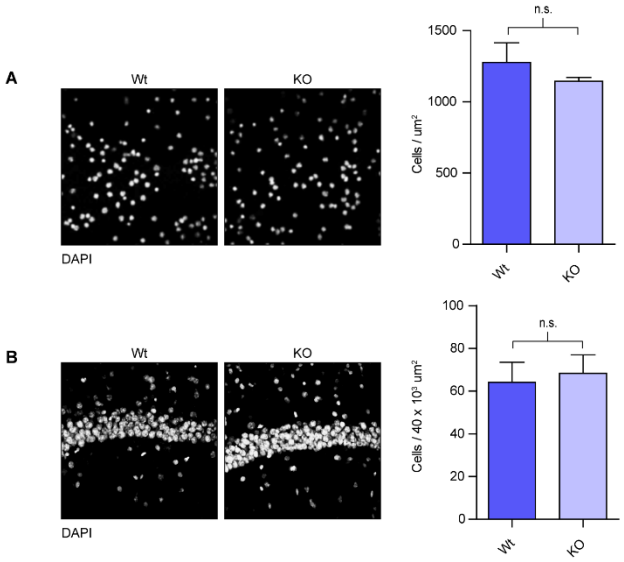

Fig. 2.S2. Deletion of OGT in postmitotic neurons does not affect cell number. (A) Left: DAPI stain of primary cultured neurons that were infected with either a wildtype virus (Wt) or a virus expressing Cre recombinase (KO). Right: quantification of DAPI stained cells (Wt n=3, KO n=3; two-tailed *t*-test: $P<0.05$). (B) Left: DAPI stain of the CA1 region of the hippocampus, where almost all cells express αCaMKII. Right: quantification of DAPI stained cells (Wt n=3, KO n=3; two-tailed *t*-test: $P<0.05$). Quantifications represent mean +/- s.e.m.

Figure 2.S3

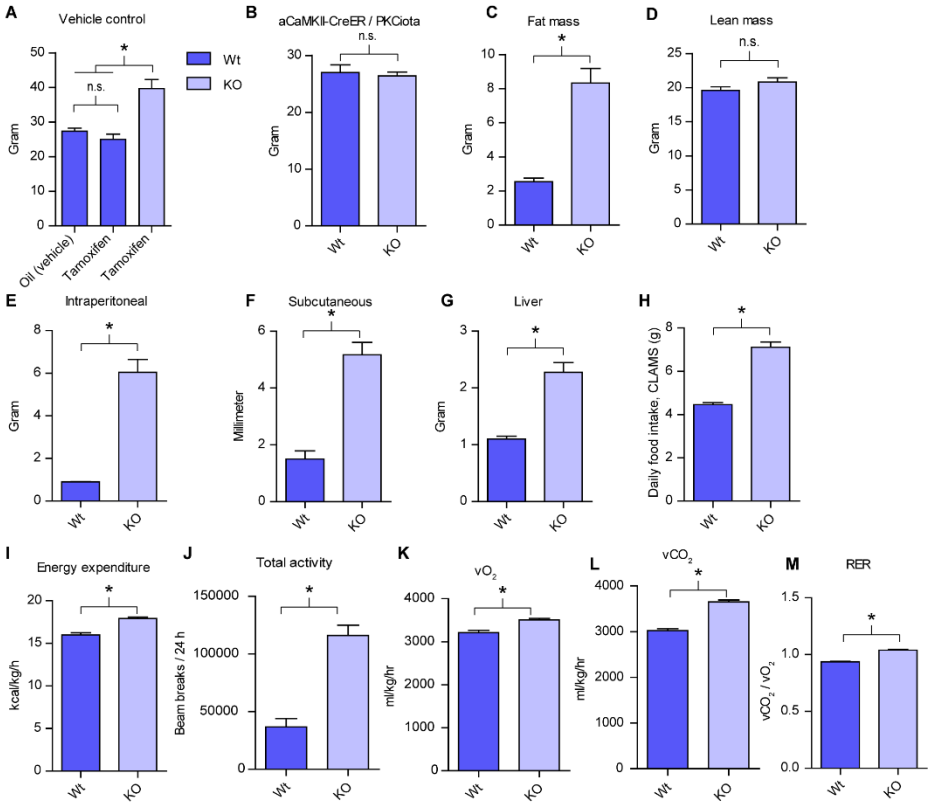

Fig. 2.S3. Loss of OGT leads to adiposity, hyperphagia and hyperactivity. (A-B) Induction of Cre recombinase by tamoxifen treatment leads to weight gain only in the presence of floxed *Ogt*. (A) Quantification of body weight; tamoxifen treatment alone does not affect body weight (n=3 for all groups; one-way ANOVA with *post hoc* Tukey's Multiple Comparison Test: $P<0.05$). (B) Quantification of body weight; αCaMKII-CreER crossed with an unrelated floxed mouse and treated with tamoxifen does not affect body weight (Wt n=5, KO n=5; two-tailed *t*-test: $P<0.05$). (C-D) Quantitative NMR of total body fat (C) and total lean body mass (D) (Wt n=7, KO n=6; two-tailed *t*-test:

P<0.05). (E-G) Quantification of amount fat in different regions the body. (E) Intraperitoneal fat. (F) Subcutaneous fat. (G) Total liver weight. (For all regions: Wt n=3, KO n=3; two-tailed *t*-test: *P*<0.05). (H-M): Data from CLAMS analysis; (H) Daily food intake. (I) Total energy expenditure as measured by exchange of respiratory gases, see Methods. (J) Physical activity. (K) Volume O_2 inhaled. (L) Volume CO_2 exhaled. (M) The respiratory exchange ratio (RER). (H-M: Wt n=17, KO n=20; two-tailed *t*-test: *P*<0.05). Quantifications represent mean +/- s.e.m.

Figure 2.S4

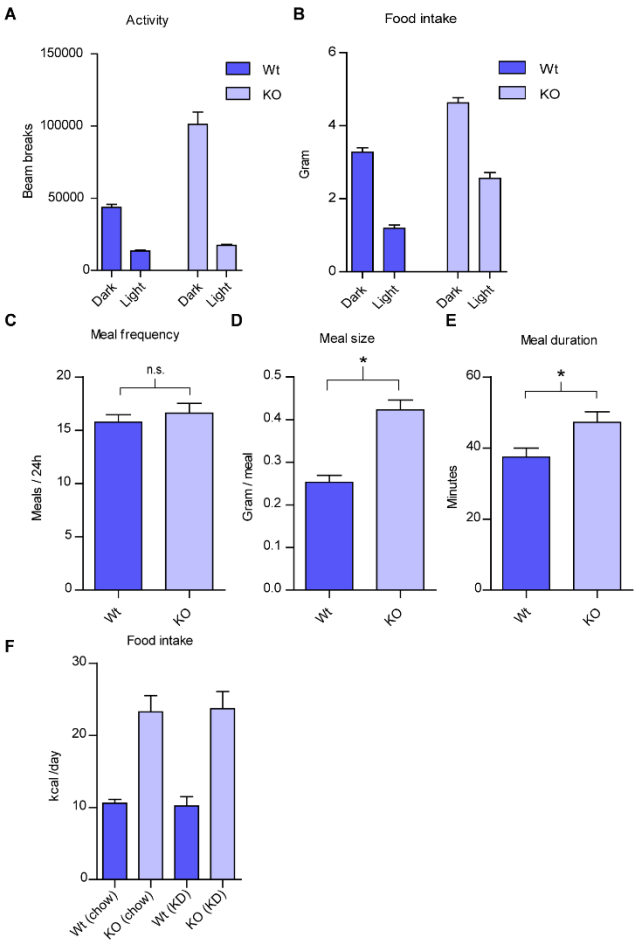

Fig. 2.S4. Diurnal rhythm and meal frequency are not perturbed in OGT KO mice while meal size and duration are increased. The OGT-dependent hyperphagia correlates with total caloric intake. (A) Quantification of total activity during CLAMS as dispersed over dark and light hours (Wt n=21, KO n=21; two-tailed *t*-test: $P<0.05$). (B) Quantification of food intake during CLAMS as dispersed over dark and light hours (Wt n=17, KO n=20; two-tailed *t*-test: $P<0.05$). (C) Quantification of the number of initiated meals during CLAMS (Wt n=17, KO n=20; two-tailed *t*-test: $P<0.05$). (D-E)

Quantification of meal size (D) and meal length (E) during CLAMS (Wt n=268, KO n=330; two-tailed *t*-test: $P<0.05$). (F) Quantification of food intake as it differs between carbohydrate-based pellets and fat-based paste (KD). (Chow (3.1 kcal/g): Wt n=10, KO n=10; KD (6.7 kcal/g): Wt n=7, KO n=5). Quantifications represent mean +/- s.e.m.

Figure 2.S5

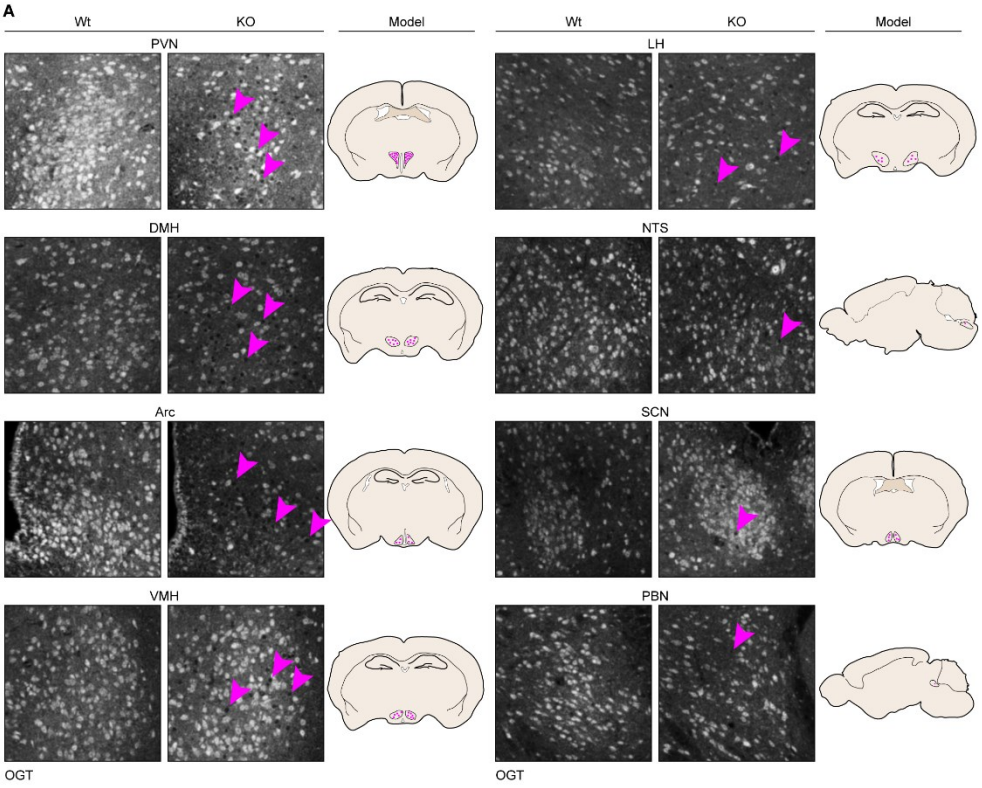

Fig. 2.S5. αCaMKII-CreER x OGT^{Fl} deletes OGT from several core feeding nuclei. (A) For each panel: left; immunohistochemistry for OGT in αCaMKII-CreER x OGT^{Fl} mice. Arrowheads indicate cells that lack OGT. Right; schematics showing general anatomical landmarks for slices that were used for imaging. The areas within each slice containing purple dots were the areas that were imaged and used for analysis. Purple dots within the schematics indicate cells that lost OGT in KO mice. Abbreviations used: Paraventricular nucleus (PVN), Dorsomedial hypothalamic nucleus (DMH), Arcuate

nucleus (Arc), Ventromedial hypothalamus (VMH), Lateral hypothalamus (LH), Nucleus of the solitary tract (NTS), Parabrachial nucleus (PBN).

Figure 2.S6

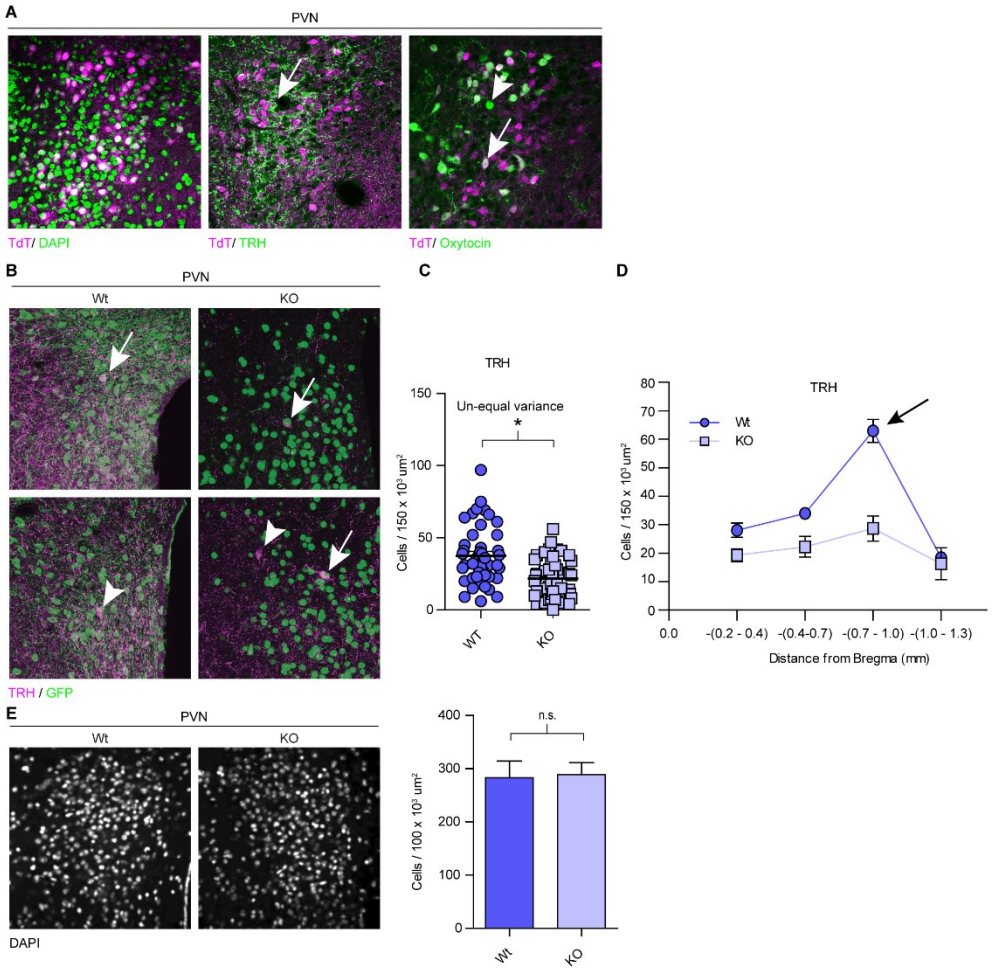

Fig. 2.S6. αCaMKII-CreER x OGT^{Fl} deletes OGT from a subpopulation of cells in the PVN with no effect on total cell number in the PVN. (A) αCaMKII-positive cells (purple) were labeled using αCaMKII-CreER^{+} x TdT^{Fl} mice. Left: DAPI (green). Middle: immunohistochemistry for TRH (green). Right: immunohistochemistry for Oxytocin (green). Arrow; cell positive for both the cell-specific marker and TdT. Arrowhead; cell positive for the cell-specific marker but not TdT. (B) Double-labeling of TRH cells and αCaMKII cells. The PVN was injected stereotactically with Wt or KO virus. TRH cells

were labeled with immunohistochemistry for TRH (purple) and αCaMKII cells with virus expressing GFP under the αCaMKII promoter (green). Arrow; cell positive for both TRH and GFP. Arrowhead; cell positive for TRH but not GFP. (C) Serial sections of the PVN were cut and subjected to *in situ* hybridization for TRH as shown in Fig. 2B. Shown is the quantification of the number of TRH positive cells per PVN slice. The distribution of TRH cells in Wts and KOs showed statistical un-equal variance, indicating that a particular subpopulation of TRH cells is affected by OGT deletion (Wt n=45, KO n=48; F-test: $P<0.05$). (D) The same data as in (C) but plotted is the number of TRH positive cells per PVN slice in relation to distance from Bregma. (E) Left: DAPI stain of the PVN. Right: quantification of DAPI stained cells (Wt n=3, KO n=3; two-tailed t-test: $P<0.05$). Quantifications represent mean +/- s.e.m.

Figure 2.S7

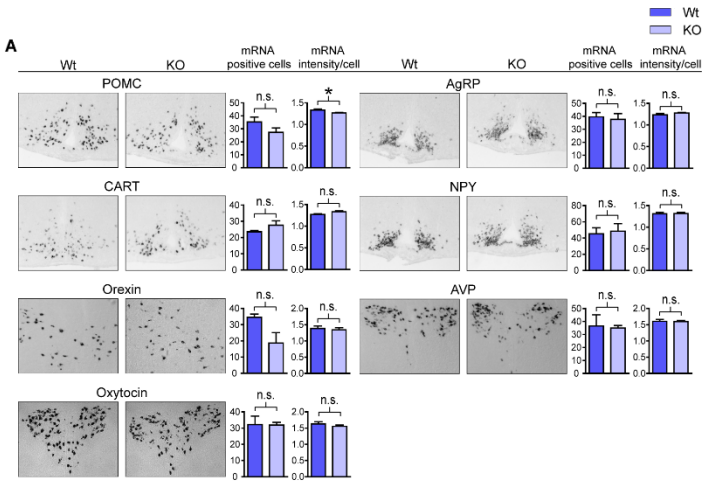

Fig. 2.S7. Deletion of OGT in αCaMKII-positive neurons leaves several major feeding circuits intact. (A) *In situ* hybridization for neuropeptide modulators in core feeding circuits two weeks after OGT KO prior to significant weight increase. For each peptide: left; image of probe staining, right; quantification of number of stained cells within the respective area (cells / 150 x 10^3 μm^2) and quantification of intensity of staining per cell (a.u.) (Wt n=4 (except for CART, and number of oxytocin positive cells, where n=3), KO n=4; two-tailed *t*-test: $P<0.05$). Quantifications represent mean +/- s.e.m.

Figure 2.S8

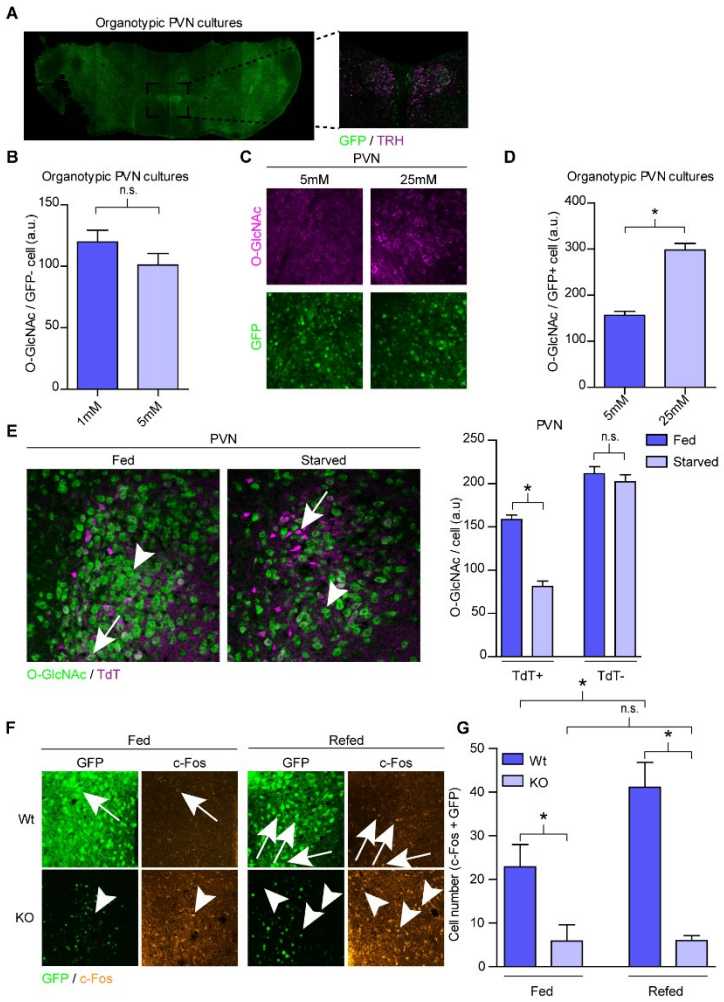

Fig. 2.S8. αCaMKII-positive PVN neurons are uniquely sensitive to physiological variations in glucose in terms of O-GlcNAc and deletion of OGT blunts feeding-induced activation of the same cells. (A-D) Hypothalamic explant with GFP expression (green) and immunohistochemistry for TRH (A) or O-GlcNAc (C) (purple). Boxed magnification in (A) shows the PVN. (B) Quantification of O-GlcNAc intensity in αCaMKII-negative cells in the PVN from Fig. 2C (1 mM n=360, 5 mM n=330; two-

tailed t-test: $P<0.05$). (D) Quantification of O-GlcNAc intensity in αCaMKII-positive cells in the PVN from (C) (5 mM n=390, 25 mM n=375; two-tailed t-test: $P<0.05$). (E) O-GlcNAc expression in the PVN in fed and starved animals (αCaMKII-CreER^{+} x TdT^{Fl} mice). Left; double-labeling of TdT expression (purple) and immunohistochemistry for O-GlcNAc (green). Arrow; cell positive for TdT. Arrowhead; cell negative for TdT. Right; quantification of O-GlcNAc expression in TdT-positive and TdT-negative cells (TdT-positive: fed n=455, starved n=259. TdT-negative: fed n=357, starved n=375; two-tailed t-test: $P<0.05$). (F) The PVN was injected stereotactically with Wt or KO virus. Double-labeling of GFP expression (green) and c-Fos (orange) in the PVN in fed and refed animals. Arrow; cell positive for both c-Fos and GFP. Arrowhead; cell positive for c-Fos but not GFP. (G) Quantification of number of cells expressing both GFP and c-Fos from (F) (Fed: Wt n=8, KO n=7. Refed: Wt n=12, KO n=10; two-tailed t-test: $P<0.05$). Quantifications represent mean +/- s.e.m.

Figure 2.S9

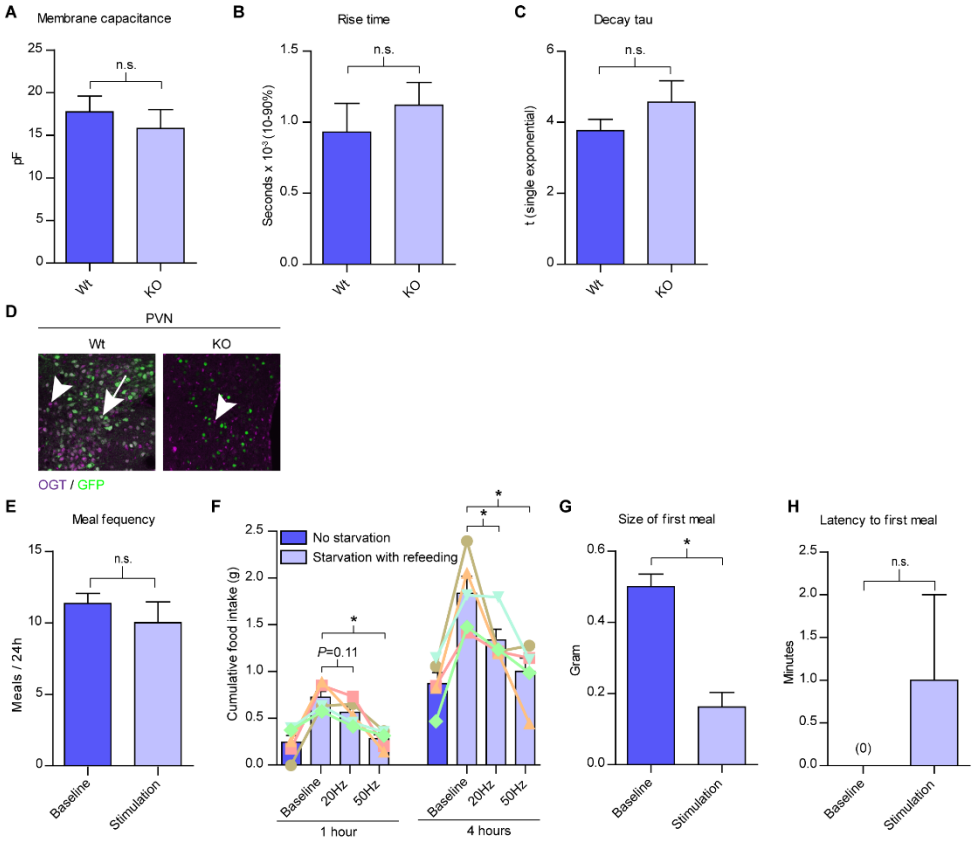

Fig. 2.S9. OGT KO does not affect membrane capacitance or EPSC shape in αCaMKII-positive cells in the PVN and optogenetic stimulation of the same cells decreases food intake. (A-C) Patch-clamp analysis of αCaMKII-positive cells in the PVN (Wt n=6, KO n=6; two-tailed t-test: $P<0.05$). (A) Membrane capacitance. (B) mEPSC peak rise time. (C) mEPSC peak decay tau. (D) GFP expression (green) and immunohistochemistry for OGT (purple) in the PVN after stereotactic injection of Wt or KO virus. Arrow; cell positive for OGT and GFP. Arrowhead; cell positive for OGT only. (E-H) Optogenetic stimulation of αCaMKII-positive cells in the PVN. (E)

Quantification of meal frequency (baseline n=11, stimulation n=11; two-tailed t-test: $P<0.05$). (F) Quantification of food intake after a light fast. Bars represent average intake over all mice and lines represent average intake per individual mouse (All conditions n=5; two-tailed t-test: '*' refers to $P<0.05$). (G) Quantification of the size of the first meal after a light fast, 50 Hz stimulation (baseline n=5, stimulation n=5; two-tailed t-test: $P<0.05$). (H) Quantification of the latency to the initiation of the first meal after a light fast, 50 Hz stimulation (baseline n=5, stimulation n=5; two-tailed t-test: $P<0.05$). Quantifications represent mean +/- s.e.m.

2.3 Materials and Methods

Animals

OGT^{Fl} and αCaMKII-$CreER^{T2}$ mice have been derived previously(6, 188). They were fully backcrossed (>N11) to the C57BL6 background. Only males were used and they were about 6 weeks old at the start of experiments. Tamoxifen was injected accordingly: 2mg twice per day for 5 days (20mg total dose). Control mice were either vehicle (sunflower seed oil injected into OGT^{Fl} x αCaMKII-$CreER^{+}$ mice) or genetic (tamoxifen injected into OGT^{Fl} x αCaMKII-$CreER^{-}$) controls. No difference between controls was seen. Therefore, all control animals were combined. Mice were fed standard chow (Teklad Global 2018SX: 24% protein, 18% fat, 58% carbohydrate) and had free access to food unless otherwise specified. Only littermates were compared. Apart from noted exceptions, the animals were kept on a 14 h/10 h light/dark cycle. For all animal studies, animals where randomly allocated to experimental groups. The experimenter was aware of the animal genotype when conducting experiments. The TdT^{Fl} mice express the fluorescent reporter TdTomato upon exposure to Cre recombinase and were originally developed by the Allen Institute (Ai9). All animals were housed according with the Johns Hopkins University Animal Care and Use Committee guidelines. All details pertaining to optogenetics experiments, including animal work, are described below under Optogenetics.

Biochemistry

Primary neuronal cell culture. Cortical neurons were prepared from timed E18 embryos, as previously described (189). Lentivirus was added at DIV (days in vitro) 2. Cells were harvested for analysis at DIV 11-13.

Western blot. Cultured cells were harvested in RIPA buffer (50mM tris, 150mM sodium chloride, 1% NP-40, 1% deoxycholate, 0.1% SDS, 1mM EDTA, including inhibitors for proteases, phosphatases and O-GlcNAcases), solubilized for 20 min at 4°C and then spun at 13000 rpm. The supernatant was used for further analysis. When tissue was analyzed, unless otherwise noted, after removal from the animal, it was homogenized in homogenization buffer (HB; 0.32M sucrose, 10mM HEPES, including inhibitors for proteases, phosphatases and O-GlcNAcases). 2X RIPA was then added to a final concentration of 1X RIPA for solubilization at 4°C for 20 min, before spun at 13000 rpm. Clear lysate, with top lipid layer discarded, was used for further analysis. Note that the muscle indicated in Fig. 2.S1A is *musculus femoris*. Western blotting was performed according to standard procedures. Briefly, after separation by SDS-PAGE and transfer to polyvinylidene fluoride (PVDF) membranes, membranes were blocked in 3% bovine serum albumin (BSA), or 5% bovine milk when blotting for O-GlcNAc, and then probed with the following antibodies: OGT (AL25, produced in-house, 1:5000), O-GlcNAc (CTD110.6, produced in-house, 1:10000), HSC70 (Santa Cruz Biotechnology, sc7298, 1:5000).

Virus

For cell culture experiments, lentivirus was used. VSVG pseudotyped lentiviral particles were produced by standard procedures. In short, a FUGW vector expressing enhanced (eGFP) alone (Wt) or eGFP and Cre recombinase (KO) together with cDNA plasmids VSVG and delta 8.9 were transfected into HEK 293T cells using Lipofectamine (*25*). The culture supernatant was collected 24 h and 48 h after transfection, then subjected to ultracentrifugation where the resulting pellet was resuspended in Neurobasal

medium. For viral infections *in vivo*, adeno-associated virus (AAV) was used. All AAV were of serotype 2.1 and purchased from University of Pennsylvania Vector Core: For Wt; #AV-1-PV1917 (AAV1.CaMKII0.4.eGFP.WPRE.rBG) and for KO; #AV-1-PV2521 (AAV1.CaMKII.HI.eGFP-Cre.WPRE.SV40). All details pertaining to optogenetics experiments are described below under Optogenetics.

Histology

Immunohistochemistry. Animals were anesthetized with avertin (0.03ml/g) and then perfused with 4% paraformaldehyde (PFA) in phosphate-buffered saline (PBS). The brain was removed and post-fixed in 4% PFA/PBS overnight. After the brain had been equilibrated in 30% sucrose/PBS, it was frozen and serial sections (25 μm) were cut on a microtome (Leica, SM2000R). Free-floating sections were blocked in IHC buffer (5-10% normal goat serum diluted in 0.25% triton X-100/PBS) overnight at 4°C, incubated with the primary antibody overnight at 4°C and then with the secondary antibody either for 2 hours in room temp or overnight at 4°C. DAPI was included with the secondary antibody. Washes after the primary and secondary antibody were done in 0.25% triton X-100/PBS and antibodies were diluted in IHC buffer. Primary antibodies used were OGT (AL25 (produced in-house), 1:5000), TRH (Santa Cruz Biotechnology, 1:100), c-Fos (ABE457, Millipore, 1:500), Oxytocin (MAB5296, Millipore, 1:1000), GFP (Abcam, 1:1000), in Figs. 2.4 and 2.S9 the signal from virally expressed GFP alone was imaged without using an antibody against GFP. For some experiments when staining for OGT alone, the animal was not perfused but fixed in 4% PFA/PBS overnight.

In situ hybridization. The brain was removed and fresh frozen in OCT (Tissue-Tek) and stored at -80°C. Serial sections were cut (25 μm) on a cryostat (Leica CM3050-S)

and stored at -80°C. Probes and hybridization protocol have been described at length previously (190, 191). Briefly, slides were fixed in 4% PFA, treated with acetic anhydride and then blocked in pre-hybridization solution (hybridization buffer without probes added: 50% formamide, 5X saline sodium citrate (SSC), 5X Denhardt's solution (Bioworld), 250ug/ml yeast tRNA, 500ug/ml sperm DNA) before application of respective probe diluted in hybridization buffer. Hybridization was done at 70°C overnight. The next day the slides were washed, re-blocked (0.1M Tris, pH 7.5, 0.15M sodium chloride, 5% sheep serum) and then incubated overnight at 4°C with an alkaline-phosphatase linked anti-digoxigenin antibody (Roche, 1:5000) diluted in blocking buffer. On the third day probes were developed after washing. Probe development was done by applying a mix of NBT (nitro-blue tetrazolium chloride), BCIP (5-bromo-4-chloro-3'-indolyphosphate p-toluidine salt) and levamisole until sufficient stain had precipitated (within the same probe, all slides were treated for the same length of time). Afterwards, slides were DAPI stained.

Brain region coordinates. Different brain regions were identified by taking advantage of the Paxinos and Franklin atlas (The Mouse Brain, in stereotaxic coordinates, second edition). Counted as distance from Bregma, the following coordinates were used: SCN (-0.34 to -0.82), PVN (-0.60 to -1.20), Arc (-1.46 to -2.20). VMH (-1.30 to -2.06), LH (-1.34 to -1.75), DMH (-1.46 to -2.06). The PBN and the NTS were identified on sagittal slices, PBN (Bregma: -5.00 to -5.45, lateral: 0.85 to 1.35), NTS (Bregma: -6.30 to -7.80, lateral: 0.36 to 0.96). Abbreviations used: Paraventricular nucleus (PVN), Dorsomedial hypothalamic nucleus (DMH), Arcuate nucleus (Arc), Ventromedial

hypothalamus (VMH), Lateral hypothalamus (LH), Nucleus of the solitary tract (NTS), Parabrachial nucleus (PBN).

Organotypic cultures

Acute coronal slices were cut from male mice around postnatal day 10 on a vibratome. The slices were cut in oxygen-bubbled dissection medium (1 mM $CaCl_2$, 5 mM $MgCl_2$, 10 mM glucose, 4 mM KCl, 26 mM $NaHCO_3$, 218 mM sucrose, 1.2 mM $NaH_2PO4(H_2O)$, 30 mM HEPES). After cutting, the dorsal half of each slice was removed and then mounted on membrane inserts in a 6 well plate (one slice per insert). Each well was filled with 1 ml slice culture media (SCM: 4.16 g/500ml MEM, 20% horse serum, 1 mM L-glutamine, 0.5 mg/500ml insulin, 2 mM $MgCl_2$, 1 mM $CaCl_2$, 3 mM glucose, 1.3 mM $NaHCO_3$, 3.58 g/500ml HEPES) and changed every 2-3 days. Explants were incubated at 35 °C. On DIV 10, virus was added by direct application on the top of each slice to label αCaMKII-positive cells (UPenn, #AV-1-PV1917 (AAV1.CaMKII0.4.eGFP.WPRE.rBG)). After about 1 week, cultures were submitted to 1 mM glucose SCM for 24 h (media changed once during those 24 h) and then changed into either fresh 1 mM or 5 mM glucose SCM for 1 h. In a second round of experiments, slices were put in 5 mM glucose SCM for 24 h and then transferred to either fresh 5 mM or 25 mM glucose SCM for 16 h. Slices were then fixed in 4% PFA in PBS for 2-7 h. The area around the fixed slices were cut out using a scalpel and then subjected to immunohistochemistry (O-GlcNAc and TRH) as described for free-floating slices.

Stereotactic virus injection

Anesthesia was induced using avertin (0.03ml/g) and thereafter kept by 1-1.5% isoflurane gas inhalation. The coordinates for the PVN were: distance from Bregma, -

0.80 mm; distance from midline, 0.20 mm; depth from surface, -4.75mm. The stereotaxic instrument used was the Leica Angle Two stereotaxic instrument. The scalp was exposed by a small incision through the skin. Bregma and Lambda were identified and two small holes drilled over the injection site. Stored virus was thawed, diluted with sterile saline to a final concentration of $1x10^9$ particles/ul and then spun for 5 min at 3000 rpm in room temperature. The virus was then loaded into a pulled glass pipette (20-40 μm) and connected to a syringe pump (WPI, sp220i). In total, 2ul virus was injected at 0.300 ul/min. After the surgery, the scalp was sutured and the animal rehydrated with saline (0.02 ml/g, intraperitoneal injection) and given buprenorphine to relieve pain (0.01 ml/g, subcutaneous injection). Upon animal harvest, the injection site and spread of the virus was controlled by immunohistochemistry. In total, 5 Wt animals and 8 KO animals were injected. In all but one case, the PVN was successfully targeted. Although there was minor spread outside the PVN, the PVN was the common denominator of areas hit across animals. In the one case when the PVN was hit only partially, the daily food intake and body weight increased but to a lesser degree, as expected (data not shown). This animal was removed from analysis. Excluding animals where the PVN had not been successfully targeted was a pre-established criterion. All details pertaining to optogenetics experiments are described below under Optogenetics.

Behavior

General feeding behavior. Animals were kept in individual cages after tamoxifen treatment or virus injection. Food intake was measured by weighing leftover food pellets. The bottom of the cage was searched to include all leftover food. For some Wt and KO tamoxifen treated animals, the animals were not separated to individual cages until two

weeks after the treatment had finished. Data from these animals were compiled with the rest as the effect on feeding behavior and body weight for all animals followed the same time course. Whereas tamoxifen treated animals were kept on a 14 h/10 h light/dark cycle, the virus injected animals were kept on a 12 h/12 h light/dark cycle.

Restricted feeding. 10 days after tamoxifen treatment, the KO animals were split into two groups. One group had continuous free access to food whereas the other group was fed 1 gram at the start of light hours and 2.5 grams at the start of dark hours, totaling 3.5 grams/day. At 21 days, free access to food was reintroduced to the latter group. Animals were kept on a 12 h/12 h light/dark cycle.

Comprehensive laboratory animal monitoring system (CLAMS). CLAMS (Columbus Instruments) is a closed chamber system that measures ventilation gases and food intake automatically. Our system was also equipped with laser beams that register physical movement. We submitted 7 Wt and 7 KO mice to CLAMS analysis two weeks after tamoxifen treatment. After several days of acclimatization, data were collected for 3 days. Data were binned in 15 min increments. Values that were the obvious result of aberrant mouse behavior or technical failure, such as spillage off the scale, were removed from analysis. There were a few small negative values recorded. These were included in the analysis, except for Fig. S.1E for which negative values were removed. The total number of beam breaks is shown as 'physical activity' in all figures. A 'meal' was defined as any multiplicative of 15 min where the amount of intake the first 15 min was 50 mg or larger and the previous 15 min had no intake registered. A meal was considered finished when no intake had been registered for another 15 min. The formulas used to

calculate different endpoints can be found at www.colinst.com. Animals were kept on a 12 h/12 h light/dark cycle.

Refeeding. For refeeding experiments in Fig. 2.S8, the food was removed for 24 h and then reintroduced for 2.5 h before animal harvest. Throughout the experiment, the animals had free access to drinking water. For the refeeding paradigm coupled with optogenetics, see Optogenetics.

Fat-based diet. Mice were fed either regular chow (3.1 kcal/g, Teklad Global 2018SX: 24% protein, 18% fat, 58% carbohydrate) or energy-dense fat-based food (6.7 kcal/g, Teklad Global TD.96355: 9.1% protein, 90.5% fat, 0.4% carbohydrate). The mice were raised on regular chow and then switched to fat-based diet either about 1 week before injected with tamoxifen or about 14 days after injections had finished. The same behavior was noticed in both regiments and the data were combined. As the data for regular chow mimicked the data in general feeding behavior experiments, all those data were combined also. The data shown are the averages during the period when daily food intake had stabilized (days 20-26 after tamoxifen injection).

Optogenetics

Animals. All experimental protocols were conducted according to U.S. National Institutes of Health guidelines for animal research and were approved by the Institutional Animal Care and Use Committee at NIDA. Male C57BL/6J mice (2–5 months old, Jackson Laboratories) were used for optogenetic experiments.

Stereotactic viral delivery and fiber guide system implantation. Mice were anesthetized with isoflurane and were placed into a stereotaxic apparatus (David Kopf Instruments), as previously described (192). A pulled glass pipette with 30-40μm tip

diameter was inserted into the brain, and one unilateral injection (30nL) of AAV2/1-CamKIIα-hChR2(H134R)-EYFP virus (titer: 3.3x1012 viral genomes/mL, Optogenetics and Transgenic Technology Core, NIDA) was made at coordinates in the paraventricular nucleus of the hypothalamus (PVN, bregma: -0.70mm, midline: +0.15mm, dorsal surface: -4.60mm). A micromanipulator (Narishige) was used to control the injection speed (30nL/min), and the pipette was withdrawn 15 min after the injection. This was followed by the insertion of a ferrule-capped optical fiber (200 μm diameter core; BFH48-200-Multimode, NA 0.48; Thorlabs) through the craniotomy. Metabond cement (C&B-METABOND Quick! Cement System, Parkell, Inc.) was used to anchor the ferrule to the skull. The fiber tip was implanted 0.7mm above the PVN. Mice were returned to their home cages for 10 – 14 days to recover and for expression of ChR2:EYFP.

Components for food consumption and photostimulation. In home cages, mice had *ad libitum* access to rodent chow (PicoLab Rodent Diet 20, 5053 tablet, TestDiet). For behavioral testing, mice were transferred into feeding cages with automatic pellet dispensers (Coulbourn Instruments) and supplied with food pellets (20 mg each) of identical composition to the food in the home cage. Pellet removal was sensed by the offset of a beam break and an additional pellet was administered after a delay (10 s). Food consumption was monitored continuously using Graphic State software (Coulbourn Instruments). Water was also available *ad libitum* during behavioral experiments, and in some cases, was monitored by optical detection (Coulbourn Instruments) of licks emitted towards the drinking spout. In addition, water bottles were manually weighed to estimate water intake every 24 hours. Mice were allowed to acclimate for 3 days before initiating the photostimulation protocols. Light was delivered to the brain through an optical fiber.

The relationship of light scattering and absorption in the brain as a function of distance has been described previously (Aravanis AM, et al., 2007). Using this relationship, the light power exiting the fiber tip (10 mW) was estimated to correspond to 2.0 mW/mm2 at the PVN, which was sufficient to drive a behavioral response. For optical delivery of light pulses with millisecond precision to multiple mice, the output beam from a 300 mW diode laser (473 nm, Opto Engine, LLC)) was split into four beams using a combination of 50/50 beam splitters and turning mirrors (Thorlabs). Each beam was controlled using an acousto-optic modulator (AOM) (Quanta Tech OPTO-ELECTRONIC) to generate light pulses that were launched into separate fiber ports (PAF-X-7, Thorlabs) and their corresponding optical fibers. Using these components, four mice could be simultaneously and independently photostimulated. LabVIEW software (National Instruments) was used control the AOMs.

Behavioral experiments. *General feeding behavior*. Food intake was recorded during a pre-stimulus (baseline) for 3 days followed by a 24 h photostimulation period. In two experiments, stimulation started during light hours and in one experiment stimulation started at the onset of darkness. In all experiments, the same behavioral response was recorded and the data were averaged over all experiments. The primary photostimulation protocol consisted of 50 light pulses (10 ms) for 1 s at 50 Hz, with the sequence repeated every 4 s for 24 h. Meals were quantified as described for CLAMS.

Hunger-induced feeding behavior. Mice were fasted for 9 hours during the light phase (with *ad libitum* access to water) before testing for evoked feeding behavior at the onset of feeding at the start of the dark phase. The primary photostimulation protocol consisted of 50 or 20 light pulses (10 ms each) which were delivered for 1 s (50 Hz or 20

Hz, respectively), and the sequence repeated every 4 seconds for 12 hours. For the no starvation control, we used the average intake during the equivalent hours over 2 days. For meals analysis, food intake was binned over 5 min. A 'meal' was defined as any multiplicative of 5 min where the amount of intake the first 5 min was 10 mg or larger and no intake had been registered prior to that period. A meal was considered finished when no intake had been registered for another 10 min.

Whole body composition analysis

Quantitative NMR to measure total fat and lean mass was done using EchoMRI. Animals were analyzed about three weeks after tamoxifen treatment.

Electrophysiology

Whole-cell patch-clamp recordings were performed to assess the excitatory synaptic function in OGT KO PVN neurons. For this, we took advantage of αCaMKII-CreER^{+} x OGT$^{Fl/Wt}$ x TdT^{Fl} mice. Acute PVN slices were prepared 17-19 days after tamoxifen injection at a similar time of day. Mice were anesthetized with isoflurane and decapitated. Brains were removed rapidly and placed in ice-cold cutting solution containing 210.3 mM sucrose, 2.5 mM KCl, 1 mM NaH_2PO_4, 26.2 mM $NaHCO_3$, 4 mM $MgCl_2$, 0.5 mM $CaCl_2$ and 11 mM D-(+)-glucose and oxygenated with 95% O_2/5% CO_2. Coronal slices (300 μm thick) were cut with a vibratome (Leica VT1200S) and were kept in ACSF (125 mM NaCl, 2.5 mM KCl, 2 mM $MgCl_2$, 2 mM $CaCl_2$, 1.0 mM NaH_2PO_4, 26.2 mM $NaHCO_3$ and 11 mM glucose, oxygenated with 95% O_2/5% CO_2) at 23–25 °C until recordings. Slices were placed in a submerged chamber and perfused with ACSF supplemented with 50 μM picrotoxin and 1 μM TTX. Targeted whole cell recordings of PVN tdTomato-positive neurons were made using pipettes of 2-5 MΩ resistance. The

intracellular solution contained 115 mM $CsMeSO_4$, 0.4 mM EGTA, 5.0 mM TEA-Cl, 1 mM QX314, 2.8 mM NaCl, 20 mM HEPES, 3.0 mM MgATP, 0.5 mM GTP and 10 mM sodium phosphocreatine (pH = 7.2 and osmolality of 285–290 mOsm). Cells were held at -70mV holding potential and recording was performed at room temperature. The junction potential was left uncorrected. Signals were measured with a MultiClamp 700B amplifier and digitized using a Digidata 1440A analog-to-digital board (Molecular Devices). Data were acquired with pClamp 10 software and digitized at 20 kHz. Cell capacitance was measured. Miniature EPSCs (mEPSCs) were analyzed with MiniAnalysis (Synaptosoft) using a detection threshold of 7 pA (>2 times root mean square noise). Decay times were obtained by single-exponential fitting of the average mEPSC traces.

Image analysis

Neuronal cell number. *In vitro*: Cell number was quantified by counting the number of DAPI stained primary cultured neurons. On each of three Wt and KO coverslips, 10 random images were taken on a confocal microscope (Zeiss, LSM 510). In ImageJ, after setting a pre-defined threshold, the number of cells was counted automatically by applying the 'Analyze particles' command. *In vivo*: Cell number was quantified by counting the number of DAPI stained cells within the CA1 region of the hippocampus and the PVN in several slices from 3 Wt and 3 KO animals (confocal microscope, Zeiss, LSM 510). All slices were matched in distance from Bregma between Wt and KO. The number of cells was counted manually in the CA1 region. For the PVN, cells were counted automatically in ImageJ as described above.

Neuropeptide transcript expression. Within the PVN, the expression of the following probes was quantified: TRH, AVP, Oxytocin. Within the arcuate nucleus, the expression

of the following probes was quantified: POMC, CART, AgRP, NPY. In the lateral hypothalamus the expression of orexin was quantified. Images for quantification were taken on a Nikon Eclipse Ti, except for orexin where an Axiophot (Zeiss) was used. Images shown in Fig. 2.2 and 2.S7 were all taken on the Axiophot (Zeiss). Animals had been harvested in the early phase when KOs had just started to develop hyperphagia without developing any major obesity (about two weeks after tamoxifen treatment). Slices from the same 4 Wt and 4 KO animals were used for all probes, except for Wt CART where slices from 3 of the animals were used. Quantification was done in ImageJ. A pre-defined region of interest (ROI) was placed over each cell. The number of cells per image and the average intensity of each cell were collected. The right and left side of each brain region were imaged separately. Data were averaged per animal. Within the same probe, all sections were matched in distance from Bregma. The investigator was blinded to whether images came from Wt or KO animals during counting.

c-Fos and OGT expression in virus-injected PVN. Prior to harvest, αCaMKII-positive cells in the PVN had been labeled with virus expressing GFP under the αCaMKII promoter by stereotaxic injection. Within the PVN, in ImageJ, all c-Fos positive cells per brain slice of the PVN were counted manually and marked as GFP-positive or GFP-negative. All sections were matched in distance from Bregma. Note that the Wt virus GFP expression was higher than the KO virus GFP expression, a result we attributed to the combined GFP and Cre recombinase expression by the KO virus while the Wt virus expressed GFP alone. Therefore, for the GFP channel in KO slices, the microscope gain was set higher to include all GFP positive cells (confocal microscope, Zeiss, LSM 510).

O-GlcNAc expression in organotypic slices and starved mice. All image analysis was done on raw, unmanipulated images in ImageJ. Cells and background were marked with a pre-defined ROI. For TdT/GFP positive cells, the ROI was placed over positive cells in the TdT/GFP channel. For TdT/GFP negative cells, cells were picked randomly in the DAPI channel and then verified as TdT/GFP negative in the TdT/GFP channel. If the ROI marked a TdT/GFP positive cell, the ROI was moved to a cell nearby. The background in each image was quantified by measuring the average intensity of three ROIs placed over cell-empty areas as judged by no DAPI signal. After placing all ROIs, the mean intensity was measured in the O-GlcNAc channel. The background value was subtracted from each cell value. The experimenter was blinded to the O-GlcNAc channel when placing the ROIs.

Image presentation. All image analysis was done on raw, unmanipulated images. For presentation purposes, most shown immunohistochemistry images and DAPI stained images were improved *post hoc*. All manipulations were applied equally within the same experiment and to Wt and KO images. The manipulations (done in Photoshop) were the following: change of Levels and Brightness/Contrast and Filtering ('Despeckle' and 'Gaussian blur' (2.0pixels)).

Statistical analysis

Statistical analyses were done using the program Prism 5. Repeated-measures two-way analysis of variance (ANOVA) analyses detected significant interaction of 'time' and 'genotype', and *post hoc* Bonferroni analyses detected statistical significance between individual time points. In Fig. 2.S3A, one-way ANOVA was applied to calculate significant interaction between all groups and then the difference between all separate

group combinations was tested *post hoc* with Tukey's Multiple Comparison Test. For *in situ* hybridization, statistical analysis compared between animals mean data averaged over all imaged slices. All Student's t-tests were two-tailed and unpaired. Star, '*', signifies $P<0.05$. All error bars represent mean +/- standard error of the mean (s.e.m.). A few animals where either some food intake or body weight value had been missed were omitted in repeated-measures two-way ANOVA analyses and post-hoc Bonferroni analyses. However, these values did not change the overall result and were included in shown graphs. The normality distribution of data used for the F-test in Fig. 2.S6C was verified using the D'Agostino-Pearson omnibus normality test.

CHAPTER 3.

OGT REGULATES EXCITATORY SYNAPSE MATURITY

Notes

Most content (e.g. text, figures and experimental results) included here is modified from work that will be submitted for publication:

1. **Lagerlöf O**, Hart GW, Huganir RL. OGT regulates excitatory synapse maturity. In preparation.

3.1 Abstract

Experience-driven synaptic plasticity is believed to underlie adaptive behavior by rearranging the way neuronal circuits process information. We have previously discovered that O-GlcNAc transferase (OGT), an enzyme that modifies protein function by attaching β-N-acetylglucosamine (GlcNAc) to serine and threonine residues of intracellular proteins (O-GlcNAc), regulates food intake through mediating excitatory synaptic function. However, how OGT affects excitatory synapse function is largely unknown. Here we demonstrate that OGT is enriched in the postsynaptic density of excitatory synapses. In the postsynaptic density, O-GlcNAcylation on multiple proteins increased upon neuronal stimulation. Removal of OGT decreased the synaptic expression of the GluA2 and GluA3, but not the GluA1, subunits of the AMPA receptor. The number of opposed excitatory presynaptic terminals was sharply reduced upon postsynaptic knock out of OGT. There were also fewer dendritic spines on OGT knock out neurons and those that were present had not developed morphology akin to mature spines. These data identify OGT as a novel molecular mechanism that regulates synapse maturity.

3.2 Introduction

Neuronal synapses, the cell-cell junctions over which neurons communicate, are formed and eliminated throughout life and their turnover has for decades been associated with the way neuronal circuits adapt to environmental challenges to optimize behavior (111, 112). In both humans and animals, early development is characterized by massive generation of new synapses. About half of all synapses are then lost during adolescence (112, 113). Most mature excitatory synapses occur on dendritic protrusions called spines and essentially all spines contain an excitatory synapse (114-116). *In vivo* imaging of individual spines for days to months has shown that adult spines are largely stable but a small subpopulation remains plastic (113, 117) and spine turnover is increased by novel experience (115, 118-120). While most new spines are thin and withdraw rapidly, some enlarge and form stable synaptic contacts (112, 113, 117, 121-124). In fact, the stabilization of a subset of new spines correlates with behavioral performance in several different tasks in multiple animal species (123, 125-127). Rather than synapse formation or density, the selection of which spines are retained once formed has been suggested to match circuit architecture with behavioral needs (128). Without affecting spine formation, deleting β-adducin, which regulates actin, perturbed the process by which nascent spines establish functional synapses and impaired long-term memory (129). Fragile X Syndrome, a common form of mental retardation, exhibits a higher than normal density of spines but more of them exhibit an immature morphology and their turnover is not affected by sensory experience (119, 130). Conversely, the protein Telencaphalin arrests the maturation of spines and its removal enhances several forms of learning (123, 131).

The association between learning and spine survival suggests that synaptic maturation is regulated by neuronal activity (112). Long-term synaptic potentiation (LTP) caused by repeated stimulation of excitatory synapses, a predominate model for encoding of learning and memory on a cellular level, protects activated spines from removal (132, 133). Likewise, Hill and Zito induced LTP specifically on individual newly formed spines through glutamate uncaging and observed potent stabilization (134). While also causing some spines to be eliminated, LTP does not consistently lead to a lasting increase in overall spine density (114, 132, 135, 136). It is widely believed that LTP is caused by insertion of α-amino-3-hydroxy-5-methyl-4-isoxazolepropionic acid (AMPA) receptors into the synaptic cleft. AMPA receptors are glutamate-gated tetrameric ion channels composed of different combinations of subunits GluA1-4 and conduct the majority of the fast excitatory neurotransmission in the brain (103). AMPA receptors may not be obligatory for spine formation in early development, as knocking out (KO) GluA1-3 shortly after birth did not change spine density (137). However, knocking down GluA1-3 increases the number of inactive presynaptic terminals and overexpression of the GluA2 as well as the GluA4 subunits recruits synapses (138-140). Nascent spines incorporate AMPA receptors within a few tens of minutes of formation and so-called 'silent spines', where AMPA receptors cannot be detected, do not correspond to the age of the spine but only its size (123, 141-144). Live imaging has shown that the frequency of local postsynaptic calcium transients within seconds to minutes upon contact between a dendritic protrusion and an axon correlates with the retention of that contact (122). While blocking glutamate signaling did not affect these early events, it did arrest subsequent molecular organization of the spine, including decreasing its long-term stability (122,

124, 133). AMPA receptor stimulation, rather than overall neuronal activity, can rescue the loss of spines that occurs upon removal of presynaptic inputs (111, 145). Similar to LTP, which occurs mainly at small spines, inhibiting AMPA receptor signaling decreases spine density by reducing the number of small and thin spines (114, 146-148). Long-term depression (LTD) of excitatory synapses involves synaptic removal of AMPA receptors and leads to fewer and smaller spines (114, 149). A downstream target of AMPA receptor-dependent regulation of spine maturation is actin, e.g. via modulation of the RhoA signaling cascade (148, 150).

Synapse formation and termination are multi-step processes where the stability, or maturity, of the spine is continuously surveyed by activity-dependent processes. Though many molecules that affect synapse number have been identified over the last decade, it is still unclear how these are regulated to refine information processing to optimize behavior (162). In neurons, the O-GlcNAc pathway has emerged recently as critical for coupling cellular function to metabolic hormones and to energy availability through nutrient-dependent flux via the hexosamine biosynthesis pathway (HBP), which produces UDP-GlcNAc, the donor substrate for OGT (Lagerlöf *et al.* (2016), *Science*. In press; (2, 179, 182)). Unlike complex glycans present on the outside of cells and in the secretory pathway, O-GlcNAc is a highly dynamic sugar that is added and removed repeatedly over the lifespan of a single peptide chain. It is expressed mainly on the inside of cells in the nucleus and cytoplasm. Only two enzymes regulate its cycling; O-GlcNAc transferase (OGT) attaches O-GlcNAc to proteins covalently, whereas O-GlcNAcase (OGA) hydrolyses O-GlcNAc from proteins. Brain is one of the organs where O-GlcNAc is the most abundant (2, 5). In the synapse, a myriad of proteins carry O-GlcNAc (3, 68, 69).

Many of these are critical for synaptic plasticity like αCaMKII and SynGAP (3, 193). O-GlcNAc signaling does affect learning and memory (8, 194). Acute inhibition of OGT or OGA pharmacologically indicated that O-GlcNAc regulates LTP and LTD by affecting AMPA receptor trafficking. However, there have been contradictory reports whether global elevation or depression of O-GlcNAc levels have a stimulatory or inhibitory effect, respectively, on excitatory synaptic function, possibly due to unspecific pharmacology against OGT or differences in mode and length of application of drugs against OGA (7, 104, 194). We developed a new mouse model where OGT was deleted genetically from mature brain neurons *in vivo* and demonstrated that OGT regulates normal food intake, at least in part, by mediating excitatory synaptic function (Lagerlöf *et al.* (2016), *Science*. In press). Using electrophysiology, we observed that knocking out OGT sharply reduced the frequency of miniature excitatory postsynaptic currents (mEPSCs). mEPSC amplitude was also decreased, but to a lesser degree. These findings indicate that OGT underlies adaptive behavior partly by mediating normal excitatory synaptic function (Lagerlöf *et al.* (2016), *Science*. In press).

Here we investigate how OGT regulates excitatory synaptic function by taking advantage of primary neuronal cell culture where OGT is deleted genetically either systemically or in sparse neurons. We discovered that OGT deletion greatly reduced the synaptic expression of GluA2/3 heteromers, a major AMPA receptor isoform. Mimicking our electrophysiological finding of lower mEPSC frequency *in vivo*, removal of OGT *in vitro* led to fewer mature morphological synapses and fewer dendritic spines. The spines that were present on OGT KO neurons were largely immature. Collectively, our observations suggest that OGT is important for the maturation of excitatory synapses, at

least in part through modulating GluA2/3 expression. The regulation of synapse maturity by OGT represents a new model for how neuronal circuits may respond to environmental challenges, such as nutrient fluctuations, to accommodate behavior.

3.3 Results

3.3.1 OGT is enriched in the postsynaptic density of excitatory synapses

Based on biochemical fractionation, it has been shown previously that OGT is present in neuronal synapses (7, 68). Electron microscopy from the cerebellum indicated that OGT is more highly expressed in presynaptic, rather than postsynaptic, nerve terminals (69). To investigate the role of OGT in postsynaptic function, we applied a fractionation protocol to forebrain homogenate that allowed purification of the postsynaptic density (PSD) of excitatory synapses. Equal amounts of all fractions were separated by SDS-PAGE and analyzed by Western blotting. Enrichment of the PSD marker PSD-95 and exclusion of the presynaptic marker synaptophysin ensured that the PSD fraction isolated PSDs specifically (Fig. 3.1A). OGT was present in all subcellular compartments, including in the PSD (Fig. 3.1A). Interestingly, compared to the whole-cell homogenate, OGT was more than twice as abundant in the PSD (Fig. 3.1B). In contrast to OGT, OGA was less abundant in the PSD (Fig. 3.1A). We then used immunohistochemistry to examine the localization of OGT in primary cultured hippocampal neurons. Along the dendrite, OGT expression was punctate and many, but not all, puncta overlapped with PSD-95 (Fig. 3.1C). Introducing a C-terminal truncation of OGT (dCTD), removing a region that has been associated with OGT's interaction with the plasma membrane (48), largely abolished OGT's postsynaptic expression (Fig. 3.1D). This effect did not depend on different expression levels between wildtype (Wt) and mutant OGT as dCTD-OGT

was confined to the soma regardless of amount of DNA used for transfection (Fig. 3.1D). In addition, the somatic expression between Wt OGT and dCTD-OGT did not differ (Fig. 3.1D). It has been shown that depolarization of cultured neuroblastoma cells using KCl activates OGT via calcium-dependent phosphorylation by CaMKIV (56). Moreover, induced seizures in rodents increased the O-GlcNAcylation of some proteins in the brain *in vivo* (71). However, whether, and to what extent, neuronal firing regulates O-GlcNAc incorporation in neurons is still unclear. Taking advantage of two-dimensional gel electrophoresis and blotting for O-GlcNAc, we observed that stimulating neuronal network activity in cortical cultures by inhibiting $GABA_A$ receptors pharmacologically (bicuculline) elevated O-GlcNAcylation in the PSD on multiple proteins (Fig. 3.1E). Together, our observations demonstrate that OGT is enriched in the PSD of excitatory synapses in forebrain neurons, where its localization relied upon its CTD. Within the PSD, O-GlcNAcylation is a dynamic and activity-dependent posttranslational modification.

3.3.2 OGT regulates the synaptic expression of AMPA receptors

Recently, we knocked out OGT in adult animals and observed a marked attenuation of excitatory synaptic currents using electrophysiology (Lagerlöf *et al.* (2016), *Science*. In press). Other groups have shown that acute inhibition of OGT or OGA activity affects LTP and LTD in the CA1 region of the hippocampus, possibly through altered AMPA receptor trafficking (7, 104, 194). Two major AMPA receptor isoforms are GluA1/2 and GluA2/3 heteromers (103, 195). Here we deleted OGT in cortical neurons cultured from floxed OGT mice (OGT^{Fl}) by applying lentivirus expressing either GFP alone (Wt) or GFP together with Cre recombinase (KO) at DIV2. After the neurons had matured, we

precipitated the surface protein population using biotinylation and blotted for the major AMPA receptor subunits. As shown in Fig. 3.2A, only proteins expressed on the surface of the cell were pulled down applying this method. There was no change in the total expression of PSD-95 upon deleting OGT (Fig. 3.2A-B). In contrast, removal of OGT caused a sharp downregulation of the surface expression of the GluA2 and the GluA3 AMPA receptor subunits but not the GluA1 subunit (Fig. 3.2A, C). Also the total expression of GluA2 and GluA3 was decreased (Fig. 3.2A-B). There was no effect on the relative surface over total expression of either subunit, albeit there was a trend towards a small decrease for GluA1 (P=0.05, n=6 for Wt and KO, Fig. 3.2D). We also isolated the PSD from OGT Wt and KO cultures. In the PSD, there was a reduction in GluA3 while there was an increase in GluA1 (Fig. 3.2E-F). GluA2, again, was expressed at a level between GluA1 and GluA3 (9% decrease, P=0.08, Fig. 3.2E-F). Next, we sparsely KO OGT in hippocampal cultures from OGT^{Fl} mice by transfecting a cell-fill (GFP) and an empty plasmid (Wt) or a plasmid expressing Cre (KO) around DIV9. At DIV14 we used immunohistochemistry to stain the surface GluA2 population using an antibody directed against its N-terminus and, after permeabilization, the total GluA2/3 population with a C-terminus-targeted antibody. There was no overt difference in the overall morphology between Wt and KO neurons (Fig. 3.3A). In the soma, the total GluA2/3 expression did not change upon OGT KO (Fig. 3.3B). In contrast, along dendrites, similar to what we showed biochemically, the number of surface GluA2 positive puncta decreased by 51% (P<0.05, Wt n=27, 4.9 ± 0.5; KO n=28, 2.4 ± 0.2, Fig. 3.3C-D). Likewise, the number of total GluA2/3 puncta was 51% lower in OGT KO neurons (P<0.05, Wt n=27, 5.4 ± 1.1, KO n=28, 2.7 ± 0.69, Fig. 3.3C, E). This change in expression was not reflected in the

size of the surface GluA2 puncta and the size of the GluA2/3 puncta was only slightly smaller (Fig. 3.3C, F-G). Using biochemistry and imaging, our results indicate that OGT is necessary cell-autonomously for normal synaptic expression of AMPA receptors, in particular the GluA2/3 heteromer.

3.3.3 Postsynaptic deletion of OGT leads to fewer presynaptic terminals

As deletion of OGT mainly affected the number of GluA2 puncta along dendrites rather than the somatic expression of GluA2/3 or the expression of surface GluA2 per punctum, we reasoned that OGT may regulate the number of synaptic contacts. This idea would be consistent with our previous electrophysiological data showing that OGT removal primarily leads to lower mEPSC frequency (Lagerlöf *et al.* (2016), *Science*. In press). After sparsely labeling and deleting OGT in hippocampal cultures as described above, immunohistochemistry was applied to stain for vGlut1, a marker for excitatory presynaptic terminals, and PSD-95 (Fig. 3.4A). The number of puncta and the size of each punctum overlapping with the cell-fill was then quantified. There was no significant change in the number or the size of PSD-95 positive puncta (Fig. 3.4A-C). In contrast, there was a 47% drop in the number of vGlut1 puncta ($P<0.05$; Wt n=21, 2.7 ± 0.4 puncta/10μm; KO n=18, 1.4 ± 0.3 puncta/10μm, Fig. 3.4A, D). The size of the vGlut1 puncta did not differ between Wt and KOs (Fig. 3.4E). Together, our data suggest that the formation of postsynaptic structures, as determined by PSD-95, is not affected by removing OGT. In contrast, deleting OGT in the postsynaptic cell prevents the specialization of opposing presynaptic terminals. These observations corroborate and expand the previous finding that the drop in mEPSC frequency upon OGT KO *in vivo* reflects a loss of functional synapses (Lagerlöf *et al.* (2016), *Science*. In press).

3.3.4 OGT removal is associated with deficient spine maturation

Most excitatory synapses occur on dendritic spines (112). Filling the neuron with a fluorescent marker, spines can be imaged and their number and shape measured. Whereas the number of spines is a function of the number of excitatory synapses, the shape of the spine indicates its maturity (114-116). Mature and stable spines typically exhibit a wider distal portion ('spine head') (Fig. 3.5a) (112, 113, 121-124, 132). Here, again, hippocampal cultures from OGT^{Fl} mice were sparsely transfected to label cells and KO OGT at DIV9 and then fixed at DIV14. Upon deletion of OGT, spine number decreased by 43% ($P<0.05$; Wt n=26, 3.9 ± 0,3 spines/10μm; KO n=28, 2.2 ± 0.2 spines/10μm, Fig. 3.5A-B). Spine shape was measured by quantifying the ratio between the width and the length of individual spines (Fig. 3.5A). Counting all spines, deleting OGT decreased their mean shape ratio by 33% ($P<0.05$, Wt n=1108, 0.85 ± 0.02, KO n=1074, 0.57 ± 0.01, Fig. 3.5C). To evaluate the proportion of mature versus immature spines, spines with a ratio above 0.5 were labeled 'mature' and those with a ratio below 0.5 'thin' (Fig. 3.5A). In Wt cells, the majority of all spines were mature (Fig. 3.5D). Of those spines that were present on OGT KO cells, in contrast, most were thin (Fig. 3.5D). To summarize, deleting OGT leads to a higher proportion of immature spines and fewer spines in total (Fig. 3.5E).

3.4 Discussion

Neuronal circuits need to constantly rearrange their connectivity pattern in order to match behavioral output to environmental influences. Here we find that OGT, a nutrient-dependent enzyme, is enriched in the postsynaptic density of excitatory synapses. In the PSD, the abundance of O-GlcNAc was dynamic and dependent on neuronal activation.

Deletion of OGT greatly depressed the synaptic expression of the GluA2 and GluA3 subunits of the AMPA receptor. The reduction in GluA2 and GluA3 expression was largely due to fewer dendritic AMPA receptor clusters rather than a decrease in the amount of AMPA receptors in each cluster, indicating that the main effect of OGT removal would be explained by a downregulation of the number of functional excitatory synapses. Indeed, removing OGT postsynaptically disrupted the formation of opposing presynaptic terminals, as determined by staining of the synaptic vesicle protein vGlut1. There were also fewer spines on OGT KO neurons. Those spines that did form were mostly immature and did not express morphological features reminiscent of stable synapses. In contrast, the total expression of PSD-95 was not affected upon OGT KO, and neither was the density of PSD-95 puncta along dendrites or their size.

Total spine number is regulated by the formation of new spines and the termination of old spines. We deleted OGT genetically before or during the period of the most extensive synapse formation in culture (DIV7-14) and observed a marked reduction in spine density. Accordingly, albeit we have not applied methods such as live imaging of individual spine turnover to verify this idea, it is likely that the decrease in total spine number upon OGT KO mainly resulted from disrupted spine formation. However, deleting OGT did not affect the expression and clustering of PSD-95, which is an integral protein of the PSD (133). At many synapses, PSD-95 clustering precedes the accumulation of presynaptic components such as synaptic vesicles (112, 129, 196, 197). In the PSD of OGT KO cells, there was a comparatively high abundance of GluA1-containing receptors while GluA3-containing receptors were lower in abundance than in Wt cells. Similarly, on the cell surface, there was a reduction in GluA2 and GluA3 but

not GluA1. As GluA2 consistently expressed at levels between GluA1 and GluA3 upon removal of OGT, the main effect of deleting OGT presumably occurs on GluA2/3 heteromers as opposed to on GluA1/2 heteromers. Early in development, GluA4 translocates into so-called silent synapses and are later replaced by GluA2-containing receptors (198-200). While synaptic insertion of GluA1 homomers and GluA1/2 heteromers require neuronal stimulation, GluA2/3-heteromers can be inserted under baseline conditions in exchange for pre-existing receptors (201, 202). However, unlike GluA1, GluA2 does not appear to enter into silent synapses (201). Sensory experience and learning increase the abundance of GluA1 homomers in the synapse, but this increase is often transient (160, 161, 202). Although the trafficking of GluA2/3 can be regulated by neuronal activity, these and other data suggest that GluA2/3 heteromers, as opposed to GluA1 homomers or GluA1/2 heteromers, are associated with the maintenance of synaptic strength in mature synapses (103, 159). Whereas total spine number was reduced, spines did develop on OGT KO cells. But of those spines that formed, most resembled immature spines and rarely evolved morphology akin to mature spines with a wider spine head as in Wt cells. Spine formation is intimately linked to synapse formation (112, 113, 121-124). The formation of presynaptic terminals on dendrites where OGT had been deleted, as determined by overlapping staining of the synaptic vesicle protein vGlut1, was interrupted. Based on the selective effect on GluA2/3 heteromers, immature spine phenotype and reduction in the number of vGlut1 puncta but not PSD-95 puncta, it appears that OGT is necessary for later, rather than early, stages of postsynaptic development when otherwise unstable spines mature into functional synapses (Fig. 3.5E).

Although the experiments presented in this paper were performed in the context of synapse formation in culture, previously we have observed a similar decrease in excitatory synapse number in adult animals. After OGT was removed acutely *in vivo*, there was a sharp drop in mEPSC frequency (Lagerlöf *et al.* (2016), *Science*. In press). In addition, other groups have shown that short-term nutritional or pharmacological manipulation of global O-GlcNAc levels in hippocampal slices affects long-term potentiation and long-term depression of excitatory CA1 synapses (7, 104, 194). At least some of these effects were related to altered trafficking of GluA2 (104, 194). Collectively, these observations suggest that OGT is important not only for the formation of new excitatory synapses during development but also for the stability of excitatory synapses in the adult. As discussed above, spines undergo constant remodeling where activity-dependent signaling through AMPA receptors, e.g. via actin, maintain their stability. Thus, it is possible that the synaptic depression of GluA2/3 heteromers upon OGT deletion prevented the development of thin spines into mature synapses. The idea that OGT underlies spine maturity via maintaining AMPA receptor expression would explain why removing OGT during development and in adult animals lead to the same phenotype; loss of excitatory synapse number.

OGT may regulate AMPA receptor expression through several pathways. We show here that the O-GlcNAc content in the PSD is dynamic. We also observed that OGT is enriched in the PSD and that its postsynaptic expression relies on the CTD of OGT, a region that has been associated with membrane translocation of OGT (48). Global and long-term deletion of OGT decreased the total expression of GluA2 and 3. In contrast, shorter and sparse OGT KO did not affect the somatic expression of GluA2/3. This

indicates that OGT regulates AMPA receptor expression by a cell-autonomous mechanism, probably, at least in part, through degradation or trafficking of the receptor, which is supported by the fact that the effect of acute manipulation of global O-GlcNAc levels on excitatory neurotransmission is GluA2-dependent (194). Moreover, we and others have shown that O-GlcNAc regulates excitatory synapse function in hypothalamic, cortical and hippocampal cells. Thus, the manipulation of synaptic AMPA receptor abundance may be a common and major endpoint for how OGT shapes neuronal circuits. Many O-GlcNAc-modified proteins known to affect AMPA receptor trafficking have been identified using mass spectrometry, e.g. SynGAP and αCaMKII (3, 193). Based on these observations, it is likely that OGT may regulate AMPA receptor expression via pathways local to the spine or the postsynaptic density, but other mechanisms cannot be excluded.

O-GlcNAc is increasingly being appreciated as an important modification of protein function. Its unique regulation where metabolic and other stimuli can affect O-GlcNAcylation on a global as well as a target-specific scale presents a novel mechanism for how cells respond to environmental challenges. Here we demonstrate that OGT is enriched in the postsynaptic density of excitatory synapses and is necessary for synapse maturation, possibly via regulating the synaptic expression and/or localization of GluA2/3 heteromers. O-GlcNAc cycling in the brain is linked to learning and memory, feeding behavior and neurodegenerative diseases (2, 8, 194). While many proteins in the excitatory postsynapse are known to be modified by O-GlcNAc, an important task will be to identify what O-GlcNAc sites are dynamically regulated to modify neuronal circuit function.

Figure 3.1

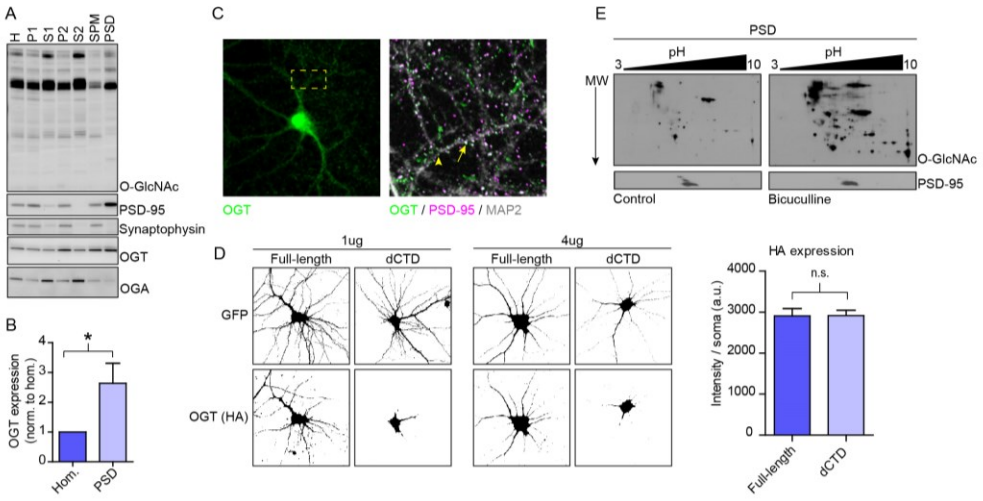

Fig. 3.1. OGT is enriched in the postsynaptic density of excitatory synapses. (A) Wb of PSD preparation fractions from brain. (B) Quantification of OGT expression in the PSD relative to the whole-cell fraction (n=7 for Hom. and PSD; two-tailed *t*-test: $P<0.05$). (C) Immunohistochemistry of OGT (green), PSD-95 (magenta) and MAP2 (gray). Right image shows boxed area from left image in higher magnification. (D) Left: Expression of GFP and different HA-tagged OGT constructs in cultured hippocampal neurons. Binary images are shown. Right: quantification of OGT expression (HA) in the soma of transfected neurons (Full-length n=13, dSPY n=8; two-tailed *t*-test: $P<0.05$). (E) Wb of two-dimensional gel electrophoresis of the PSD fraction from control and stimulated neurons. Quantifications represent mean ± s.e.m.

Figure 3.2

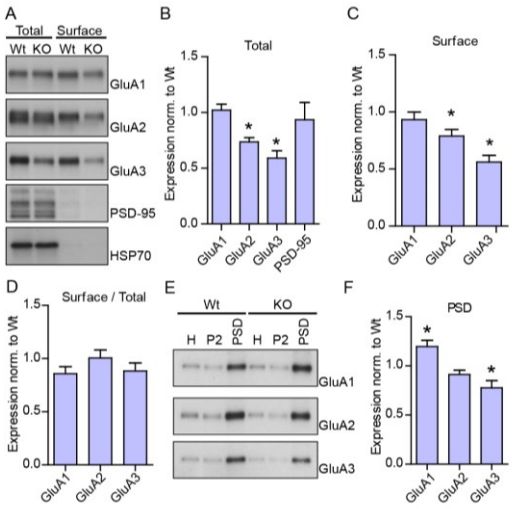

Fig. 3.2. OGT regulates the synaptic expression of AMPA receptors. (A) Wb of the total and surface expression of GluA1-3. (B) Quantifications of the total expression from (A) (GluA1-3: n=5 for Wt and KO; PSD-95: n=3 for Wt and KO; two-tailed *t*-test: $P<0.05$). (C) Quantifications of the surface expression from (A) (GluA1-3: n=6 for Wt and KO; two-tailed *t*-test: $P<0.05$). (D) Quantifications of the surface over total expression from (A) (GluA1-3: n=6 for Wt and KO; two-tailed *t*-test: $P<0.05$). (E) Wb of PSD preparation fractions from Wt and KO cells. (F) Quantification of GluA1-3 expression in the PSD (n=3 for Wt and KO; two-tailed *t*-test: $P<0.05$). Quantifications represent mean ± s.e.m.

Figure 3.3

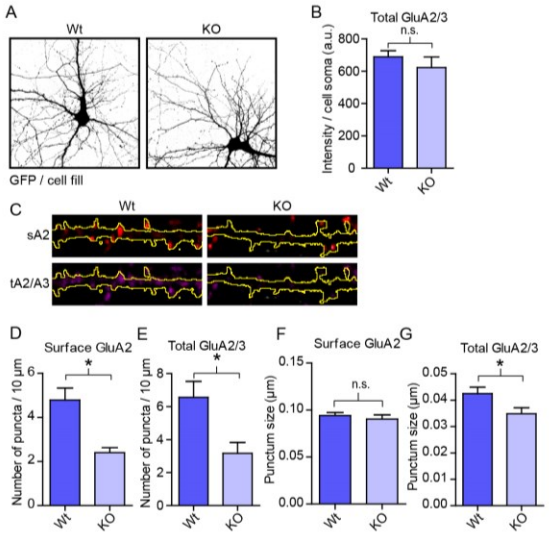

Fig. 3.3. Deletion of OGT leads to fewer surface GluA2 clusters. (A) Thresholded images of GFP expression in Wt and KO hippocampal neurons. (B) Quantification of the total expression of GluA2/3 in the cell soma of individual hippocampal neurons (Wt n=18, KO n=20; two-tailed *t*-test: $P<0.05$). (C) Immunohistochemistry of the surface expression of GluA2 and total expression of GluA2/3 in dendrites from transfected neurons. The outlines of the cell (GFP expression) are shown in yellow. (D-G) Quantifications from (C) (Wt n=27, KO n=28, two-tailed *t*-test: $P<0.05$). Quantifications represent mean ± s.e.m.

Figure 3.4

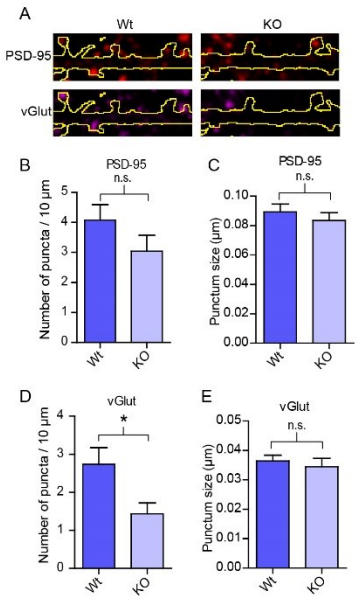

Fig. 3.4. OGT regulates the number of mature synaptic contacts. (A) Immunohistochemistry of vGlut1 and PSD-95 overlapping with transfected neurons. The outlines of the cell (GFP expression) are shown in yellow. (B-E) Quantifications from (Wt n=21, KO n=18, except for vGlut puncta size where n=16, two-tailed *t*-test: $P<0.05$). Quantifications represent mean ± s.e.m.

Figure 3.5

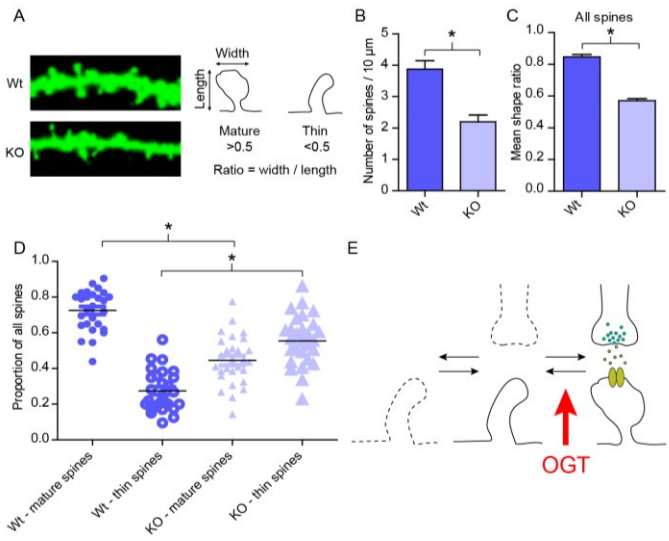

Fig. 3.5. Fewer and more immature spines on OGT KO neurons. (A) Left: Expression of GFP in dendrites from Wt and KO hippocampal neurons. Right: Schematic of measurements taken to quantify spine shape. (B) Quantification of spine density (Wt n=26, KO n=28, two-tailed *t*-test: $P<0.05$). (C) Quantification of the mean spine shape ratio (Wt n=1108, KO n=1074, two-tailed *t*-test: $P<0.05$. (D) Quantification of the proportion of mature and thin spines along dendrites. (Wt n=27, KO n=28, two-tailed *t*-test: $P<0.05$). (E) Model of how OGT, at least in part, regulates excitatory synapse function; OGT inhibits the maturation of dendritic spines leading to fewer and more immature synapses. Quantifications represent mean ± s.e.m.

3.5 Materials and Methods

Materials. Mice where an exon in the *Ogt* locus has been floxed (OGT^{Fl}) to delete OGT has been described previously (Lagerlöf *et al.* (2016), *Science*. In press; (6). Antibodies used were: OGT (AL25 and AL28, produced in-house, 1:5000), O-GlcNAc (110.6, produced in-house, 1:10000), OGA (345, produced in-house, 1:5000), HSP70 (Santa Cruz Biotechnology, 1:1000-5000), PSD-95 (NeuroMab, Wb; 1:5000, IF; 1:2000), GluA1 (4.9D, produced in-house, 1:10000), GluA2 (Wb; Mab, produced in-house, 1:5000, IF; 15F1, a kind gift from Dr Eric Gouaux, 1:500-1000), GluA3 (JH4300, produced in-house, 1:5000), GluA2/3 (JH4854, produced in-house, 1:250), MAP2 (nb300-213, Novus biologicals, 1:10000), Synaptophysin (SVP-38, Sigma, 1:10000), HA (12CA5, 1:200), vGlut1 (AB5905, Millipore, 1:2500), GFP (ab13970, Abcam, 1:2500). All plasmid inserts used had been generated by standard cloning techniques previously in-house. All animals were housed according to the Johns Hopkins University Animal Care and Use Committee guidelines.

Primary neuronal cell culture. For biochemistry, rat and mice E18 cortical neurons were prepared as previously described (Lagerlöf *et al.* (2016), *Science*. In press). Briefly, after dissociation, cells were plated on poly-L-lysine coated dishes in neuronal growth media with 5% serum, NM5 (Neurobasal growth medium (GIBCO), 2% B27 (Invitrogen), 2 mM Glutamax (GIBCO), 5% Fetal Bovine Serum and PenStrep (GIBCO)). Dividing cells were removed using 5 mM uridine and 5 mM (+)-5-fluor-2'-deoxyuridine in NM1 (1% serum) at days *in vitro* (DIV) 3-5). Then, every 3-4 days, half of the culture media was exchanged for glia-conditioned NM1 until harvest. For OGT KO experiments, lentivirus was added on DIV 2. SDS-PAGE and Western blotting were

done according to standard procedures. For imaging, mice E16.5-17 and rat E18 hippocampal neurons were cultured in serum-free media (NM0). Upon transfection, half of the media was exchanged for fresh NM0. Transfections were done using Lipofectamin 2000 (Fisher).

Imaging. Mature hippocampal neurons were fixed with 4% paraformaldehyde and 4% sucrose. When surface staining was performed, the fix was applied for 4.5 min in room temp, which did not break the cell membrane. Thereafter, the GluA2 antibody raised against the N-terminus of GluA2 was applied in room temp for 2 h in a blocking buffer (0.1% gelatin, 250 mM NaCl, 15 mM phosphate buffer, pH7.4) that did not contain any detergent. After washing, other primary antibodies were introduced in blocking buffer that did contain detergent (0.25 % Tx-100) for 2 h at room temp. Secondary antibodies, diluted in blocking buffer plus 0.25% triton, were added for 1 h after washing. For other staining, the neurons were fixed using the same solution but for 15 min at 4°C, permeabilized for 10 min at 4°C (0.25% Tx-100 in PBS) and blocked for at least 1 h (5-10% normal goat serum in PBS). All antibodies were diluted in the same blocking buffer and applied for 1-2 h.

Lentivirus. To KO OGT in cultured neurons, pseudotyped VSV-G lentivirus expressing GFP alone (Wt) or GFP together with Cre recombinase (KO) was produced according to standard procedures (Lagerlöf *et al.* (2016), *Science*. In press).

PSD isolation. From neuronal culture: Cells were harvested and homogenized in homogenization buffer (0.32 M sucrose, 4mM HEPES pH7.4, including inhibitors for proteases, phosphatases and O-GlcNAcases). After homogenization, in all subsequent steps including adding any solution, the same inhibitors as used for the homogenization

buffer were added. The homogenate (H) was centrifuged (1000xg, 10 min, 4°C). The supernatant was spun again (10000xg, 15 min, 4°C). The pellet was resuspended in homogenization buffer and spun again (10000xg, 15 min, 4°C). The pellet was lyzed by hypo-osmotic shock in H_2O (P1000 pipet x 20-30 times) and then adjusted to 4 mM HEPES, pH7.4. This fraction was used as P2. The remained material was rotated at 4°C for 30 min before ultracentrifugation (25000xg, 20 min 4°C). The pellet was resuspended in 50 mM HEPES, pH 7.4, e mM EDTA). After 0.5% Triton X100 had been added, the solution was rotated at 4°C for 15 min and then centrifuged again (32000xg, 20 min, 4°C) to yield the PSD fraction. From brain (the cerebellum and most of the midbrain and brainstem were removed): the tissue was homogenized (fraction H, 0.32 M sucrose, 10 mM HEPES, pH 7.4, including inhibitors for proteases, phosphatases and O-GlcNAcases) and then centrifuged (1000xg, 10 min, 4°C) to yield the P1 fraction. After homogenization, in all subsequent steps including adding any solution, the same inhibitors as used for the homogenization buffer were added. The supernatant (S1) was spun again (13800xg, 20 min, 4°C) where the supernatant was collected as S2. The pellet (P2) was resuspended in homogenization buffer and layered on a sucrose gradient (P2 - 0.85 M - 1.0 M - 1.2 M sucrose in 1mM HEPES, pH 7.4) and centrifuged (82500xg, 2 h, 4°C). The material between the 1.0 M and 1.2 M layers was collected and diluted with 2.5 volumes of 10 mM HEPES, pH 7.4 before centrifugation (150000xg, 30 min, 4°C). The pellet (SPM) was resuspended in 80 mM Tris-HCl, pH 8.0, and then diluted with 1.0% Triton X100 to a final concentration of 0.5% Triton X100. The solution was rotated for 15 min (4°C) and then centrifuged (32000xg, 20 min, 4°C) to yield the PSD fraction (the pellet).

Surface biotinylation. Cells were washed 2-3 times in aCSF (143 mM NaCl, 5 mM KCl, 2 mM $CaCl_2$ 1 mM $MgCl_2$, 10 mM HEPES pH 7.4, 10 mM D-glucose) and then incubated on ice fro 20 min in Sulfo-NHS-SS-Biotin (Fisher) diluted in aCSF. Remaining active biotin was quenced with TBS three times (4°C, 5 min each wash) and then lyzed in RIPA buffer (50mM tris, 150mM sodium chloride, 1% NP-40, 1% deoxycholate, 0.1% SDS, 1mM EDTA, including inhibitors for proteases, phosphatases and O-GlcNAcases). Biotinylated proteins were pulled down using neutravidin beads (Fisher).

Isoelectrofocusing. Two-dimensional electrophoresis was done according to standard procedures (57). Briefly, from mature neuronal cell cultures (DIV14-20) treated with vehicle or bicuculline (40 μM) for 5 h, the PSD fraction was isolated and resuspended in 7 M urea, 2 M thiourea, 2% dodecyl maltoside (D4641, Sigma), 50 mM DTT, 0.2% ampholytes (BioLyte 3–10 IEF buffer from Bio-Rad) and inhibitors for proteases, phosphatases and O-GlcNAcases. The sample was then swelled overnight at room temperature onto Readystrip IPG Strips (pI 3–10) (Bio-Rad), isoelectrofocused and treated with DTT and iodoacetamide before separated using SDS-PAGE. Subsequent Western blotting was done according to standard procedures.

Image quantification and presentation. All analysis was done on non-manipulated, raw images in ImageJ. For quantification of puncta number and size, the cell-fill channel (GFP) was thresholded and then used to create a mask tracing the border of the cell. Only secondary and tertiary dendrites were included, and their total length measured per image. Then the channel for each type of punctum was thresholded and counted within the cell-fill mask using the 'analyze particles' function. The number and size of each punctum was recorded. The number of puncta was divided by the length of

the corresponding dendrite, and both spine density and spine shape were quantified per image. Spines were counted manually. Only secondary and tertiary dendrites were included, and their total length measured per image. The total spine number was divided by the length of the corresponding dendrite per image. The length between the tip of each spine and the junction between the spine and the dendrite and the width of the head of each spine were measured manually on 50 randomly picked spines per image. The shape of each spine was calculated by dividing the width by the length of each spine. This ratio was compared between all Wt and KO spines. For expression analysis comparing full-length and truncated OGT, the laser intensity varied slightly between images to account for differences in expression level per cell. The differences were minor and were not consistently lower or higher for either mutant and did not affect the interpretation of the experiment. While all analysis was done on raw, unmanipulated images, for image presentation purposes, most images shown in the figures were improved *post hoc*. Within the same experiment, all changes were done in the same way between Wt and KO images. The manipulations were applied in Photoshop and MS Paint and included: Levels and Brightness/Contrast and Filtering ('Despeckle' and 'Gaussian blur').

Statistical analysis. Student's t-tests were unpaired and two-tailed. Star, '*', represents $P<0.05$. Error bars represent mean +/- standard error of the mean (s.e.m.).

CHAPTER 4.

CHARACTERIZATION OF THE O-GLCNACYLATION OF PROTEIN 4.1N AND GLUA2

4.1 Introduction

Several studies have reported that multiple proteins in the brain are O-GlcNAcylated. Those studies that identify what particular proteins contain O-GlcNAc are mostly based on mass spectrometry (3, 193). We have shown that O-GlcNAc transferase (OGT) is highly expressed in the postsynaptic density and regulates AMPA receptor expression, probably via a posttranscriptional mechanism (Lagerlöf *et al.* (2016), *Science*. In press, Lagerlöf *et al*. In preparation). Here we tested whether protein 4.1N, a protein that binds GluA1 and is critical for the cell surface expression of GluA1, or GluA1-3 are O-GlcNAcylated.

4.2 Results

4.2.1 Protein 4.1N

Protein 4.1N was immunoprecipitated from forebrain and probed for O-GlcNAc using Western blotting with an O-GlcNAc antibody (Fig. 4.1A). The band corresponding to protein 4.1N reacted against an O-GlcNAc antiobdy, and this signal could be competed off with 0.5M free GlcNAc. We treated neuronal cell cultures with either vehicle or Thiamet-G (an inhibitor to OGA). After 4 h, the O-GlcNAc signal on 4.1N was dramatically increased (Fig. 4.1B). Interestingly, adding NMDA to the cultures also appeared to increase the O-GlcNAc signal on 4.1N (but the effect did not reach significance, P=0.09, not shown) (Fig. 4.1C). 4.1N was then overexpressed in autologous cell culture, immunopreciptated and mixed with in vitro-purified OGT together with radiolabeled UDP-GlcNAc. After only a few days, we picked up a strong OGT-dependent signal from 4.1N (Fig. 4.1D).

4.2.2 GluA1-3

GluA1 and GluA2 were immunoprecipitated from neuronal cultures or the brain (not shown) and then Western blotted for O-GlcNAc. While there was a band reacting against the O-GlcNAc antibody laying very close to the band specific for GluA2, they did not exactly overlap (Fig. 4.2A). For GluA1, there were O-GlcNAc bands also in the GluA1 immunoprecipitate but these were, in comparison to GluA2, farther away from the GluA1 band (Fig. 4.2A). When GluA1 and GluA2 were overexpressed and pulled down from autologous cell culture, there was no specific signal from O-GlcNAc corresponding to either AMPA receptor isoform (Fig. 4.2B). However, when the C-terminal tails were overexpressed and pulled down in a similar way, O-GlcNAc appeared to react against the GluA1 and the GluA2 C-tails; the O-GlcNAc antibody also stained the tag linked to the C-tails used for the pull-down but to a lesser degree (Fig. 4.2C). We also overexpressed and mixed the C-tail pull-downs with *in vitro*-purified OGT and radiolabeled UDP-GlcNAc. After months of exposure, we observed signal from GluA2, but also GluA1 to some extent (Fig. 4.2D). Similar result was seen with the C-tail of GluA3 (not shown). Next, to increase any possible O-GlcNAcylated population of GluA2, brain lysate was first mixed and pulled down with sWGA beads (which bind terminal GlcNAc). The pulled-down material was eluted with either GlcNAc or GalNAc and then immunoprecipitated with an antibody against GluA2 and blotted for O-GlcNAc. GluA2 did enrich in the sWGA precipitate and O-GlcNAc signal was only observed in the GlcNAc-eluted GluA2 immunoprecipitate (Fig. 4.2E). In another experiment, GluA2 was immunoprecipitated from brain lysate and then mixed with enzymes cleaving any O-linked or N-linked sugars before blotted for O-GlcNAc. Hydrolysis of O-linked sugars

removed the O-GlcNAc staining from the GluA2-related band. While hydrolysis of N-linked sugars did cause a mobility shift in GluA2, as expected from a transmembrane protein, it did not cause a similar shift in the O-GlcNAc band. After the mobility shift, there was no O-GlcNAc band detected near GluA2 (Fig. 4.2F).

4.3 Discussion

Here we present preliminary data validating older mass spectrometric reports that protein 4.1N, a protein that binds GluA1 and is critical for the cell surface expression of GluA1, is O-GlcNAcylated (3). Our observations indicate that 4.1N may be dynamically modified, including by NMDA-dependent signaling. We have also characterized whether the AMPA receptor subunits GluA1-3 are O-GlcNAcylated. GluA1-3 appear to be substrates of OGT *in vitro*. While we reproduce a previous finding that immunoprecipitation of GluA2 reacts against an antibody for O-GlcNAc, our preliminary data suggest that this signal comes from a GluA2-binding protein and not GluA2 itself (194).

Figure 4.1

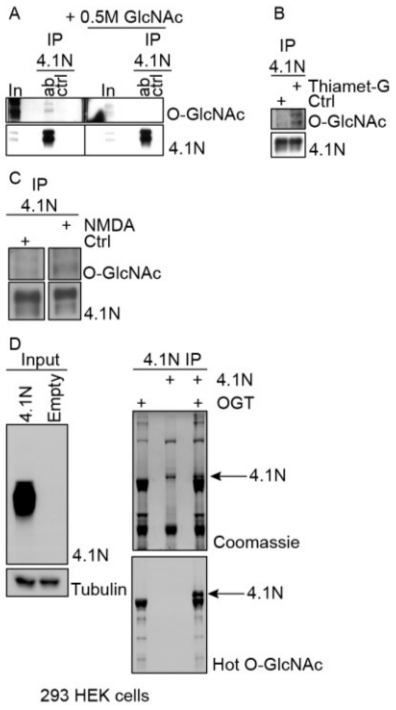

Fig. 4.1. Protein 4.1N is O-GlcNAcylated. (A) Wb of immunoprecipitation of 4.1N form brain. (B) Wb of immunoprecipitation of 4.1N form neuronal culture after treatment with Thiamet-G. (C) Wb of immunoprecipitation of 4.1N form culture after treatment with NMDA. (D) *In vitro* labeling of 4.1N with radioactive O-GlcNAc. Left: Wb of lysate from 293 cells transfected with 4.1N or an empty plasmid. Right: 4.1N was immunoprecipitated and radiolabeled and then separated using SDS-PAGE.

Figure 4.2

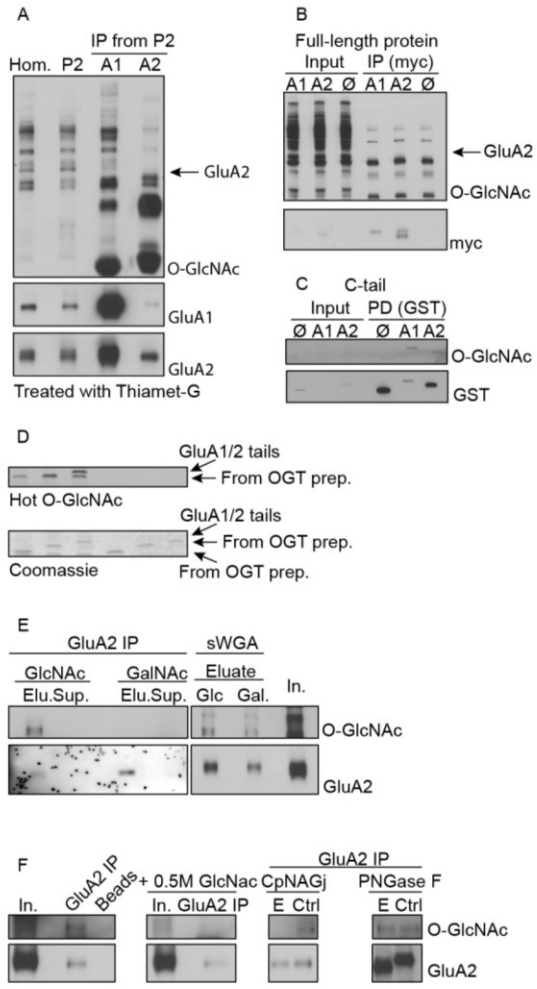

Fig. 4.2. The GluA2 C-terminus may be a target of OGT *in vitro*. (A) Wb probing for O-GlcNAc on GluA1 and GluA2 immunoprecipitates from neuronal culture. (B). 293 cells were transfected with GluA1, GluA2 or empty vector. The image is showing Wb probing for O-GlcNAc on immunoprecipitates. (C) 293 cells were transfected with the C-terminus of GluA1, GluA2 or empty vector. The image is showing Wb probing for O-GlcNAc on immunoprecipitates. (D) *In vitro* labeling of GluA1/2 C-termini with radioactive O-GlcNAc. 293 cells were transfected with the C-terminus of GluA1, GluA2 or empty vector. The C-termini were pulled down and radiolabeled and then separated

using SDS-PAGE. (E) Wb of sWGA-enriched GluA2 immunoprecipitates. (F) Wb probing for O-GlcNAc on immunoprecipitates of GluA2 after treatment with various enzymes.

4.4 Materials and Methods

Materials. Antibodies used were: O-GlcNAc (110.6, produced in-house, 1:10000), GluA1 (4.9D and JH4294, produced in-house, 1:10000 and 1:5000, respectively), GluA2 (Wb; Mab, produced in-house, 1:5000, GluA3 (JH4300, produced in-house, 1:5000). All plasmid inserts used had been generated by standard cloning techniques previously in-house. All animals were housed according to the Johns Hopkins University Animal Care and Use Committee guidelines.

Primary neuronal cell culture. Rat neurons were prepared from cortex according to standard procedures, see chapter 3. SDS-PAGE and Western blotting were done according to standard procedures.

Protein isolation, labeling and blotting. Cells were lysed in RIPA buffer (50mM tris, 150mM sodium chloride, 1% NP-40, 1% deoxycholate, 0.1% SDS, 1mM EDTA, including inhibitors for proteases, phosphatases and O-GlcNAcases). The lysates were mixed with the given antibody for 2-4 h and then with beads for 1-2 h and eluted with SDS sample buffer. N-linked sugars were cleaved using PNGase F and O-GlcNAc was cleaved using CpNAGj. For sWGA pull-downs, the lysate was first mixed with commercially available sWGA beads and eluted with free GlcNAc or GalNAc before immunoprecipitation with a GluA2 antibody was started. Western blotting, *in vitro* purification of OGT and O-GlcNAc radiolabeling was performed according as described (57).

CHAPTER 5.

FINAL REMARKS AND OUTLOOK

Notes

Most content included here is modified from work published previously, including:

1. **Lagerlöf O** and Hart GW (2014). O-GlcNAcylation of Neuronal Proteins: Roles in Neuronal Functions and in Neurodegeneration. *Book Chapter in the book 'Glycobiology of the nervous system'*. Springer.

5.1 Final remarks and Outlook

Every time we think, act and feel information is passed between neurons in the brain. Neurons are extraordinary cells with complex morphology and a lifespan that matches the lifespan of the organism. The posttranslational modification O-GlcNAc, the attachment of β-N-acetylglucosamine to serine and threonine, is expressed in all compartments of the neuron. By the help of only two enzymes, OGT and OGA, O-GlcNAc regulates thousands of proteins underlying diverse cellular processes such as gene transcription and signal transduction. In this dissertation, we have established a role for O-GlcNAc as a regulator of excitatory synaptic function and adaptive behavior. In particular, our observations indicate that the regulation of excitatory synapse number by OGT is an important pathway by which the brain controls food intake and meal size. The big challenge for the future will be to derive a mechanistic picture how specific O-GlcNAc sites affect protein function and thereby synaptic transmission. Recently, several new techniques have been developed that improve and simplify the detection of O-GlcNAc. Nevertheless, more tools such as site-specific antibodies for O-GlcNAc are needed to make the O-GlcNAc field more accessible to the broader neuroscience research community. It may appear a distant goal, but eventually the field needs efficient methods

enabling putting on or taking off O-GlcNAc at single and specific sites *in vivo*. Understanding the way O-GlcNAc works in the nervous system will not only afford fundamental principles of brain function but also provide novel targets for the treatment of neurocognitive disease.

BIBLIOGRAPHY

1. Torres CR & Hart GW (1984) Topography and polypeptide distribution of terminal N-acetylglucosamine residues on the surfaces of intact lymphocytes. Evidence for O-linked GlcNAc. *J Biol Chem* 259(5):3308-3317.
2. Hart GW, Slawson C, Ramirez-Correa G, & Lagerlof O (2011) Cross talk between O-GlcNAcylation and phosphorylation: roles in signaling, transcription, and chronic disease. *Annu Rev Biochem* 80:825-858.
3. Trinidad JC*, et al.* (2012) Global identification and characterization of both O-GlcNAcylation and phosphorylation at the murine synapse. *Mol Cell Proteomics* 11(8):215-229.
4. Alfaro JF*, et al.* (2012) Tandem mass spectrometry identifies many mouse brain O-GlcNAcylated proteins including EGF domain-specific O-GlcNAc transferase targets. *Proc Natl Acad Sci U S A* 109(19):7280-7285.
5. Kreppel LK, Blomberg MA, & Hart GW (1997) Dynamic glycosylation of nuclear and cytosolic proteins. Cloning and characterization of a unique O-GlcNAc transferase with multiple tetratricopeptide repeats. *J Biol Chem* 272(14):9308-9315.
6. O'Donnell N, Zachara NE, Hart GW, & Marth JD (2004) Ogt-Dependent X-Chromosome-Linked Protein Glycosylation Is a Requisite Modification in Somatic Cell Function and Embryo Viability. *Molecular and Cellular Biology* 24(4):1680-1690.
7. Tallent MK*, et al.* (2009) In vivo modulation of O-GlcNAc levels regulates hippocampal synaptic plasticity through interplay with phosphorylation. *J Biol Chem* 284(1):174-181.
8. Rexach JE*, et al.* (2012) Dynamic O-GlcNAc modification regulates CREB-mediated gene expression and memory formation. *Nat Chem Biol* 8(3):253-261.
9. Arnold CS*, et al.* (1996) The microtubule-associated protein tau is extensively modified with O-linked N-acetylglucosamine. *J Biol Chem* 271(46):28741-28744.
10. Liu F, Iqbal K, Grundke-Iqbal I, Hart GW, & Gong CX (2004) O-GlcNAcylation regulates phosphorylation of tau: a mechanism involved in Alzheimer's disease. *Proc Natl Acad Sci U S A* 101(29):10804-10809.
11. Yuzwa SA*, et al.* (2012) Increasing O-GlcNAc slows neurodegeneration and stabilizes tau against aggregation. *Nat Chem Biol* 8(4):393-399.
12. Wang Z*, et al.* (2010) Enrichment and site mapping of O-linked N-acetylglucosamine by a combination of chemical/enzymatic tagging, photochemical cleavage, and electron transfer dissociation mass spectrometry. *Mol Cell Proteomics* 9(1):153-160.
13. Marotta NP, Cherwien CA, Abeywardana T, & Pratt MR (2012) O-GlcNAc modification prevents peptide-dependent acceleration of alpha-synuclein aggregation. *Chembiochem* 13(18):2665-2670.
14. Fang B & Miller MW (2001) Use of galactosyltransferase to assess the biological function of O-linked N-acetyl-d-glucosamine: a potential role for O-GlcNAc during cell division. *Exp Cell Res* 263(2):243-253.
15. Webster DM*, et al.* (2009) O-GlcNAc modifications regulate cell survival and epiboly during zebrafish development. *BMC Dev Biol* 9:28.

16. Banerjee S, Robbins PW, & Samuelson J (2009) Molecular characterization of nucleocytosolic O-GlcNAc transferases of Giardia lamblia and Cryptosporidium parvum. *Glycobiology* 19(4):331-336.
17. Benko DM, Haltiwanger RS, Hart GW, & Gibson W (1988) Virion basic phosphoprotein from human cytomegalovirus contains O-linked N-acetylglucosamine. *Proc Natl Acad Sci U S A* 85(8):2573-2577.
18. Caillet-Boudin ML, Strecker G, & Michalski JC (1989) O-linked GlcNAc in serotype-2 adenovirus fibre. *Eur J Biochem* 184(1):205-211.
19. Halim A*, et al.* (2015) Discovery of a nucleocytoplasmic O-mannose glycoproteome in yeast. *Proc Natl Acad Sci U S A* 112(51):15648-15653.
20. Schirm M*, et al.* (2004) Flagellin from Listeria monocytogenes is glycosylated with beta-O-linked N-acetylglucosamine. *J Bacteriol* 186(20):6721-6727.
21. Fredriksen L*, et al.* (2012) The major autolysin Acm2 from Lactobacillus plantarum undergoes cytoplasmic O-glycosylation. *J Bacteriol* 194(2):325-333.
22. Selzer J*, et al.* (1996) Clostridium novyi alpha-toxin-catalyzed incorporation of GlcNAc into Rho subfamily proteins. *J Biol Chem* 271(41):25173-25177.
23. Hart GW, Housley MP, & Slawson C (2007) Cycling of O-linked beta-N-acetylglucosamine on nucleocytoplasmic proteins. *Nature* 446(7139):1017-1022.
24. Holt GD & Hart GW (1986) The subcellular distribution of terminal N-acetylglucosamine moieties. Localization of a novel protein-saccharide linkage, O-linked GlcNAc. *J Biol Chem* 261(17):8049-8057.
25. Zhang F*, et al.* (2003) O-GlcNAc modification is an endogenous inhibitor of the proteasome. *Cell* 115(6):715-725.
26. Zeidan Q, Wang Z, De Maio A, & Hart GW (2010) O-GlcNAc cycling enzymes associate with the translational machinery and modify core ribosomal proteins. *Mol Biol Cell* 21(12):1922-1936.
27. Roquemore EP, Chevrier MR, Cotter RJ, & Hart GW (1996) Dynamic O-GlcNAcylation of the small heat shock protein alpha B-crystallin. *Biochemistry* 35(11):3578-3586.
28. Holt GD*, et al.* (1987) Nuclear pore complex glycoproteins contain cytoplasmically disposed O-linked N-acetylglucosamine. *J Cell Biol* 104(5):1157-1164.
29. Miller MW, Caracciolo MR, Berlin WK, & Hanover JA (1999) Phosphorylation and glycosylation of nucleoporins. *Arch Biochem Biophys* 367(1):51-60.
30. Zachara NE*, et al.* (2004) Dynamic O-GlcNAc modification of nucleocytoplasmic proteins in response to stress. A survival response of mammalian cells. *J Biol Chem* 279(29):30133-30142.
31. Kearse KP & Hart GW (1991) Lymphocyte activation induces rapid changes in nuclear and cytoplasmic glycoproteins. *Proc Natl Acad Sci U S A* 88(5):1701-1705.
32. Carrillo LD, Froemming JA, & Mahal LK (2011) Targeted in vivo O-GlcNAc sensors reveal discrete compartment-specific dynamics during signal transduction. *J Biol Chem* 286(8):6650-6658.
33. Whelan SA, Dias WB, Thiruneelakantapillai L, Lane MD, & Hart GW (2010) Regulation of insulin receptor substrate 1 (IRS-1)/AKT kinase-mediated insulin

signaling by O-Linked beta-N-acetylglucosamine in 3T3-L1 adipocytes. *J Biol Chem* 285(8):5204-5211.
34. Whelan SA, Lane MD, & Hart GW (2008) Regulation of the O-linked beta-N-acetylglucosamine transferase by insulin signaling. *J Biol Chem* 283(31):21411-21417.
35. Cheung WD & Hart GW (2008) AMP-activated protein kinase and p38 MAPK activate O-GlcNAcylation of neuronal proteins during glucose deprivation. *J Biol Chem* 283(19):13009-13020.
36. Housley MP*, et al.* (2009) A PGC-1alpha-O-GlcNAc transferase complex regulates FoxO transcription factor activity in response to glucose. *J Biol Chem* 284(8):5148-5157.
37. Haltiwanger RS, Holt GD, & Hart GW (1990) Enzymatic addition of O-GlcNAc to nuclear and cytoplasmic proteins. Identification of a uridine diphospho-N-acetylglucosamine:peptide beta-N-acetylglucosaminyltransferase. *J Biol Chem* 265(5):2563-2568.
38. Dong DL & Hart GW (1994) Purification and characterization of an O-GlcNAc selective N-acetyl-beta-D-glucosaminidase from rat spleen cytosol. *J Biol Chem* 269(30):19321-19330.
39. Gao Y, Wells L, Comer FI, Parker GJ, & Hart GW (2001) Dynamic O-glycosylation of nuclear and cytosolic proteins: cloning and characterization of a neutral, cytosolic beta-N-acetylglucosaminidase from human brain. *J Biol Chem* 276(13):9838-9845.
40. Shafi R*, et al.* (2000) The O-GlcNAc transferase gene resides on the X chromosome and is essential for embryonic stem cell viability and mouse ontogeny. *Proc Natl Acad Sci U S A* 97(11):5735-5739.
41. Nolte D & Muller U (2002) Human O-GlcNAc transferase (OGT): genomic structure, analysis of splice variants, fine mapping in Xq13.1. *Mamm Genome* 13(1):62-64.
42. Muller U, Steinberger D, & Nemeth AH (1998) Clinical and molecular genetics of primary dystonias. *Neurogenetics* 1(3):165-177.
43. Hanover JA*, et al.* (2003) Mitochondrial and nucleocytoplasmic isoforms of O-linked GlcNAc transferase encoded by a single mammalian gene. *Arch Biochem Biophys* 409(2):287-297.
44. Iyer SP & Hart GW (2003) Roles of the tetratricopeptide repeat domain in O-GlcNAc transferase targeting and protein substrate specificity. *J Biol Chem* 278(27):24608-24616.
45. Kreppel LK & Hart GW (1999) Regulation of a cytosolic and nuclear O-GlcNAc transferase. Role of the tetratricopeptide repeats. *J Biol Chem* 274(45):32015-32022.
46. Jinek M*, et al.* (2004) The superhelical TPR-repeat domain of O-linked GlcNAc transferase exhibits structural similarities to importin alpha. *Nat Struct Mol Biol* 11(10):1001-1007.
47. Lazarus MB, Nam Y, Jiang J, Sliz P, & Walker S (2011) Structure of human O-GlcNAc transferase and its complex with a peptide substrate. *Nature* 469(7331):564-567.

48. Yang X, *et al.* (2008) Phosphoinositide signalling links O-GlcNAc transferase to insulin resistance. *Nature* 451(7181):964-969.
49. Banerjee PS, Hart GW, & Cho JW (2013) Chemical approaches to study O-GlcNAcylation. *Chem Soc Rev* 42(10):4345-4357.
50. Marz P, *et al.* (2006) Ataxin-10 interacts with O-linked beta-N-acetylglucosamine transferase in the brain. *J Biol Chem* 281(29):20263-20270.
51. Liu Y, *et al.* (2012) Developmental regulation of protein O-GlcNAcylation, O-GlcNAc transferase, and O-GlcNAcase in mammalian brain. *PLoS One* 7(8):e43724.
52. Haltiwanger RS, Blomberg MA, & Hart GW (1992) Glycosylation of nuclear and cytoplasmic proteins. Purification and characterization of a uridine diphospho-N-acetylglucosamine:polypeptide beta-N-acetylglucosaminyltransferase. *J Biol Chem* 267(13):9005-9013.
53. Shen DL, Gloster TM, Yuzwa SA, & Vocadlo DJ (2012) Insights into O-linked N-acetylglucosamine ([0-9]O-GlcNAc) processing and dynamics through kinetic analysis of O-GlcNAc transferase and O-GlcNAcase activity on protein substrates. *J Biol Chem* 287(19):15395-15408.
54. Cheung WD, Sakabe K, Housley MP, Dias WB, & Hart GW (2008) O-linked beta-N-acetylglucosaminyltransferase substrate specificity is regulated by myosin phosphatase targeting and other interacting proteins. *J Biol Chem* 283(49):33935-33941.
55. Yang X, Zhang F, & Kudlow JE (2002) Recruitment of O-GlcNAc transferase to promoters by corepressor mSin3A: coupling protein O-GlcNAcylation to transcriptional repression. *Cell* 110(1):69-80.
56. Song M, *et al.* (2008) o-GlcNAc transferase is activated by CaMKIV-dependent phosphorylation under potassium chloride-induced depolarization in NG-108-15 cells. *Cell Signal* 20(1):94-104.
57. Bullen JW, *et al.* (2014) Cross-talk between two essential nutrient-sensitive enzymes: O-GlcNAc transferase (OGT) and AMP-activated protein kinase (AMPK). *J Biol Chem* 289(15):10592-10606.
58. Li X, Lu F, Wang JZ, & Gong CX (2006) Concurrent alterations of O-GlcNAcylation and phosphorylation of tau in mouse brains during fasting. *Eur J Neurosci* 23(8):2078-2086.
59. Heckel D, *et al.* (1998) Novel immunogenic antigen homologous to hyaluronidase in meningioma. *Hum Mol Genet* 7(12):1859-1872.
60. Bertram L, *et al.* (2000) Evidence for genetic linkage of Alzheimer's disease to chromosome 10q. *Science* 290(5500):2302-2303.
61. Twine NA, Janitz K, Wilkins MR, & Janitz M (2011) Whole transcriptome sequencing reveals gene expression and splicing differences in brain regions affected by Alzheimer's disease. *PLoS One* 6(1):e16266.
62. Dennis RJ, *et al.* (2006) Structure and mechanism of a bacterial beta-glucosaminidase having O-GlcNAcase activity. *Nat Struct Mol Biol* 13(4):365-371.
63. Butkinaree C, *et al.* (2008) Characterization of beta-N-acetylglucosaminidase cleavage by caspase-3 during apoptosis. *J Biol Chem* 283(35):23557-23566.

64. Toleman C, Paterson AJ, Whisenhunt TR, & Kudlow JE (2004) Characterization of the Histone Acetyltransferase (HAT) Domain of a Bifunctional Protein with Activable O-GlcNAcase and HAT Activities. *Journal of Biological Chemistry* 279(51):53665-53673.
65. Toleman CA, Paterson AJ, & Kudlow JE (2006) The histone acetyltransferase NCOAT contains a zinc finger-like motif involved in substrate recognition. *J Biol Chem* 281(7):3918-3925.
66. Yuzwa SA*, et al.* (2008) A potent mechanism-inspired O-GlcNAcase inhibitor that blocks phosphorylation of tau in vivo. *Nat Chem Biol* 4(8):483-490.
67. Lubas WA, Frank DW, Krause M, & Hanover JA (1997) O-Linked GlcNAc transferase is a conserved nucleocytoplasmic protein containing tetratricopeptide repeats. *J Biol Chem* 272(14):9316-9324.
68. Cole RN & Hart GW (2001) Cytosolic O-glycosylation is abundant in nerve terminals. *J Neurochem* 79(5):1080-1089.
69. Akimoto Y*, et al.* (2003) Localization of the O-GlcNAc transferase and O-GlcNAc-modified proteins in rat cerebellar cortex. *Brain Res* 966(2):194-205.
70. Wang Z*, et al.* (2010) Extensive crosstalk between O-GlcNAcylation and phosphorylation regulates cytokinesis. *Sci Signal* 3(104):ra2.
71. Khidekel N*, et al.* (2007) Probing the dynamics of O-GlcNAc glycosylation in the brain using quantitative proteomics. *Nat Chem Biol* 3(6):339-348.
72. Rexach JE*, et al.* (2010) Quantification of O-glycosylation stoichiometry and dynamics using resolvable mass tags. *Nat Chem Biol* 6(9):645-651.
73. Lisman J, Schulman H, & Cline H (2002) The molecular basis of CaMKII function in synaptic and behavioural memory. *Nat Rev Neurosci* 3(3):175-190.
74. Dias WB & Hart GW (2007) O-GlcNAc modification in diabetes and Alzheimer's disease. *Mol Biosyst* 3(11):766-772.
75. Kelly WG, Dahmus ME, & Hart GW (1993) RNA polymerase II is a glycoprotein. Modification of the COOH-terminal domain by O-GlcNAc. *J Biol Chem* 268(14):10416-10424.
76. Comer FI & Hart GW (1999) O-GlcNAc and the control of gene expression. *Biochim Biophys Acta* 1473(1):161-171.
77. Ranuncolo SM, Ghosh S, Hanover JA, Hart GW, & Lewis BA (2012) Evidence of the involvement of O-GlcNAc-modified human RNA polymerase II CTD in transcription in vitro and in vivo. *J Biol Chem* 287(28):23549-23561.
78. Sakabe K, Wang Z, & Hart GW (2010) Beta-N-acetylglucosamine (O-GlcNAc) is part of the histone code. *Proc Natl Acad Sci U S A* 107(46):19915-19920.
79. Fujiki R*, et al.* (2011) GlcNAcylation of histone H2B facilitates its monoubiquitination. *Nature* 480(7378):557-560.
80. Ozcan S, Andrali SS, & Cantrell JE (2010) Modulation of transcription factor function by O-GlcNAc modification. *Biochim Biophys Acta* 1799(5-6):353-364.
81. Andrali SS, Qian Q, & Ozcan S (2007) Glucose mediates the translocation of NeuroD1 by O-linked glycosylation. *J Biol Chem* 282(21):15589-15596.
82. Jang H*, et al.* (2012) O-GlcNAc regulates pluripotency and reprogramming by directly acting on core components of the pluripotency network. *Cell Stem Cell* 11(1):62-74.

83. Datta B, Ray MK, Chakrabarti D, Wylie DE, & Gupta NK (1989) Glycosylation of eukaryotic peptide chain initiation factor 2 (eIF-2)-associated 67-kDa polypeptide (p67) and its possible role in the inhibition of eIF-2 kinase-catalyzed phosphorylation of the eIF-2 alpha-subunit. *J Biol Chem* 264(34):20620-20624.
84. Ray MK*, et al.* (1992) The eukaryotic initiation factor 2-associated 67-kDa polypeptide (p67) plays a critical role in regulation of protein synthesis initiation in animal cells. *Proc Natl Acad Sci U S A* 89(2):539-543.
85. Sayat R, Leber B, Grubac V, Wiltshire L, & Persad S (2008) O-GlcNAc-glycosylation of beta-catenin regulates its nuclear localization and transcriptional activity. *Exp Cell Res* 314(15):2774-2787.
86. Geng F, Zhu W, Anderson RA, Leber B, & Andrews DW (2012) Multiple post-translational modifications regulate E-cadherin transport during apoptosis. *J Cell Sci* 125(Pt 11):2615-2625.
87. Fiederling A, Ewert R, Andreyeva A, Jungling K, & Gottmann K (2011) E-cadherin is required at GABAergic synapses in cultured cortical neurons. *Neurosci Lett* 501(3):167-172.
88. Clark PM*, et al.* (2008) Direct in-gel fluorescence detection and cellular imaging of O-GlcNAc-modified proteins. *J Am Chem Soc* 130(35):11576-11577.
89. Guinez C*, et al.* (2008) Protein ubiquitination is modulated by O-GlcNAc glycosylation. *FASEB J* 22(8):2901-2911.
90. Chou TY, Dang CV, & Hart GW (1995) Glycosylation of the c-Myc transactivation domain. *Proc Natl Acad Sci U S A* 92(10):4417-4421.
91. Chou TY, Hart GW, & Dang CV (1995) c-Myc is glycosylated at threonine 58, a known phosphorylation site and a mutational hot spot in lymphomas. *J Biol Chem* 270(32):18961-18965.
92. Dias WB, Cheung WD, Wang Z, & Hart GW (2009) Regulation of calcium/calmodulin-dependent kinase IV by O-GlcNAc modification. *J Biol Chem* 284(32):21327-21337.
93. Wang Z, Gucek M, & Hart GW (2008) Cross-talk between GlcNAcylation and phosphorylation: site-specific phosphorylation dynamics in response to globally elevated O-GlcNAc. *Proc Natl Acad Sci U S A* 105(37):13793-13798.
94. Dias WB, Cheung WD, & Hart GW (2012) O-GlcNAcylation of kinases. *Biochem Biophys Res Commun* 422(2):224-228.
95. Slawson C*, et al.* (2005) Perturbations in O-linked beta-N-acetylglucosamine protein modification cause severe defects in mitotic progression and cytokinesis. *J Biol Chem* 280(38):32944-32956.
96. Slawson C, Lakshmanan T, Knapp S, & Hart GW (2008) A mitotic GlcNAcylation/phosphorylation signaling complex alters the posttranslational state of the cytoskeletal protein vimentin. *Mol Biol Cell* 19(10):4130-4140.
97. Wang P*, et al.* (2012) O-GlcNAc cycling mutants modulate proteotoxicity in Caenorhabditis elegans models of human neurodegenerative diseases. *Proc Natl Acad Sci U S A* 109(43):17669-17674.
98. Francisco H*, et al.* (2009) O-GLcNAc post-translational modifications regulate the entry of neurons into an axon branching program. *Dev Neurobiol* 69(2-3):162-173.

99. Hanley JG (2008) AMPA receptor trafficking pathways and links to dendritic spine morphogenesis. *Cell Adh Migr* 2(4):276-282.
100. Lynch MA (2004) Long-term potentiation and memory. *Physiol Rev* 84(1):87-136.
101. Verpelli C & Sala C (2012) Molecular and synaptic defects in intellectual disability syndromes. *Curr Opin Neurobiol* 22(3):530-536.
102. Grant SG (2012) Synaptopathies: diseases of the synaptome. *Curr Opin Neurobiol* 22(3):522-529.
103. Shepherd JD & Huganir RL (2007) The cell biology of synaptic plasticity: AMPA receptor trafficking. *Annu Rev Cell Dev Biol* 23:613-643.
104. Kanno T, Yaguchi T, Nagata T, Mukasa T, & Nishizaki T (2010) Regulation of AMPA receptor trafficking by O-glycosylation. *Neurochem Res* 35(5):782-788.
105. Koffie RM, Hyman BT, & Spires-Jones TL (2011) Alzheimer's disease: synapses gone cold. *Mol Neurodegener* 6(1):63.
106. Schulz-Schaeffer WJ (2010) The synaptic pathology of alpha-synuclein aggregation in dementia with Lewy bodies, Parkinson's disease and Parkinson's disease dementia. *Acta Neuropathol* 120(2):131-143.
107. Griffith LS, Mathes M, & Schmitz B (1995) Beta-amyloid precursor protein is modified with O-linked N-acetylglucosamine. *J Neurosci Res* 41(2):270-278.
108. Biessels GJ, Staekenborg S, Brunner E, Brayne C, & Scheltens P (2006) Risk of dementia in diabetes mellitus: a systematic review. *Lancet Neurol* 5(1):64-74.
109. de la Monte SM & Wands JR (2008) Alzheimer's disease is type 3 diabetes-evidence reviewed. *J Diabetes Sci Technol* 2(6):1101-1113.
110. Kazemi Z, Chang H, Haserodt S, McKen C, & Zachara NE (2010) O-linked beta-N-acetylglucosamine (O-GlcNAc) regulates stress-induced heat shock protein expression in a GSK-3beta-dependent manner. *J Biol Chem* 285(50):39096-39107.
111. Bailey CH & Kandel ER (1993) Structural changes accompanying memory storage. *Annu Rev Physiol* 55:397-426.
112. Bhatt DH, Zhang S, & Gan WB (2009) Dendritic spine dynamics. *Annu Rev Physiol* 71:261-282.
113. Zuo Y, Lin A, Chang P, & Gan WB (2005) Development of long-term dendritic spine stability in diverse regions of cerebral cortex. *Neuron* 46(2):181-189.
114. McKinney RA (2010) Excitatory amino acid involvement in dendritic spine formation, maintenance and remodelling. *J Physiol* 588(Pt 1):107-116.
115. Trachtenberg JT*, et al.* (2002) Long-term in vivo imaging of experience-dependent synaptic plasticity in adult cortex. *Nature* 420(6917):788-794.
116. Lai KO & Ip NY (2013) Structural plasticity of dendritic spines: the underlying mechanisms and its dysregulation in brain disorders. *Biochim Biophys Acta* 1832(12):2257-2263.
117. Holtmaat AJ*, et al.* (2005) Transient and persistent dendritic spines in the neocortex in vivo. *Neuron* 45(2):279-291.
118. Zuo Y, Yang G, Kwon E, & Gan WB (2005) Long-term sensory deprivation prevents dendritic spine loss in primary somatosensory cortex. *Nature* 436(7048):261-265.

119. Chen CC, Lu J, & Zuo Y (2014) Spatiotemporal dynamics of dendritic spines in the living brain. *Front Neuroanat* 8:28.
120. Sanders J, Cowansage K, Baumgartel K, & Mayford M (2012) Elimination of dendritic spines with long-term memory is specific to active circuits. *J Neurosci* 32(36):12570-12578.
121. Knott GW, Holtmaat A, Wilbrecht L, Welker E, & Svoboda K (2006) Spine growth precedes synapse formation in the adult neocortex in vivo. *Nat Neurosci* 9(9):1117-1124.
122. Lohmann C & Bonhoeffer T (2008) A role for local calcium signaling in rapid synaptic partner selection by dendritic filopodia. *Neuron* 59(2):253-260.
123. Yoshihara Y, De Roo M, & Muller D (2009) Dendritic spine formation and stabilization. *Curr Opin Neurobiol* 19(2):146-153.
124. De Roo M, Klauser P, Mendez P, Poglia L, & Muller D (2008) Activity-dependent PSD formation and stabilization of newly formed spines in hippocampal slice cultures. *Cereb Cortex* 18(1):151-161.
125. Xu T*, et al.* (2009) Rapid formation and selective stabilization of synapses for enduring motor memories. *Nature* 462(7275):915-919.
126. Yang G, Pan F, & Gan WB (2009) Stably maintained dendritic spines are associated with lifelong memories. *Nature* 462(7275):920-924.
127. Roberts TF, Tschida KA, Klein ME, & Mooney R (2010) Rapid spine stabilization and synaptic enhancement at the onset of behavioural learning. *Nature* 463(7283):948-952.
128. Jontes JD & Phillips GR (2006) Selective stabilization and synaptic specificity: a new cell-biological model. *Trends Neurosci* 29(4):186-191.
129. Bednarek E & Caroni P (2011) beta-Adducin is required for stable assembly of new synapses and improved memory upon environmental enrichment. *Neuron* 69(6):1132-1146.
130. Pan F, Aldridge GM, Greenough WT, & Gan WB (2010) Dendritic spine instability and insensitivity to modulation by sensory experience in a mouse model of fragile X syndrome. *Proc Natl Acad Sci U S A* 107(41):17768-17773.
131. Nakamura K*, et al.* (2001) Enhancement of hippocampal LTP, reference memory and sensorimotor gating in mutant mice lacking a telencephalon-specific cell adhesion molecule. *Eur J Neurosci* 13(1):179-189.
132. De Roo M, Klauser P, & Muller D (2008) LTP promotes a selective long-term stabilization and clustering of dendritic spines. *PLoS Biol* 6(9):e219.
133. Ehrlich I, Klein M, Rumpel S, & Malinow R (2007) PSD-95 is required for activity-driven synapse stabilization. *Proc Natl Acad Sci U S A* 104(10):4176-4181.
134. Hill TC & Zito K (2013) LTP-induced long-term stabilization of individual nascent dendritic spines. *J Neurosci* 33(2):678-686.
135. Engert F & Bonhoeffer T (1999) Dendritic spine changes associated with hippocampal long-term synaptic plasticity. *Nature* 399(6731):66-70.
136. Bagal AA, Kao JP, Tang CM, & Thompson SM (2005) Long-term potentiation of exogenous glutamate responses at single dendritic spines. *Proc Natl Acad Sci U S A* 102(40):14434-14439.

137. Lu W, *et al.* (2009) Subunit composition of synaptic AMPA receptors revealed by a single-cell genetic approach. *Neuron* 62(2):254-268.
138. Saglietti L, *et al.* (2007) Extracellular interactions between GluR2 and N-cadherin in spine regulation. *Neuron* 54(3):461-477.
139. Tracy TE, Yan JJ, & Chen L (2011) Acute knockdown of AMPA receptors reveals a trans-synaptic signal for presynaptic maturation. *EMBO J* 30(8):1577-1592.
140. Sia GM, *et al.* (2007) Interaction of the N-terminal domain of the AMPA receptor GluR4 subunit with the neuronal pentraxin NP1 mediates GluR4 synaptic recruitment. *Neuron* 55(1):87-102.
141. Zito K, Scheuss V, Knott G, Hill T, & Svoboda K (2009) Rapid functional maturation of nascent dendritic spines. *Neuron* 61(2):247-258.
142. Zhang Y, Cudmore RH, Lin DT, Linden DJ, & Huganir RL (2015) Visualization of NMDA receptor-dependent AMPA receptor synaptic plasticity in vivo. *Nat Neurosci* 18(3):402-407.
143. Takumi Y, Ramirez-Leon V, Laake P, Rinvik E, & Ottersen OP (1999) Different modes of expression of AMPA and NMDA receptors in hippocampal synapses. *Nat Neurosci* 2(7):618-624.
144. Groc L, Gustafsson B, & Hanse E (2006) AMPA signalling in nascent glutamatergic synapses: there and not there! *Trends Neurosci* 29(3):132-139.
145. McKinney RA, Capogna M, Durr R, Gahwiler BH, & Thompson SM (1999) Miniature synaptic events maintain dendritic spines via AMPA receptor activation. *Nat Neurosci* 2(1):44-49.
146. Matsuzaki M, Honkura N, Ellis-Davies GC, & Kasai H (2004) Structural basis of long-term potentiation in single dendritic spines. *Nature* 429(6993):761-766.
147. Mateos JM, *et al.* (2007) Synaptic modifications at the CA3-CA1 synapse after chronic AMPA receptor blockade in rat hippocampal slices. *J Physiol* 581(Pt 1):129-138.
148. Kang MG, Guo Y, & Huganir RL (2009) AMPA receptor and GEF-H1/Lfc complex regulates dendritic spine development through RhoA signaling cascade. *Proc Natl Acad Sci U S A* 106(9):3549-3554.
149. Tada T & Sheng M (2006) Molecular mechanisms of dendritic spine morphogenesis. *Curr Opin Neurobiol* 16(1):95-101.
150. Fortin DA, *et al.* (2010) Long-term potentiation-dependent spine enlargement requires synaptic Ca2+-permeable AMPA receptors recruited by CaM-kinase I. *J Neurosci* 30(35):11565-11575.
151. Patterson MA, Szatmari EM, & Yasuda R (2010) AMPA receptors are exocytosed in stimulated spines and adjacent dendrites in a Ras-ERK-dependent manner during long-term potentiation. *Proc Natl Acad Sci U S A* 107(36):15951-15956.
152. Kennedy MJ, Davison IG, Robinson CG, & Ehlers MD (2010) Syntaxin-4 defines a domain for activity-dependent exocytosis in dendritic spines. *Cell* 141(3):524-535.
153. Anggono V & Huganir RL (2012) Regulation of AMPA receptor trafficking and synaptic plasticity. *Curr Opin Neurobiol* 22(3):461-469.

154. Lu W & Roche KW (2012) Posttranslational regulation of AMPA receptor trafficking and function. *Curr Opin Neurobiol* 22(3):470-479.
155. Nakagawa T, Cheng Y, Ramm E, Sheng M, & Walz T (2005) Structure and different conformational states of native AMPA receptor complexes. *Nature* 433(7025):545-549.
156. Fukaya M*, et al.* (2006) Abundant distribution of TARP gamma-8 in synaptic and extrasynaptic surface of hippocampal neurons and its major role in AMPA receptor expression on spines and dendrites. *Eur J Neurosci* 24(8):2177-2190.
157. Granger AJ, Shi Y, Lu W, Cerpas M, & Nicoll RA (2013) LTP requires a reserve pool of glutamate receptors independent of subunit type. *Nature* 493(7433):495-500.
158. Lee HK*, et al.* (2003) Phosphorylation of the AMPA receptor GluR1 subunit is required for synaptic plasticity and retention of spatial memory. *Cell* 112(5):631-643.
159. Kessels HW & Malinow R (2009) Synaptic AMPA receptor plasticity and behavior. *Neuron* 61(3):340-350.
160. Clem RL & Barth A (2006) Pathway-specific trafficking of native AMPARs by in vivo experience. *Neuron* 49(5):663-670.
161. Clem RL & Huganir RL (2010) Calcium-permeable AMPA receptor dynamics mediate fear memory erasure. *Science* 330(6007):1108-1112.
162. Sharma K*, et al.* (2013) High-throughput genetic screen for synaptogenic factors: identification of LRP6 as critical for excitatory synapse development. *Cell Rep* 5(5):1330-1341.
163. Lewis CE*, et al.* (2009) Mortality, health outcomes, and body mass index in the overweight range: a science advisory from the American Heart Association. *Circulation* 119(25):3263-3271.
164. Gustavsson A*, et al.* (2011) Cost of disorders of the brain in Europe 2010. *Eur Neuropsychopharmacol* 21(10):718-779.
165. Sohn JW, Elmquist JK, & Williams KW (2013) Neuronal circuits that regulate feeding behavior and metabolism. *Trends Neurosci* 36(9):504-512.
166. van Gestel MA, Kostrzewa E, Adan RA, & Janhunen SK (2014) Pharmacological manipulations in animal models of anorexia and binge eating in relation to humans. *Br J Pharmacol* 171(20):4767-4784.
167. Salamone JD & Correa M (2013) Dopamine and food addiction: lexicon badly needed. *Biol Psychiatry* 73(9):e15-24.
168. De Silva A, Salem V, Matthews PM, & Dhillo WS (2012) The use of functional MRI to study appetite control in the CNS. *Exp Diabetes Res* 2012:764017.
169. Williams KW & Elmquist JK (2012) From neuroanatomy to behavior: central integration of peripheral signals regulating feeding behavior. *Nat Neurosci* 15(10):1350-1355.
170. von Hausswolff-Juhlin Y, Brooks SJ, & Larsson M (2015) The neurobiology of eating disorders--a clinical perspective. *Acta Psychiatr Scand* 131(4):244-255.
171. Ben-Tovim DI*, et al.* (2001) Outcome in patients with eating disorders: a 5-year study. *The Lancet* 357(9264):1254-1257.

172. Halmi KA*, et al.* (2002) Relapse predictors of patients with bulimia nervosa who achieved abstinence through cognitive behavioral therapy. *Arch Gen Psychiatry* 59(12):1105-1109.
173. Morton GJ, Meek TH, & Schwartz MW (2014) Neurobiology of food intake in health and disease. *Nat Rev Neurosci* 15(6):367-378.
174. Wu Q, Boyle MP, & Palmiter RD (2009) Loss of GABAergic signaling by AgRP neurons to the parabrachial nucleus leads to starvation. *Cell* 137(7):1225-1234.
175. Betley JN, Cao ZF, Ritola KD, & Sternson SM (2013) Parallel, redundant circuit organization for homeostatic control of feeding behavior. *Cell* 155(6):1337-1350.
176. Speliotes EK*, et al.* (2010) Association analyses of 249,796 individuals reveal 18 new loci associated with body mass index. *Nat Genet* 42(11):937-948.
177. Gutierrez-Aguilar R, Kim DH, Woods SC, & Seeley RJ (2012) Expression of new loci associated with obesity in diet-induced obese rats: from genetics to physiology. *Obesity (Silver Spring)* 20(2):306-312.
178. Wolosker H*, et al.* (1998) Molecularly cloned mammalian glucosamine-6-phosphate deaminase localizes to transporting epithelium and lacks oscillin activity. *FASEB J* 12(1):91-99.
179. Ruan HB*, et al.* (2014) O-GlcNAc transferase enables AgRP neurons to suppress browning of white fat. *Cell* 159(2):306-317.
180. Vijayan E & McCann SM (1977) Suppression of feeding and drinking activity in rats following intraventricular injection of thyrotropin releasing hormone (TRH). *Endocrinology* 100(6):1727-1730.
181. Steffens AB, Scheurink AJ, Porte D, Jr., & Woods SC (1988) Penetration of peripheral glucose and insulin into cerebrospinal fluid in rats. *Am J Physiol* 255(2 Pt 2):R200-204.
182. Pekkurnaz G, Trinidad JC, Wang X, Kong D, & Schwarz TL (2014) Glucose regulates mitochondrial motility via Milton modification by O-GlcNAc transferase. *Cell* 158(1):54-68.
183. Karnani M & Burdakov D (2011) Multiple hypothalamic circuits sense and regulate glucose levels. *Am J Physiol Regul Integr Comp Physiol* 300(1):R47-55.
184. Sutton AK*, et al.* (2014) Control of food intake and energy expenditure by Nos1 neurons of the paraventricular hypothalamus. *J Neurosci* 34(46):15306-15318.
185. Xu Y*, et al.* (2013) Glutamate mediates the function of melanocortin receptor 4 on Sim1 neurons in body weight regulation. *Cell Metab* 18(6):860-870.
186. Wallen-Mackenzie A*, et al.* (2009) Restricted cortical and amygdaloid removal of vesicular glutamate transporter 2 in preadolescent mice impacts dopaminergic activity and neuronal circuitry of higher brain function. *J Neurosci* 29(7):2238-2251.
187. American Diabetes A (2001) Postprandial blood glucose. American Diabetes Association. *Diabetes Care* 24(4):775-778.
188. Erdmann G, Schutz G, & Berger S (2007) Inducible gene inactivation in neurons of the adult mouse forebrain. *BMC Neurosci* 8:63.
189. Takamiya K, Mao L, Huganir RL, & Linden DJ (2008) The glutamate receptor-interacting protein family of GluR2-binding proteins is required for long-term synaptic depression expression in cerebellar Purkinje cells. *J Neurosci* 28(22):5752-5755.

190. Shimogori T*, et al.* (2010) A genomic atlas of mouse hypothalamic development. *Nat Neurosci* 13(6):767-775.
191. Blackshaw S (2013) High-throughput RNA in situ hybridization in mouse retina. *Methods Mol Biol* 935:215-226.
192. Aponte Y, Atasoy D, & Sternson SM (2011) AGRP neurons are sufficient to orchestrate feeding behavior rapidly and without training. *Nat Neurosci* 14(3):351-355.
193. Vosseller K*, et al.* (2006) O-linked N-acetylglucosamine proteomics of postsynaptic density preparations using lectin weak affinity chromatography and mass spectrometry. *Mol Cell Proteomics* 5(5):923-934.
194. Taylor EW*, et al.* (2014) O-GlcNAcylation of AMPA receptor GluA2 is associated with a novel form of long-term depression at hippocampal synapses. *J Neurosci* 34(1):10-21.
195. Wenthold RJ, Petralia RS, Blahos J, II, & Niedzielski AS (1996) Evidence for multiple AMPA receptor complexes in hippocampal CA1/CA2 neurons. *J Neurosci* 16(6):1982-1989.
196. Gerrow K*, et al.* (2006) A preformed complex of postsynaptic proteins is involved in excitatory synapse development. *Neuron* 49(4):547-562.
197. McAllister AK (2007) Dynamic aspects of CNS synapse formation. *Annu Rev Neurosci* 30:425-450.
198. Zhu JJ, Esteban JA, Hayashi Y, & Malinow R (2000) Postnatal synaptic potentiation: delivery of GluR4-containing AMPA receptors by spontaneous activity. *Nat Neurosci* 3(11):1098-1106.
199. Isaac JT, Ashby MC, & McBain CJ (2007) The role of the GluR2 subunit in AMPA receptor function and synaptic plasticity. *Neuron* 54(6):859-871.
200. Pickard L, Noel J, Henley JM, Collingridge GL, & Molnar E (2000) Developmental changes in synaptic AMPA and NMDA receptor distribution and AMPA receptor subunit composition in living hippocampal neurons. *J Neurosci* 20(21):7922-7931.
201. Shi S, Hayashi Y, Esteban JA, & Malinow R (2001) Subunit-specific rules governing AMPA receptor trafficking to synapses in hippocampal pyramidal neurons. *Cell* 105(3):331-343.
202. Takahashi T, Svoboda K, & Malinow R (2003) Experience strengthening transmission by driving AMPA receptors into synapses. *Science* 299(5612):1585-1588.

CURRICULUM VITAE

Karl Olof Lagerlöf

15 Charles Plaza, apt. 1504 klagerl1@jhmi.edu
Baltimore, Maryland, 21201
Born: 27 July 1983, Mölndal, Sweden

EDUCATION

Ph.D.	**2010-*present***	**Program in Biochemistry, Cellular and Molecular Biology (BCMB), Departments of Biological Chemistry and Neuroscience, Johns Hopkins University School of Medicine (JHU SOM), Baltimore, MD U.S.A.** **Mentors: Gerald W. Hart, Ph.D., and Richard L. Huganir, Ph.D.** Thesis: On the regulation of excitatory synapses and feeding behavior by O-GlcNAc transferase *Anticipated graduation February 2016*
M.D.	2002-2010	Gothenburg University, Sweden
B.A.	2007-2009	Cambridge University, England Philosophy
M.S.	2007	Gothenburg University, Sweden Human Biology

RESEARCH EXPERIENCE

Research

2010-2016 Johns Hopkins University

Mentors: Dr Richard L. Huganir & Dr Gerald W. Hart

2009 **Harvard University**

Mentors: Dr Margaret A. Niznikiewicz & Dr Robert W. McCarley

2007 **Yale University**

Mentor: Dr Michael J. Caplan

2002-2008 **Gothenburg University**

Mentors: Dr Susann Teneberg & Dr Thomas Jansson

Clinical Work

2008-2010 **Physician ('Underläkare'), Sahlgrenska University Hospital**

Department of Psychiatry, during summer and winter breaks from school. (NB: In Sweden senior medical students may be given a temporary doctor's license by the Swedish Health Care authorities)

2004 **Khartoum Teaching Hospital, Sudan**

Assisting as a medical student the general surgeon and worked for a program providing free clinical consultation on the Sudanese countryside

Publications

Biomedical research

1. **Lagerlöf O**, Slocomb J, Hong I, Aponte Y, Blackshaw S, Hart GW, Huganir RL. The nutrient sensor OGT in PVN neurons regulates feeding. In press (*Science*)

2. **Lagerlöf O**, Hart GW, Huganir RL. OGT is a synaptic proteins that regulates excitatory synapse maturity. In preparation

3. **Lagerlöf O** and Hart GW (2014). O-GlcNAcylation of Neuronal Proteins: Roles in Neuronal Functions and in Neurodegeneration. *Book Chapter in the book 'Glycobiology of the nervous system'*. Springer

4. Prendergast J, Umanah GK, Yoo SW, **Lagerlöf O**, Motari MG, Cole RN, Huganir RL, Dawson TM, Dawson VL, Schnaar RL (2014). Ganglioside regulation of AMPA receptor trafficking. *J Neurosci*

5. Hart GW, Slawson C, Ramirez-Correa G, **Lagerlöf O** (2011). Cross Talk Between O-GlcNAcylation and Phosphorylation: Roles in Signaling, Transcription, and Chronic Disease. *Annu Rev Biochem*

6. Roos S, **Lagerlöf O**, Wennergren M, Powell T, Jansson T (2009). Regulation of amino acid transporters by glucose and growth factors in cultured primary trophoblast cells is mediated by mTOR signaling. *Am J Physiol Cell Physiol*

Medical/Education policy

1. **Lagerlöf O**, Sallin K, Friberg P (2009). Grades should be used in Swedish medical schools. *Läkartidningen* (Sweden's leading health care journal)

2. **Lagerlöf O** and Olsson D (2008). A new medical student research program in Goteborg. *SLS Aktuellt* (Swedish health care journal)

Awards and Honors

2015 **Young Investigator Award, Johns Hopkins University**

The Nupur Dinesh Thekdi Award, for excellence in research

2013 **Marine Biological Laboratory, Woods Hole**

Research and academic scholarship

2010 **Johns Hopkins University**

Full graduate scholarship

Adlerbertska Foundation Award

Scholarship for academic excellence

2009 **Harvard University Medical School**

Research scholarship

Adlerbertska Foundation Award

Scholarship for academic excellence

Cambridge University

The Worts Travelling Scholars Fund Award

Cambridge University

St Edmund's College Tutorial Award

Wilhelm and Martina Lundgrens Science Foundation Award

Research scholarship

Stiftelsen Längmanska Kulturfonden

Research award

2008 **Cambridge University**

Cambridge European Trust Award

Glycoconjugates in Biological Systems (GLIBS) Scholarship

Travel award

Willinska Foundation Award

Research scholarship

2007	**Cambridge University**
	Cambridge European Trust Award,
	Glycoconjugates in Biological Systems (GLIBS) Scholarship
	Travel award
	Gothenburg University
	Research scholarship
2006	**Gothenburg University**
	Research Scholarship, awarded twice
2005	**Gothenburg University**
	Research scholarship
2004	**Gothenburg University**
	Research scholarship
	Gothenburg University School of Medicine
	'Best Poster' Winner, including scholarship
	Gothenburg University School of Medicine
	Teaching Position (“amanuens”) Scholarship
2003	**Gothenburg University**
	Research scholarship, awarded twice

Teaching

2012	**Graduate course, Johns Hopkins University Medical School**
	Helped develop and instructed and graded the graduate school course
	Method & Logic (teaching assistant, ‘TA’)
2009	**Sahlgrenska University Hospital**

Lecture, Department of Clinical Physiology

2004 **Gothenburg University School of Medicine**

Lecture series and practical sessions for junior medical students ("amanuens", Anatomy)